Submitted in accordance with the requirements for the degree of
Doctor of Philosophy

UNIVERSITY OF LEEDS

SCHOOL OF PHYSICS & ASTRONOMY

Reservoir Engineering for Quantum Information Processing

Jonathan Busch

September 2010

Acknowledgements

Abstract

Jonathan Busch, "Reservoir Engineering for Quantum Information Processing",

Ph.D. thesis, University of Leeds, May 2010.

This thesis concerns possible implementations of quantum computing schemes and tries to overcome some standard limitations. The central result is a technique we call reservoir engineering that is applied to optical cavity QED based quantum computing. The usual problem for quantum computing with atomic qubits in cavities is scalability as this requires either the coupling of photons leaking from cavities, using linear optics elements and measurements or shuttling of ions into and out of cavities. We propose an alternative that applies strong dissipative coupling to an environment as a control on fibre-coupled cavity systems. The control mechanism is effectively an overdamping of certain common cavity modes that restricts the time evolution of the qubit-cavity system onto a smaller subsystem consisting of only one common cavity modes. Within this subsystem, we then show that it is possible to implement quantum computing schemes that apply otherwise only to atomic qubits in the same cavity.

Thesis Publications

1. J. Busch, E.S. Kyoseva, M. Trupke and A. Beige, *Entangling distant quantum dots using classical interference* Phys. Rev. A, **78** 040301, (2008); ArXiv Quantum Physics e-prints, quant-ph/0801.0942, (2008).

2. J. Busch and A. Beige, *Protecting subspaces by acting on the outside* J. Phys.: Conf. Ser. (in press); arXiv Quantum Physics e-prints, quant-ph/1002.3479, (2010).

3. J. Busch and A. Beige, *Generating single-mode behavior in fiber-coupled optical cavities* Phys. Rev. A, **82** 053824, (2010); arXiv Quantum Physics e-prints, quant-ph/1009.1011, (2010).

Contents

Contents

List of Figures

Chapter 1

Introduction

Quantum Information Processing has seen great progress in the last two decades. The combination of groundbreaking experimental techniques and new theoretical insights into the fundamental aspects of Quantum Mechanics, have been combined to push the boundaries of our understanding of physics on the single atom and single photon level. A byproduct of this is the potential to build new technologies, including quantum computers and quantum cryptography, that harness these new discoveries. The most significant progress experimentally has been on systems of single atom and photon interactions and these have been used as testbeds for new technologies. However, there remain significant challenges to building systems that can perform quantum information processing tasks and scale to a level where they would be useful. Problems arise from the difficulty in isolating individual quantum systems from their environment and engineering controlled interactions between them. This thesis represents a proposal for new experimental techniques that overcome some of these problems.

The type of system that is worked on consists of single qubits coupled to optical cavities. In order for this to include solid state based qubits, the system has certain restriction including the inability to shuttle qubits in and out of cavities. A standard alternative to this is to effect an interaction through single photons that are emitted and absorbed by the cavities and measured by detectors. We use a more general

interaction with a common reservoir to engineer an effective interaction between two separate cavities. By engineering the form of the reservoir and observing it in a specific way, we can produce an effective interaction that performs useful quantum information processing tasks, specifically, generating an entangled state.

For a proper introduction, we begin by introducing the setting for the work of this thesis properly - starting with a brief explanation of how it fits into the rapidly growing field of quantum information processing; then moving on to a description of the physical systems we have in mind, the physics used to describe them and the inherent problems with these that we address. We then introduce the tools used in developing our technique. The first of these is the use of the quantum jump approach as a tool to analyse the dynamics of a system coupled to a reservoir, the second is the application of the reservoir coupling to induce a quantum control on the system that results in an effective dynamics.

1.1   Computing with Quantum

Whilst cavity quantum electrodynamics (cavity QED) and Quantum Jumps are the setting for most of the physics in this thesis, quantum information science is its motivation. The field of quantum information science lies in the interaction of quantum physics with computer science. At its heart is the question of how information is stored, manipulated and exchanged in a quantum universe. To put the work contained in this thesis into its proper context, a brief overview of where it fits into the field of Quantum Information now follows.

The basic unit of classical computing is the bit which can hold a value of 0 or 1. Bits can be stored, transmitted through channels and manipulated through logical operations. Information theory provides a mathematical framework to study the storage and transmission of information. It provides, for example, measures for the information content of messages and the capacity of channels. Computation by manipulation of bits is the subject of study for computer science. Logical operations on bits are combined into algorithms that perform useful computational tasks.

Quantum Information comes into the picture when we consider the physical systems used to implement bits and logical operations on them. In a classical computer, these are all macroscopic systems, at least to the extent that describing them with bits is consistent. Quantum Mechanics describes the physics of how semiconductors are used in a modern computer but the logic they implement through the manipulation of currents and magnetic storage is still classical. However, in 1959, Richard Feynman questioned what would happen when these physical systems where miniaturised to the point of bits being stored on single atoms or transmitted by single electrons. In this case, Feynman pointed out, quantum mechanics would have to be used. Computation performed with these devices would follow different rules [1].

To formalise these ideas, in quantum information the bit is replaced by the qubit (quantum bit). The qubit still has values 0 and 1 but its behaviour is described by quantum mechanics so it may also be in a superposition of 0 and 1. Although Feynman pointed out the possibility of quantum computing in 1959, the implications of this where not seriously studied until the 1980's. In 1982, Feynman followed up his earlier observation by showing that a quantum computer could efficiently simulate a quantum system [2]. This was built on in 1985 when David Deutsch introduced the idea of a universal quantum computer as the quantum analog to the classical Turing machine [3].

The 1990's saw the development of a number of algorithms for quantum computers that are more efficient than their classical counterparts. The most notable of these are Shor's factoring [4], Grover's search [5] and the Deutsch-Josza [6] algorithm. In addition, quantum analogues of error correcting codes have been proposed that mitigate the effects of quantum decoherence on quantum computation [7].

The contribution to this field made by this thesis lies between the level of qubits and that of algorithms. The algorithms mentioned above function at a level that is more abstract than anything we address here, their relevance is that they define the resources required to perform useful quantum computing tasks. Algorithms are often described using circuit diagrams where quantum gates perform operations on

qubits. This entails qubits undergoing some interaction or joint evolution the result of which performs the desired gate operation. How these qubits can be implemented in hardware and induced to undergo the desired evolution is the setting for this thesis.

A particularly interesting theoretical construct for quantum computing is that of measurement based quantum computing. First proposed by Raussendorf and Briegel in 2001 [8], this method uses only large (many qubit) entangled states as a resource. Using only these 'cluster states' and carefully arranged measurements on them, it is possible to show equivalence to a universal quantum computer. To us, this means that the ability to generate entanglement between qubits in a way that can be scaled to many qubits, is a significant step towards building a universal quantum computer. This is why the example we choose to demonstrate an application of our reservoir engineering is that of generating entanglement between two qubits. In 2001, it was shown that linear optics elements and photon detection where sufficient to perform measurement based quantum computation [9]. A number of implementations based on these linear optics that produce cluster states of matter qubits have been proposed [10, 11, 12].

In parallel to the development of Quantum Computing was the development of Quantum Cryptography - a field of study kick-started by Charles Bennett and Gilles Brassard in 1984 [13]. They developed a protocol for secret key distribution that is provably information theoretically secure by the laws of quantum mechanics. The security of this scheme is essentially based on superpositions of quantum states and the no-cloning theorem. An alternative key distribution based on entanglement was proposed by Ekert in 1991 [14].

Quantum cryptography is currently held back by the difficulty in integrating it with networks. Quantum Cryptography requires a direct link between any two communicating partners for the direct transmission of photons provided either by a single mode fibre or a line of sight through free space. This both limits the range achievable and rules out the use of straightforward switches and routers for

networking. Implementing networked quantum cryptography, or more generally just the transmission of quantum information in networks, will require the development of new technologies such as quantum memories and quantum repeaters [15]. In principle, the reservoir engineering scheme we develop here could also be used in this capacity.

1.2 Cavity quantum electrodynamics

The physics used to describe the hardware implementations for the qubits we work with in this thesis is cavity QED. Since its inception in the early 20th century, the theory of quantum mechanics has been applied to the interactions of light and matter. Cavity QED is the most modern setting for this study as it allows the reduction of the physics to describing a single atom interacting with a single mode of the quantised electromagnetic field. This system, though deceptively simple, has produced an astonishingly rich array of new physical phenomena.

Perhaps the earliest theoretical prediction relating to atom-cavity systems was that of the enhancement of spontaneous emission on resonance by Purcell in 1946 [16]. Although this was not experimentally verified until 1983 [17], this Purcell factor really lies at the heart of why cavity QED is so interesting. In a free-field, the interaction between atoms and light is very small. The change in the electromagnetic field caused by the boundary conditions imposed by the presence of the cavity mirrors greatly enhances this interaction and the effects associated with it. The quantisation of field modes can also bring about an inhibition of spontaneous emission [18] when the cavity field mode and atomic transition frequencies are far from resonance. This effect has also been experimentally observed [19].

In 1963, Jaynes and Cummings derived a description of a single atom coupled to a single cavity mode that is analytically tractable [20]. The Jaynes-Cummings Hamiltonian is the basis of many further predictions of the behaviour of such systems [1]. Predictions from this model include vacuum Rabi oscillations [23], vacuum

---

[1]the corresponding Hamlitonian for a many atom-cavity system is the Tavis-Cummings Hamil-

Rabi splitting [24, 25], photon anti-bunching [26] and the collapse and revival of Rabi oscillations [27]. Advances in experimental techniques in the 1980's with the development of high Q cavities made the direct observation of these effects possible [27], leading to increasingly impressive examples of non-classical behaviour of light [23].

It is the combination of the physical effects and the analytical progress in describing them described above that has made atom cavity systems a prime candidate for the implementation of quantum information processing. In general, there are many different architectures that need not include atoms or what one might consider a cavity that can be described by the same theory. In the following we shall refer to atom-like qubits (as opposed to atomic qubits) as not just the conventional qubits formed by the energy levels of electronic states of an atom but also qubits that are formed from 'artificial' atoms such as quantum dots, superconducting qubits and nitrogen-vacancy centres (NV-centres) in diamond. Atomic qubits in cavities are currently one of the most successfully studied systems for quantum information processing. Atomic qubits have the useful properties of being relatively long lived and easily manipulated by laser pulses making them useful candidates for QIP. Photonic qubits, using for example the polarisation states of light, are particularly useful for the transmission of quantum information over long distance. An atom-cavity setup allows the combination of the advantages of both systems.

To illustrate the kind of experimental progress that has been made on atom-cavity systems for QIP, we now list some of the most advanced and impressive experiments. For this, we consider not only atomic qubit systems but also atom-like qubits.

- **Trapped Ions -** Atomic ions have been used to produce some of the most impressive demonstrations yet of quantum information processing. They have proved to be excellent candidates for this task due to their long trapping times, long coherence times and easy access to manipulation of their internal

---

tonian [21, 22].

states. By direct interaction of trapped ions, experiments have been performed that produce three-qubit entangled states [28] and deterministic entanglement swapping [29]. The problem with trapped ion based quantum computing is that the interactions utilised for the above experiments are all local. It is very difficult to do anything with distant trapped ions as they are difficult to couple efficiently to photonic qubits. Entanglement between distant ions has been achieved [30] but as the ions coupled to a free radiation field, the success probability was extremely small. Recently, efforts have been made to overcome this issue with the trapping of a single ion inside an optical cavity [31] which was used to produce an entangled state between the ion and a single photon. Further development along these lines, including the addition of fibre-cavities on microchip-mounted ion traps, should make ion trap based systems suitable for quantum networking technologies.

- **Neutral Atoms -** In contrast to trapped ions, neutral atoms have been very successfully coupled to optical cavities. Neutral atoms are essentially the prototype for cavity QED and thus also as an interface between atomic and photonic qubits. The problem with these systems has been keeping the atoms inside the cavities. Recent progress on atom-cavity systems has been focused on improving the quality of the cavities through miniaturisation and improving the trapping times for the atoms inside the cavities. A number of groups have by now improved the trapping times to exceeding 15 seconds [32, 33, 34] and combined this with optical readout of the atomic state, a process that usually knocks the atom out of the cavity. The quality of these experiments has improved to the point that they are well into the strong coupling regime with cooperativity parameters ($C = \frac{g^2}{\kappa \Gamma}$) in excess of 30 [35]. On the miniaturisation front, fibre based cavities are being developed by a number of groups [36, 37, 38] with promising results in detection of atomic states [39]. One of the goals promised by these experiments is fibre coupling of cavities with atoms trapped within them.

- **Solid State -** Solid states systems such as quantum dots and NV-centres in diamond have only begun to be studied more recently and are thus still somewhat lagging behind in the results achieved. The promise of these systems is that they may be more scalable than true atomic systems which require complicated experimental procedures to localise the qubits, and that coupling to nuclear spins can provide excellent storage for qubit states [40]. Solid state systems have been shown to be feasible for the generation of entanglement [41, 42], but the coupling of solid state qubits to cavities in the strong coupling regime is still proving to be extremely challenging [43, 44]. Another highly impressive set of results has been produced by experiments using superconducting qubits in the microwave regime [45]. These have achieved strong coupling between qubits and single photons [46] as well as producing highly entangled states between two matter qubits [47]. However, these systems are not appropriate for the schemes proposed in this thesis. One characteristic of the microwave is that the environment cannot be assumed to be a vacuum as it is in the optical regime. Much of the later analysis in this thesis is based on this assumption and the results may not hold for a thermal reservoir where the system decoherence may take a different form.

As all of these implementations still face great challenges in implementing a really scalable quantum computer prototype, theoreticians have worked to develop schemes that could be implemented with less demanding experimental requirements. A large number of entanglement schemes for both two-partite entanglement and cluster state generation have been proposed in the literature and a few of these have been implemented experimentally. Ideas include entangling atoms in fibre-coupled cavities [48], entangling atoms in a single cavity by measuring reflected photons [49] or a macroscopic fluorescence signal [50, 51] and using control strategies [52, 53] or cooling [54] to reach an entangled steady state. Schemes for entangling atomic ensembles for quantum memories and repeaters are also becoming more numerous [55, 56].

The aim of many of these schemes is very similar to the purpose of this thesis: to develop new techniques for coupling separate atom-cavity systems. In particular, similar ideas have been proposed that couple two cavities directly with an optical fibre [57, 58, 59]. These assume that the fibre that couples two cavities can itself be treated effectively as a cavity. From this, they derive an effective interaction between the qubits that can generate entanglement or perform gate operations. The technique we employ takes a different approach in that we use the coupling fibre as a reservoir for the cavity modes and then employ it for quantum control techniques.

1.3 Reservoir modelling

As was mentioned above, the coupling of qubit systems to reservoirs forms a central theoretical component of this thesis. Historically, the description of how a quantum system behaves when coupled to a reservoir has been at the centre of a great deal of debate. A particular feature of this has been the occurrence of quantum jumps in individual quantum systems. Quantum jumps represent perhaps the most striking example of quantum behaviour [60, 61] and their history is itself quite interesting. The idea of quantum jumps has been at the heart of philosophical debate on quantum mechanics since its very beginning. Schrödinger and Bohr disagreed on the very idea of applying the formalism of quantum mechanics to single realisations of quantum systems. Schrödingers claim was that this would necessarily lead to nonsense such as quantum jumps. Bohr believed that the problem simply lay with the limitations of the experiments of the day.

The debate gets really interesting in 1975, when Dehmelt pointed out that quantum jump behaviour could be observed as macroscopic fluorescence signals [62]. With a three level atom with one metastable state and appropriate laser driving, the state of the atom can be heralded by the stimulated emission of large photon numbers or the lack thereof when the atom is *shelved* in the metastable state. Transitions between these two states would be observed as *macroscopic quantum jumps* in the fluorescence behaviour of the atom. The actual experimental observation of

this was first made by Nagourney *et.al.* [63]. More recent experiments have shown quantum jumps between hyperfine ground states of a single atom [35] and of photon number states in an optical cavity [64]. A good theoretical treatment of quantum jumps may be found in Carmichael's book on the subject [65].

For the purposes of this thesis, quantum jumps are understood to be a result of the interaction between system and reservoir. The aspect we are particularly interested in is that the reservoir has an action on the system, altering its dynamics. The form of the reservoir and the resulting action it causes has been used similarly [66] to explain the results of an experiment on interference of spontaneously emitted photons from two ions [67]. In this paper, the observed interference effect is explained by a derivation of the jump operators that act on the ions when a photon is spontaneously emitted. In this thesis, we use the same approach to derive the jump operators for atom-cavity systems that couple to reservoirs. The resulting dynamical effects of these operators are used as a tool to generate desirable dynamics, for example to separate the dynamics of cavity mode subspaces by symmetry or to produce entangled states.

The theoretical framework we use to describe the system reservoir coupling is that of the quantum jump approach (QJA), which was developed to describe accurately the behaviour of individual quantum systems coupled to reservoirs and the resulting quantum jumps. This formalism is used extensively throughout the thesis and chapter 2 is devoted to using it to describe the dynamics of a single atom-cavity system coupled to an environment.

1.4 Quantum Control

A further tool used in this thesis is that of quantum control. Quantum control can be broadly defined as techniques that generate specific dynamical evolutions of quantum systems in order to drive them towards some goal. The simplest case is that where the system to control has a finite dimensional Hilbert space. In this case, the general approach is to manipulate the Hamiltonian dynamics of the system, usually

using adiabatic evolutions, as in stimulated Raman adiabatic passages (STIRAP) [68, 69]), or shaped laser pulses [70]. These techniques have been shown to be very successful [71, 72, 73].

In general however, the system to be controlled is embedded in an infinite dimensional Hilbert space as will be the case in this thesis where qubits couple to cavity modes and infinite reservoir modes. The general approach then must take account of the reservoir coupling present in the system dynamics. A particular strategy is to induce strong interaction outside of the control subspace. This introduces a timescale to the system dynamics that is shorter than control system dynamics, thus disrupting the normal evolution of the control system. This is the approach we use in this thesis and it has many similarities with the well known 'bang-bang' and dynamical decoupling techniques [74, 75, 76].

1.5 Outlook

The content of this thesis combines the four concepts outlined above. To state it in one sentence, we develop a technique for quantum information processing using qubits embedded in cavity QED systems that uses reservoir modelling and quantum control as tools.

The main problem this thesis seeks to address is that of scalability in cavity QED systems. For the implementation of large scale quantum information processing tasks (such as building cluster states) interaction between qubits must be able to connect a set of qubits. This can be achieved by either placing all qubits into the same cavity field which then mediates the interaction or by passing photons between cavities and performing measurements on them. The problem with the first method is that it requires many qubits to be placed into the same cavity, all at once or by shuttling them in and out. This is hard to reconcile with the small mode volume required for a good cavity. The second method is based on being able to reliably operate with and measure single photons, which is also technically very demanding.

The solution we present is a method for coupling two cavities such that qubits

placed into them experience a coupling to a single common cavity mode. A full description of the two cavities requires two modes. These can be written in a basis where there are two common modes that each have some amplitude in both cavities. By manipulating the environment that the cavity modes couple to, two common modes can be made to couple to two separate environments. We use reservoir modelling as described above to show how this is achieved for two cases: one where interference from sub-wavelength fibres is used and one where one of the reservoirs is created by a single mode fibre connecting the cavities.

Once the cavity modes are separated by their coupling to different reservoirs, the quantum control techniques outlined above are applied. By making the cavity mode coupling to one reservoir much larger than the other, this cavity mode undergoes a time evolution that is faster than any other system dynamics. It becomes effectively decoupled from the rest of the system dynamics. The effect is achieved in the fibre coupling case by an atomic vapour around the fibre that measures the evanescent field of the fibre for the presence of photons. The description used for this is of rapidly repeated measurement on the common cavity mode. The effect is an overdamping of this common cavity mode that is analogous to the quantum Zeno effect [77, 78, 79]. Once this is achieved, qubits placed into the cavities interact only with the remaining common cavity mode and experience an effective dynamical evolution that is the same as if they where placed into a single cavity.

The separation of subspaces of the cavity modes we achieve by coupling to a single mode fibre between them is similar to the fibre coupled cavities that have been proposed by other authors [57, 58, 59]. The difference between these proposals and the one described in this thesis is encapsulated in the previous paragraph. We explicitly add dissipation to the connecting fibre as a control mechanism. This has the effect of relaxing some of the physical requirements for treating the fibre as a cavity. In particular, we do not need the fibre to hold a photon for as long as a cavity description would imply.

Finally, we explicitly derive an example where this reservoir engineering tech-

nique is used to implement an entanglement generation scheme for two atoms in a single cavity [51]. As we have developed this technique with a view towards applying it to solid state systems where it is even more difficult to place multiple qubits into a cavity and impossible to shuttle qubits around, this entanglement scheme is derived for quantum dot qubits with their associated decay mechanisms taken into account. The entanglement scheme presented has the advantages of being reasonably robust against decoherence, not relying on the measurement of individual photons and not requiring the coherent control of qubits.

The organisation of the thesis is as follows. Chapter 2 shows the application of the Quantum Jump Approach to a system consisting of a single cavity in a reservoir. This will later be used as the blueprint for the application of this method to a setup consisting of two fibre coupled cavities. Chapter 3 shows how decoherence can be used as a control mechanism to protect states in a subspace of the total system Hilbert space. This is done using a number of toy systems and analysing how well populations in their ground states can be protected from losses. In chapter 4, we show how the analysis of chapter 2 applied to coupled cavity systems can, with the addition of the technique from chapter 3, engineer a system that behaves as a single common cavity mode across two physical cavities. This forms the basis of the entanglement scheme presented in chapter 5 where a quantum dot qubit is placed into each of the two cavities. These qubits can be projected into an entangled state which is heralded by a macroscopic fluorescence signal. Finally, in the conclusion, we draw together the results presented in preceding chapters and discuss some potentially interesting avenues for future research.

Chapter 2

Quantum jump approach for cavity QED

2.1   Introduction

The type of system studied in this thesis can essentially be reduced to atomic qubits, quantised electromagnetic fields in resonators, free electromagnetic fields and couplings between them. In this chapter, we will introduce the simplest possible model that incorporates all of these elements in order to build a framework for the more complicated systems analysed in later chapters.

An even greater simplification would be considering only a single atom coupled to a single resonator mode. This system is described by the Jaynes-Cummings model [20]. This model has been very widely studied due to its relative simplicity and analytic tractability. What we consider in this chapter is an extension to this model that adds spontaneous emission into a free radiation field. The addition of this reservoir adds considerable complexity to the analysis of the system as we add an infinite number of degrees of freedom for the infinite modes of the free field. Such systems are treated as *open quantum systems*, where the state of the environment is traced out and only the time evolution of the system of interest is analysed. We will employ the methodology of the Quantum Jump Approach (QJA) which is
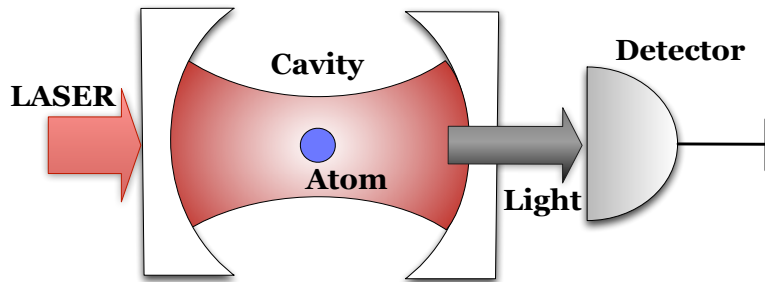
Figure 2.1: Experimental setup of a single cavity driven by a laser field. The photons leaking out through the cavity mirrors are monitored by a detector.

particularly suited to applications of single or few atoms [80].

We derive, using this approach, a master equation that is commonly used in the literature. However, the derivation of this master equation using the method we apply here is not found in the literature. We show this derivation to illustrate the perspective used in this thesis on the treatment of open quantum systems. This method of deriving the effect of the reservoir on the system is well suited to incorporating particular features of the reservoir related to the placement of detectors. A good example of where the same approach is used for an experiment on interference of spontaneously emitted photons from two ions [67] can be found in [81].

2.2 Experimental Setup

As was stated above, the system we analyse here consists of a single atom in an optical cavity where both the atom and cavity couple to a free radiation field and the atom is driven by a laser field, as shown in Fig. 2.1. In this case the atomic and the cavity states will be referred to as the system. The level structure of the atom consists simply of a ground level $|0\rangle$ and an excited level $|1\rangle$ with a transition frequency denoted by ω_0. We assume that the cavity supports only a single mode that is in resonance with the atomic transition frequency and denote this mode in the Hamiltonian by creation and annihilation operators $c^\dagger$ and c. The frequency of this cavity mode is denoted by ω_c. Analogously, the free-field modes will be denoted by creation and annihilation operator $a^\dagger_{\mathbf{k}\lambda}$ and $a_{\mathbf{k}\lambda}$ where $\mathbf{k}$ is the wave-vector of the

16

free-field mode, λ is its polarisation and ω_k its frequency.

The full Hamiltonian of this system takes the form

$$H = H_0 + H_{\mathrm{dip}} \,, \tag{2.1}$$

where H_0 represents the non-interacting parts and H_{dip} represents the appropriate dipole coupling terms between the atom, the cavity field, the free field and the laser field. The non-interacting parts of the Hamiltonian corresponding to the atom, cavity field and free field are [82]

$$
\begin{aligned}
H_{\mathrm{atom}} &= \hbar\omega_0 |1\rangle\langle 1| \\
H_{\mathrm{cavity}} &= \hbar\omega_c c^\dagger c \\
H_{\mathrm{field}} &= \sum_{\mathbf{k}\lambda} \hbar\omega_k a_{\mathbf{k}\lambda}^\dagger a_{\mathbf{k}\lambda} \,,
\end{aligned} \tag{2.2}
$$

where the zero point energy terms of the cavity and free fields have been removed by applying a normal ordering.

For the interaction part of the Hamiltonian expressions for the Dipole moment of the atom, $\mathbf{D}$, the external field, $\mathbf{E}$, and the cavity field, $\mathbf{E}_c$, are required. These are [82]

$$
\begin{aligned}
\mathbf{D} &= \mathbf{D}_{01}(|1\rangle\langle 0| + |0\rangle\langle 1|) \\
\mathbf{E} &= \mathrm{i}\sum_{\mathbf{k}\lambda} \epsilon_{\mathbf{k}\lambda} \left(\frac{\hbar\omega_k}{2\epsilon_0 V} \right)^{\frac{1}{2}} [a_{\mathbf{k}\lambda} - a_{\mathbf{k}\lambda}^\dagger] \\
\mathbf{E}_c &= \mathrm{i}\epsilon_c \left(\frac{\hbar\omega_c}{2\epsilon_0 V_c} \right)^{\frac{1}{2}} [c - c^\dagger] \,,
\end{aligned} \tag{2.3}
$$

where $\epsilon_{\mathbf{k}\lambda}$ and ϵ_c are the polarisation vectors and V and V_c are the quantisation volumes for the free-field and the cavity field respectively.

The atom-free field and atom-cavity interaction Hamiltonians are given by $\mathbf{D}\cdot\mathbf{E}$ and $\mathbf{D}\cdot\mathbf{E}_c$ respectively whilst the free field-cavity interaction Hamiltonian is simply

given by $\mathbf{E} \cdot \mathbf{E}_c$. First, we evaluate the atom-free field interaction

$$
\begin{aligned}
H_{\text{atom}-\text{field}} &= e\mathbf{D} \cdot \mathbf{E} \\
&= \mathrm{i}e\sum_{\mathbf{k}\lambda}\left(\frac{\hbar\omega_k}{2\epsilon_0 V}\right)^{\frac{1}{2}}\epsilon_{\mathbf{k}\lambda}\cdot\mathbf{D}_{01}[a_{\mathbf{k}\lambda}-a_{\mathbf{k}\lambda}^{\dagger}][|1\rangle\langle 0|+|0\rangle\langle 1|] \\
&= \mathrm{i}\sum_{\mathbf{k}\lambda}\hbar g_{\mathbf{k}\lambda}[a_{\mathbf{k}\lambda}-a_{\mathbf{k}\lambda}^{\dagger}][|1\rangle\langle 0|+|0\rangle\langle 1|]\,, \quad\quad (2.4)
\end{aligned}
$$

where

$$
g_{\mathbf{k}\lambda} = e\sqrt{\frac{\omega_k}{2\epsilon_0\hbar V}}\epsilon_{\mathbf{k}\lambda}\cdot\mathbf{D}_{01} \quad\quad (2.5)
$$

is the coupling between the atom and the free-field.

The calculations for the atom-cavity and cavity-free field interactions are largely the same with the following results

$$
\begin{aligned}
H_{\text{atom}-\text{cavity}} &= \mathrm{i}\hbar g_c[c-c^{\dagger}][|1\rangle\langle 0|+|0\rangle\langle 1|] \\
H_{\text{cavity}-\text{field}} &= \sum_{\mathbf{k}\lambda}\hbar s_{\mathbf{k}\lambda}[a_{\mathbf{k}\lambda}^{\dagger}-a_{\mathbf{k}\lambda}][c-c^{\dagger}]\,, \quad\quad (2.6)
\end{aligned}
$$

where

$$
\begin{aligned}
g_c &= e\sqrt{\frac{\omega_c}{2\epsilon_0\hbar V_c}}\epsilon_c\cdot\mathbf{D}_{01} \quad\text{and} \\
s_{\mathbf{k}\lambda} &= \frac{\sqrt{\omega_c\omega_k}}{2\epsilon_0\sqrt{VV_c}}\epsilon_{\mathbf{k}\lambda}\epsilon_c \quad\quad (2.7)
\end{aligned}
$$

are the couplings between the atom and the cavity, and the cavity and the free-field respectively.

The final interaction term is between the laser field and the atomic states. As the effect of adding or removing photons from a laser field has only a negligible effect on it, it can be treated as a classical field. Its interaction Hamiltonian with the atom is

$$
H_{\text{laser}} = \frac{1}{2}\hbar\Omega\left[|0\rangle\langle 1|e^{\mathrm{i}\omega_L t}+|1\rangle\langle 0|e^{-\mathrm{i}\omega_L t}\right]\,, \quad\quad (2.8)
$$

18

where

$$\Omega = \frac{2e}{\hbar} D_{01} \cdot E \,, \tag{2.9}$$

is the Rabi frequency of the laser and ω_L is its frequency. Combining all of the above non-interacting ($H_0 = H_{\text{atom}} + H_{\text{cavity}} + H_{\text{field}}$) and interaction ($H_{\text{dip}} = H_{\text{atom}-\text{field}} + H_{\text{atom}-\text{cavity}} + H_{\text{cavity}-\text{field}} + H_{\text{laser}}$) parts gives a Hamiltonian that describes the full system in the Schrödinger picture.

Whilst this is a complete description, it is not in a very useful form as the explicit time dependence of the Hamiltonian makes it difficult to solve analytically. To simplify this, we now rewrite the Hamiltonian in an interaction picture where it has no explicit time dependence.

2.3   Interaction Picture Hamiltonian

Formally, the Schrödinger picture refers to a description where all the time dependence is in the quantum states and the quantum mechanical operators are time independent. Conversely, in the Heisenberg picture all the time dependence is in the quantum mechanical operators and the states are time independent. An interaction picture is one where both operators and states have time dependence. The transformation from the Schrödinger picture to an interaction picture is achieved through a time dependent unitary transformation of the states and operators. More precisely, the Schrödinger picture Hamiltonian may be written $H_S = H_0 + H_{S,I}$ where H_0 contains the time-dependence we wish to remove and is used to construct the unitary transform. The quantum state in the interaction picture is then given by

$$|\Psi_I(t)\rangle = e^{-\frac{i}{\hbar} H_0 t}|\Psi_S(t)\rangle \,, \tag{2.10}$$

19

where $|\Psi_S(t)\rangle$ is the quantum state in the Schrödinger picture. Similarly, the interaction picture Hamiltonian is given by

$$H_I = U_0^\dagger(t) H_{S,I} U_0(t) , \qquad (2.11)$$

where

$$U_0(t) \equiv e^{-\frac{i}{\hbar} H_0 t} . \qquad (2.12)$$

We now apply this technique to the Hamiltonian for our atom cavity system choosing the non-interacting parts of the Hamiltonian as H_0. In this case, the transformation unitary is

$$\begin{aligned}
U_0(t) &= e^{-\frac{i}{\hbar} H_0 t} \\
&= e^{-i\omega_0 |1\rangle_{aa}\langle 1| t - i\omega_c c^\dagger c t - i\sum_{\mathbf{k}\lambda} \omega_k a_{\mathbf{k}\lambda}^\dagger a_{\mathbf{k}\lambda} t} ,
\end{aligned} \qquad (2.13)$$

where the a subscript on $|1\rangle_a$ denotes an atomic state. Analogously, c and k subscripts will be used to denote cavity and free-field states respectively.

Using the definition for the function of a Hermitian operator

$$f(A) = \sum_n f(\lambda_n) |\lambda_n\rangle\langle\lambda_n| , \qquad (2.14)$$

where $\{\lambda_n\}$ is the set of eigenvalues of A corresponding to the complete set of orthonormal eigenvectors $\{|\lambda_n\rangle\}$, we can write

$$\begin{aligned}
U_0(t) &= \left(|0\rangle_{aa}\langle 0| + e^{i\omega_0 t} |1\rangle_{aa}\langle 1| \right) \otimes \sum_{n=0}^{\infty} e^{in\omega_c t} |n\rangle_{cc}\langle n| \\
&\otimes \sum_{n=0}^{\infty} \sum_{\mathbf{k}\lambda} e^{in\omega_k t} |n\rangle_{\mathbf{kk}}\langle n| .
\end{aligned} \qquad (2.15)$$

20

We apply this transformation to the Hamiltonian as follows

$$
\begin{aligned}
H_{\mathrm{I}} &= U_0^\dagger(t)\Bigg\{ \frac{1}{2}\hbar\Omega\left[|0\rangle\langle 1|e^{i\omega_L t} + |1\rangle\langle 0|e^{-i\omega_L t}\right] \\
&\quad + i\hbar g_c[c - c^\dagger][|1\rangle\langle 0| + |0\rangle\langle 1|] \\
&\quad + i\sum_{\mathbf{k}\lambda}\hbar g_{\mathbf{k}\lambda}[a_{\mathbf{k}\lambda} - a_{\mathbf{k}\lambda}^\dagger][|1\rangle\langle 0| + |0\rangle\langle 1|] \\
&\quad + \sum_{\mathbf{k}\lambda}\hbar s_{\mathbf{k}\lambda}[a_{\mathbf{k}\lambda}^\dagger - a_{\mathbf{k}\lambda}][c - c^\dagger]\Bigg\} U_0(t) \\
&= \frac{1}{2}\hbar\Omega\left[|0\rangle\langle 1|e^{i(\omega_L - \omega_0)t} + |1\rangle\langle 0|e^{-i(\omega_L - \omega_0)t}\right] \\
&\quad + i\hbar g_c\Big[c|1\rangle\langle 0|e^{i(\omega_c - \omega_0)t} - c^\dagger|1\rangle\langle 0|e^{-i(\omega_c + \omega_0)t} + c|0\rangle\langle 1|e^{i(\omega_c + \omega_0)t} \\
&\quad - c^\dagger|0\rangle\langle 1|e^{-i(\omega_c - \omega_0)t}\Big] \\
&\quad + i\sum_{\mathbf{k}\lambda}\hbar g_{\mathbf{k}\lambda}\Big[a_{\mathbf{k}\lambda}|1\rangle\langle 0|e^{i(\omega_{k\lambda} - \omega_0)t} - a_{\mathbf{k}\lambda}^\dagger|1\rangle\langle 0|e^{-i(\omega_{k\lambda} + \omega_0)t} \\
&\quad + a_{\mathbf{k}\lambda}|0\rangle\langle 1|e^{-i(\omega_{k\lambda} - \omega_0)t} - a_{\mathbf{k}\lambda}^\dagger|0\rangle\langle 1|e^{i(\omega_{k\lambda} + \omega_0)t}\Big] \\
&\quad + \sum_{\mathbf{k}\lambda}\hbar s_{\mathbf{k}\lambda}\Big[a_{\mathbf{k}\lambda}^\dagger c\,e^{i(\omega_c - \omega_{k\lambda})t} - a_{\mathbf{k}\lambda}c\,e^{i(\omega_c + \omega_{k\lambda})t} - a_{\mathbf{k}\lambda}^\dagger c^\dagger e^{-i(\omega_c + \omega_{k\lambda})t} \\
&\quad + a_{\mathbf{k}\lambda}c^\dagger e^{-i(\omega_c - \omega_{k\lambda})t}\Big]
\end{aligned}
\tag{2.16}
$$

We can now eliminate the rapidly oscillating terms according to the rotating wave approximation and find that the resulting interaction picture Hamiltonian is

$$
\begin{aligned}
H_{\mathrm{I}} &= \frac{1}{2}\hbar\Omega(|0\rangle\langle 1| + |1\rangle\langle 0|) \\
&\quad + \sum_{\mathbf{k}\lambda}\hbar g_{\mathbf{k}\lambda}\left[e^{i(\omega_0 - \omega_k)t}|1\rangle\langle 0|a_{\mathbf{k}\lambda} + e^{-i(\omega_0 - \omega_k)t}|0\rangle\langle 1|a_{\mathbf{k}\lambda}^\dagger\right] \\
&\quad + \hbar g_c\left[|1\rangle\langle 0|c + |0\rangle\langle 1|c^\dagger\right] \\
&\quad + \sum_{\mathbf{k}\lambda}\hbar s_{\mathbf{k}\lambda}\left[c\,a_{\mathbf{k}\lambda}^\dagger e^{i(\omega_k - \omega_c)t} + c^\dagger a_{\mathbf{k}\lambda}e^{-i(\omega_k - \omega_c)t}\right],
\end{aligned}
\tag{2.17}
$$

where we have also assumed that the laser, atom and cavity are all in resonance, i.e. $\omega_L = \omega_0 = \omega_c$. A further simplification made is absorbing an i into the definition of $c^{(\dagger)}$ and $a_{\mathbf{k}\lambda}^{(\dagger)}$ thus removing an i from two of the coupling terms. Note that all the explicit time dependence in this Hamiltonian is now in the free-field coupling terms.

This is the appropriate form for the next step in the analysis.

2.4   Open Quantum System Approach

In general, the Hamiltonian in Eq. 2.17 is still very difficult to deal with. There is an infinite number of degrees of freedom in the free radiation field that we are not interested in, but that change the dynamics of the atom cavity system that we are interested in. The general approach to dealing with this type of situation is to treat the atom-cavity subsystem as an open quantum system. This means, we restrict our description to only the states of the atom and the cavity and trace out all the degrees of freedom of the free-field, reducing its effect to a small number of *dissipative* operators. Using this approach, a master equation can be derived that describes the approximate time evolution of the system without the environment.

2.4.1   The master equation

We now present a brief outline of the derivation of the master equation that follows the derivation found in [83]. For this derivation, we start with the interaction Hamiltonian in an interaction picture as defined by Eq. 2.11 with the density matrix equivalently given by

$$\rho_I(t) = U_0(t)^\dagger \rho(t) U_0(t) \,. \tag{2.18}$$

The time evolution of the density matrix is given by the standard Liouville-von Neumann equation

$$\frac{\mathrm{d}}{\mathrm{d}t} \rho_I(t) = -\frac{\mathrm{i}}{\hbar} \left[H_I(t), \rho_I(t) \right] \,. \tag{2.19}$$

What we are looking for, however, is an equation that gives the time evolution of the system density matrix without describing the evolution of the environment. This

system density matrix may be expressed as

$$\rho_S, I(t) = \text{Tr}_\text{E} \left\{ \rho_I(t) \right\} , \tag{2.20}$$

where Tr_E is a partial trace over the environment. A formal integration of Eq. 2.19 and substituting this back into Eq.. 2.19 results in

$$\frac{\mathrm{d}}{\mathrm{d}t} \rho_{S,I}(t) = -\frac{1}{\hbar^2} \int_0^t \mathrm{d}t' \text{Tr}_\text{E} \left[H_I(t), [H_I(t), \rho_I(t)] \right] . \tag{2.21}$$

Up to this point, this derivation has been exact. To get any further, we now have to invoke first the Born approximation and then the Markov approximation.

The Born approximation assumes that system-environment interactions are weak such that the density matrix describing both the system and environment may be written as a product

$$\rho_I(t) = \rho_{S,I}(t) \otimes \rho_E \tag{2.22}$$

where ρ_E is also assumed to remain in an equilibrium state and thus has no time dependence. With this approximation, the master equation may now be written

$$\frac{\mathrm{d}}{\mathrm{d}t} \rho_{S,I}(t) = -\frac{1}{\hbar^2} \int_0^t \mathrm{d}t' \text{Tr}_\text{E} \left[H_I(t), [H_I(t), \rho_{S,I}(t) \otimes \rho_E] \right] . \tag{2.23}$$

Applying the Markov approximation assumes that any correlations created between the system and the environment decay on a time scale that is much shorter than the scale on which $\rho_{S,I}$ evolves in time. This is like saying that the environment has no memory ad very quickly forgets its past interactions with the system. Via the introduction of a correlation function, the details of which will be omitted here but may be found in [83], it is straightforward to show that the master equation may now be written

$$\frac{\mathrm{d}}{\mathrm{d}t} \rho_s(t) = \frac{i}{\hbar} [H_S, \rho_S(t)] - \frac{1}{\hbar^2} \sum_\alpha \left\{ [S_\alpha, B_\alpha \rho_S(t)] + [\rho_S(t) C_\alpha, S_\alpha] \right\} \tag{2.24}$$

where B_α and C_α are time independent terms derived from the correlation function mentioned above and the system parts of the interaction Hamiltonian S_α, which is defined by

$$H_{S,I} = \sum_\alpha S_\alpha \otimes E_\alpha \,. \qquad (2.25)$$

Eq. 2.24 is the Born-Markov master equation. This equation may be transformed into the Lindblad form if one further assumption is made: the rotating wave approximation. In this case, the master equation may be written as

$$\frac{\mathrm{d}}{\mathrm{d}t}\rho_S(t) = -\frac{i}{\hbar}\left[H_S, \rho_S(t)\right] - \frac{1}{2}\sum_\mu \kappa_\mu \left\{ L_\mu^\dagger L_\mu \rho_S(t) + \rho_S(t) L_\mu^\dagger L_\mu - 2 L_\mu \rho_S(t) L_\mu^\dagger \right\} \,, (2.26)$$

where L_μ are the so-called Lindblad operators. This form of the master equation also ensures the positivity of the reduced density matrix $\rho_S(t)$, which the Born-Markov master equation does not necessarily.

This master equation may be used to derive many details of the behaviour of open quantum systems. However, when dealing with a quantum system consisting of few atoms, there are some aspects of the time evolution of the quantum state of a single experimental realisation that the master equation does not address. For this purpose, we now turn to the Quantum Jump Approach (QJA).

2.4.2 The Quantum Jump Approach

When dealing with a single realisation of quantum systems such as a single atom or, as here, a single atom and cavity, the issue of quantum jumps appears. A quantum jump occurs when, in the interaction of the system with an environment, the state of the system spontaneously changes from one state to another. A good example is the spontaneous emission of a photon from a single atom leaving the atom in its ground state.

This spontaneous jumping of a quantum system was already discussed by Schrödinger and Bohr. Schrödinger stated that quantum mechanics should not be applied

to single quantum systems as it would necessarily lead to such non-sense as quantum jumps. Bohr, in contrast, believed that the problem simply lay with the experiments of the time. The argument is reflected in the master equation which, describing only ensemble averages, does not describe the occurrence of quantum jumps: a new formalism is required to show them.

The QJA (or quantum trajectories) was developed simultaneously in Göttingen, Aarhus and Oregon as a tool to aid the understanding of the dynamics of open quantum systems where the systems consist of single or few atoms [84, 85, 86, 80] and quantum jumps may occur. In particular, the macroscopic dark periods seen in the Dehmelt V system [62] where modelled using this approach. The QJA is essentially equivalent to both the Monte Carlo wave function approach [87] and the quantum trajectories approach [65].

The derivation of the QJA begins by assuming measurements on the environment carried out at time intervals Δt. The interval Δt must be long enough to avoid running into the quantum Zeno effect [88] but short enough compared to the system lifetimes that only single emission events occur in each time step. In terms of the characteristic timescales of an atom-cavity system, the time interval must be much greater than the systems characteristic frequency (the cavity frequency ω_c) and much shorter the system decay rates (κ and Γ), i.e.

$$\frac{1}{\omega_c} \ll \Delta t \ll \frac{1}{\kappa} \, , \, \frac{1}{\Gamma} \, . \tag{2.27}$$

These continuous measurements are known as *environment induced measurements* to reflect the fact that they do not necessarily require an actual detector to absorb the photons, simply a large environment that absorbs them. The environment induced measurements are the equivalent of the Markov approximation in the master equation in that they destroy any entanglement between the system and environment that could otherwise be created.

At each time interval, Δt, a photon is either detected by the environment or not with a probability that is determined by the Hamiltonian describing the system.

In the case of no photon detection, a conditional (reduced) Hamiltonian, H_{cond}, is derived to describe the dynamics of the system. The state of the whole system under this condition is then $|\Psi(t)\rangle|0_{ph}\rangle$, where $|\Psi(t)\rangle$ is the state of the system and $|0_{ph}\rangle$ is the zero photon state of the external field. Now let $\mathbb{P}_0$ be the projector onto the zero photon subspace of the free field,

$$\mathbb{P}_0 \equiv |0_{ph}\rangle \mathbb{I}_s \langle 0_{ph}| \tag{2.28}$$

and $U(\Delta t, 0)$ the time-evolution operator of the complete system including external field,

$$U(\Delta t, 0) \equiv \mathcal{T} e^{-\frac{i}{\hbar} \int_0^{\Delta t} H(t) dt} \tag{2.29}$$

where $\mathcal{T}$ is the time ordering operator and H is the Hamiltonian describing the complete system including external field. Given the state of the system at time $t = 0$, the state at time Δt under the condition of no photon emission is then given by

$$|\Psi(\Delta t)\rangle|0_{\mathrm{ph}}\rangle = \mathbb{P}_0 \, U(\Delta t, 0)|\Psi(0)\rangle|0_{\mathrm{ph}}\rangle \,. \tag{2.30}$$

The time evolution of the system state $\Psi(t)$ is here effectively described by a conditional time evolution operator

$$U_{\mathrm{cond}}(\Delta t, 0) \equiv \langle 0_{\mathrm{ph}}|U(\Delta t, 0)|0_{\mathrm{ph}}\rangle \tag{2.31}$$

which furthermore relates to a conditional Hamiltonian H_{cond} as

$$U_{\mathrm{cond}}(\Delta t, 0) = \mathcal{T} e^{-\frac{i}{\hbar} \int_0^{\Delta t} H_{\mathrm{cond}}(t') dt'} \,. \tag{2.32}$$

The conditional time evolution operator may be calculated from the Hamiltonian

26

of the complete system using time-dependent perturbation theory as follows

$$
\begin{aligned}
U_{\text{cond}}(\Delta t, 0) \;=\; & \langle 0_{\text{ph}} | \mathbb{I} | 0_{\text{ph}} \rangle - \frac{i}{\hbar} \int_0^{\Delta t} dt \langle 0_{\text{ph}} | H(t) | 0_{\text{ph}} \rangle \\
& - \frac{1}{\hbar^2} \int_0^{\Delta t} dt \int_0^t dt' \langle 0_{\text{ph}} | H(t) H(t') | 0_{\text{ph}} \rangle
\end{aligned}
\tag{2.33}
$$

From this, the conditional Hamiltonian is easily determined. The calculation of the conditional Hamiltonian for the atom cavity system follows in the next section.

For a full description, the reset operator is required, which describes the change in the state of the system when a photon is emitted. If there is a photon emission, then a complimentary projection operator $\mathbb{P}_{1,\mathbf{k}\lambda} = |1_{\mathbf{k}\lambda}\rangle\langle 1_{\mathbf{k}\lambda}| \otimes \mathbb{I}_s$ corresponding to a photon of wavevector $\mathbf{k}$ and polarisation λ is used in Eq (2.30), ie.

$$
|1_{\mathbf{k}\lambda}\rangle|\Psi(\Delta t)\rangle = \mathbb{P}_{1,\mathbf{k}\lambda} U(\Delta t, 0)|0_{\text{ph}}\rangle|\Psi(0)\rangle \,.
\tag{2.34}
$$

This event is effectively described by the Reset (or jump) operator

$$
R_{\mathbf{k}\lambda} \equiv \langle 1_{\mathbf{k}\lambda}|U(\Delta t, 0)|0_{\text{ph}}\rangle \,,
\tag{2.35}
$$

acting on the pre-measurement state of the system. This corresponds to the system evolving normally as described by $U(\Delta t, 0)$ and then projected onto the subspace where one photon was emitted. Note again that only the possibility of one photon emission in a single time step is considered and emissions of more than one photon are neglected. This is because the time steps are very short compared to the average time between photon emissions.

Now we have both the conditional Hamiltonian and the Reset operators. The application of these two operators provides a quantum trajectory for the system, analogous to the individual trajectories of a Monte-Carlo simulation. By introducing the jump superoperator

$$
R(\rho) \equiv \sum_{\mathbf{k}\lambda} R_{\mathbf{k}\lambda} \rho R_{\mathbf{k}\lambda}^{\dagger}
\tag{2.36}
$$

the master equation in Eq. 2.26 may be expressed as

$$\dot{\rho}_S = -\frac{\mathrm{i}}{\hbar}\left[H_{\mathrm{cond}}\rho_S - \rho_S H_{\mathrm{cond}}^\dagger\right] + R(\rho_S)\,. \tag{2.37}$$

2.4.3   Derivation of H_{cond}

We now turn to the application of the QJA to the system represented by the interaction Hamiltonian in Eq. (2.17). We begin by considering the expression for the perturbative expansion of the conditional time evolution operator in Eq. (2.33). We will take the first three terms in this expansion to retain all terms up to order $\mathcal{O}(\Delta t)$ and denote them by

$$
\begin{aligned}
\mathrm{I}_1 &= \langle 0_{\mathrm{ph}}|\mathbb{I}|0_{\mathrm{ph}}\rangle\\
\mathrm{I}_2 &= -\frac{\mathrm{i}}{\hbar}\int_0^{\Delta t}\mathrm{d}t\,\langle 0_{\mathrm{ph}}|H_{\mathrm{I}}(t)|0_{\mathrm{ph}}\rangle\\
\mathrm{I}_3 &= -\frac{1}{\hbar^2}\int_0^{\Delta t}\mathrm{d}t\int_0^t\mathrm{d}t'\,\langle 0_{\mathrm{ph}}|H_{\mathrm{I}}(t)H_{\mathrm{I}}(t')|0_{\mathrm{ph}}\rangle\,.
\end{aligned}
\tag{2.38}
$$

The first term is trivially the identity for the system states $\mathbb{I}_S$. The second term is

$$\mathrm{I}_2 = -\frac{\mathrm{i}}{2}\Omega\left[|0\rangle\langle 1| + |1\rangle\langle 0|\right]\Delta t - \mathrm{i}g_c\left[|1\rangle\langle 0|c + |0\rangle\langle 1|c^\dagger\right]\Delta t\,, \tag{2.39}$$

as only the terms without free-field creation or annihilation operators can remain and these have no time dependence. The most complicated is the third term which contains the $H_{\mathrm{I}}(t)H_{\mathrm{I}}(t')$. A straightforward simplification can be made by noticing that only terms with $a_{\mathbf{k}\lambda}a_{\mathbf{k}\lambda}^\dagger$ will remain after tracing out with $\langle 0_{\mathrm{ph}}|X|0_{\mathrm{ph}}\rangle$. We furthermore recognise that the atom and cavity will emit photons into different field modes, i.e.

$$g_{\mathbf{k}\lambda}\cdot s_{\mathbf{k}\lambda} = 0\,, \tag{2.40}$$

28

for all $\mathbf{k}$ and λ. This means any cross terms in these couplings will also disappear. The remaining terms are

$$
\text{I}_3 = -\int_0^{\Delta t} \mathrm{d}t \int_0^t \mathrm{d}t \sum_{\mathbf{k}\lambda} \left[|g_{\mathbf{k}\lambda}|^2 e^{\mathrm{i}(\omega_k - \omega_0)(t'-t)} |1\rangle\langle 1| + |s_{\mathbf{k}\lambda}|^2 e^{\mathrm{i}(\omega_k - \omega_c)(t'-t)} c^\dagger c \right], \quad (2.41)
$$

where, in multiplying the two summations over $\mathbf{k}\lambda$ together, one of them has been removed as

$$
\sum_{\mathbf{k}\lambda} \langle n_{\mathbf{k}\lambda} | n_{\mathbf{k}'\lambda'} \rangle = \delta(\mathbf{k}, \mathbf{k}') \delta(\lambda, \lambda'). \quad (2.42)
$$

The laser driving term contributions have also been dropped here as they give rise to terms of order Δt^2.

The next step is to swap the integrations and summation and introduce a new variable $\tau = t' - t$. The term in Eq. 2.41 then becomes

$$
\text{I}_3 = \sum_{k\lambda} \int_0^{\Delta t} \mathrm{d}t \int_0^t \mathrm{d}\tau \left[e^{i(\omega_{k\lambda} - \omega_0)\tau} |g_{k\lambda}|^2 |1\rangle\langle 1| + e^{i(\omega_{k\lambda} - \omega_c)\tau} |s_{k\lambda}|^2 c^\dagger c \right]. \quad (2.43)
$$

Now, since the inner integral limit t is in general much greater than $1/\omega_c$, the limit of the τ integration can be taken to infinity. This assumption is equivalent to the Markov approximation and allows this integral to be evaluated to give

$$
\begin{aligned}
\text{I}_3 = \sum_{k\lambda} \int_0^{\Delta t} \mathrm{d}t &\left[|g_{k\lambda}|^2 \left\{ \pi\delta(\omega_{k\lambda} - \omega_0) + i\mathcal{P}\frac{1}{\omega_{k\lambda} - \omega_0} \right\} |1\rangle\langle 1| \right. \\
&\left. + |s_{k\lambda}|^2 \left\{ \pi\delta(\omega_{k\lambda} - \omega_c) + i\mathcal{P}\frac{1}{\omega_{k\lambda} - \omega_c} \right\} c^\dagger c \right].
\end{aligned} \quad (2.44)
$$

The principal value term is analogous to a level shift (similar to the Lamb shift) and can be absorbed into the definitions of frequencies [86].

The final step in the evaluation of this term is to substitute in expressions for the coupling parameters $g_{\mathbf{k}\lambda}$ and $s_{\mathbf{k}\lambda}$ from Eq's 2.5 and 2.7, turn the sum over $\mathbf{k}\lambda$ into an integral and evaluate the remaining integrals. The final result of this is

$$
\text{I}_3 = -\frac{\Gamma}{2} |1\rangle\langle 1| \Delta t - \frac{\kappa}{2} c^\dagger c \Delta t, \quad (2.45)
$$

29

where

$$\Gamma = \frac{e^2 D_{01} \cdot D_{01}^*}{6\pi\epsilon_0 \hbar c^3}\omega_0^3 \quad \text{and} \quad \kappa = \frac{2\pi}{\mathcal{N}}\sum_{\mathbf{k}\lambda} s_{\mathbf{k}\lambda}\delta(\omega_{k\lambda} - \omega_c)\,, \tag{2.46}$$

are known as the atom and cavity spontaneous decay rates respectively, where $\mathcal{N}$ depends for example on the quantisation volume of the reservoir.

All the first order terms in the expansion of U_{cond} are now known and the full expression is

$$
\begin{aligned}
U_{\text{cond}}(\Delta t, 0) &= \text{I}_1 + \text{I}_2 + \text{I}_3 \\
&= \mathbb{I}_S - \frac{\mathrm{i}}{2}\Omega(|0\rangle\langle 1| + |1\rangle\langle 0|)\Delta t - \mathrm{i}g_c\left[|1\rangle\langle 0|c + |0\rangle\langle 1|c\right]\Delta t \\
&\quad - \frac{\Gamma}{2}|1\rangle\langle 1|\Delta t - \frac{\kappa}{2}c^\dagger c\Delta t\,.
\end{aligned}
\tag{2.47}
$$

From this expression, the conditional Hamiltonian can be derived using a first order expansion with $\Delta t \to 0$ to be

$$
\begin{aligned}
H_{\text{cond}} &= \frac{1}{2}\hbar\Omega(|0\rangle\langle 1| + |1\rangle\langle 0|) + \hbar g_c\left[|1\rangle\langle 0|c + |0\rangle\langle 1|c^\dagger\right] \\
&\quad - \frac{\mathrm{i}\hbar}{2}\Gamma|1\rangle\langle 1| - \frac{\mathrm{i}\hbar}{2}\kappa c^\dagger c\,.
\end{aligned}
\tag{2.48}
$$

This conditional Hamiltonian describes the time evolution of the sub-ensemble where no spontaneous emission has occurred. The non-Hermitian terms in this Hamiltonian reflect the decreasing probability of finding the system in this sub-ensemble.

2.4.4 Derivation of the Reset Operator

The derivation of the Reset Operator $R_{k\lambda}$ is very similar to the derivation of H_{cond}. The same form of series expansion for the time evolution operator is initially used

in Eq. 2.35

$$
\begin{aligned}
R_{\mathbf{k}\lambda} &= \langle 1_{\mathbf{k}\lambda}|\Big\{ \mathbb{I}_S - \frac{i}{\hbar} \int_0^{\Delta t} \mathrm{d}t H_I(t) - \frac{1}{\hbar} \int_0^{\Delta t} \mathrm{d}t \int_0^t \mathrm{d}t' H_I(t) H_I(t') \Big\}|0_{ph}\rangle \\
&= \langle 1_{\mathbf{k}\lambda}|\mathbb{I}|0_{ph}\rangle - \frac{i}{\hbar} \int_0^{\Delta t} \mathrm{d}t \langle 1_{\mathbf{k}\lambda}|H_I(t)|0_{ph}\rangle \\
&\quad - \frac{1}{\hbar} \int_0^{\Delta t} \mathrm{d}t \int_0^t \mathrm{d}t' \langle 1_{\mathbf{k}\lambda}|H_I(t) H_I(t')|0_{ph}\rangle \,.
\end{aligned}
\tag{2.49}
$$

Of these only the first order term remains as a significant term and higher orders are ignored. As before, we now also assume that spontaneously emitted photons from the atom and cavity couple to different modes and should be represented by different Reset operators. For this purpose, we define two Reset operators $R_{a,\mathbf{k}\lambda}$ and $R_{c,\mathbf{k}\lambda}$ to represent these two emissions from the atom and cavity respectively. Their expressions become

$$
R_{a,\mathbf{k}\lambda} = -\frac{i}{\hbar} \int_0^{\Delta t} \mathrm{d}t \, \hbar \langle 1_{\mathbf{k}\lambda}|\Big\{ \sum_{\mathbf{k}\lambda} e^{i(\omega_k - \omega_0)t} g_{\mathbf{k}\lambda}|0\rangle\langle 1|a_{\mathbf{k}\lambda}^\dagger \Big\}|0_{ph}\rangle \,,
\tag{2.50}
$$

and

$$
R_{c,\mathbf{k}\lambda} = -\frac{i}{\hbar} \int_0^{\Delta t} \mathrm{d}t \, \hbar \langle 1_{\mathbf{k}\lambda}|\Big\{ \sum_{\mathbf{k}\lambda} e^{i(\omega_k - \omega_0)t} s_{\mathbf{k}\lambda} c a_{\mathbf{k}\lambda}^\dagger \Big\}|0_{ph}\rangle \,.
\tag{2.51}
$$

Given the orthogonality of the free-field modes, the sum over $\mathbf{k}\lambda$ is removed once the inner product of $\langle 1_{\mathbf{k}\lambda}|a_{\mathbf{k}\lambda}^\dagger|0_{ph}\rangle$ is taken. This would result in a reset operator for each reservoir mode. However, as the precise wavevector and polarisation of the reservoir modes have no impact on the evolution of the atom-cavity system, a sum over all these operators allows us to define two single reset operators for the atom and cavity. This description is also more appropriate given that the environment performing the measurements most likely cannot distinguish accurately between different reservoir modes. The remaining expressions for R_a and R_c above can be evaluated analogously to the conditional time evolution operator to give

$$
R_a = \sqrt{\Gamma}|0\rangle\langle 1| \quad \text{and} \quad R_c = \sqrt{\kappa} c \,.
\tag{2.52}
$$

31

These operators act on the detection of a photon emitted by the atom and cavity respectively.

2.4.5   The Master Equation

The conditional Hamiltonian and Reset operators derived above provide a single trajectory description of the time evolution of the cavity system. They can also be used, as described in section 2.4.2, to derive the master equation through the relation in Eq. 2.37 where the reset superoperator is now given by

$$R(\rho) = R_a \rho R_a^\dagger + R_c \rho R_c^\dagger \tag{2.53}$$

Substituting this expression and the one in Eq. 2.48 for H_{cond} into Eq. 2.37 gives

$$
\begin{aligned}
\dot{\rho} =\ & -\mathrm{i}\Big[\Omega(|0\rangle\langle 1| + |1\rangle\langle 0|)\rho - \Omega^*\rho(|0\rangle\langle 1| + |1\rangle\langle 0|)\Big] \\
& -\mathrm{i}\Big[g_c(|1\rangle\langle 0|c + |0\rangle\langle 1|c^\dagger)\rho - g_c^*\rho(|1\rangle\langle 0|c + |0\rangle\langle 1|c^\dagger)\Big] \\
& -\frac{1}{2}\Gamma\Big[|1\rangle\langle 1|\rho + \rho|1\rangle\langle 1| - 2|0\rangle\langle 1|\rho|1\rangle\langle 0|\Big] \\
& -\frac{1}{2}\kappa\Big[c^\dagger c\rho + \rho c^\dagger c - 2c\rho c^\dagger\Big].
\end{aligned}
\tag{2.54}
$$

For those more familiar with the standard Lindblad form of the master equation, it is now apparent that the Reset operators derived above are in fact equivalent to the Lindblad operators in Eq. 2.26 (with a factor of 2 thrown in by convention).

This master equation is the starting point of many possible analyses of the system dynamics. For particularly simple systems, it may be used to analytically calculate the density matrix of the system or at least its steady state. For our purposes in this thesis, the full solution of the density matrix will not be required. For us, it is sufficient to be able to determine certain steady state values such as the mean photon number in the cavity modes. The details of such calculations will be given in later chapters when they are needed.

2.5 Summary

The final result of this chapter is the master equation in Eq. 2.54, which describes the time evolution of the density matrix of an atom cavity system including the effect of reservoir coupling. This result is often used as a starting point in the literature. However, the derivation presented here, via the QJA is not found in the literature. The QJA is used to describe the evolution of a state vector. Physically, this means it describes the time evolution of one, individual realisation of the system. This is in contrast to the master equation which describes only the ensemble average time evolution. The evolution of an individual realisation takes a stochastic form where a continuous evolution described by a conditional Hamiltonian is interrupted by instantaneous jumps in the state vector represented by the action of reset operators whenever a spontaneous emission occurs. For the atom cavity system described in this chapter, the conditional Hamiltonian is given in Eq. 2.48 whilst the reset operators are given in Eq's. 2.50 and 2.51.

The purpose of this chapter was to derive the master equation in Eq. 2.54 using the quantum jump approach with a view to applying the same technique to analyse the dynamics of systems with more complicated, structured reservoirs. The application of the QJA also provides a conditional Hamiltonian and reset operators. The derivation of these is well suited to including effects due to the reservoir having a particular structure, a feature that will become important in later chapters of this thesis.

Chapter 3

Protecting quantum states with dissipation

3.1 Introduction

In this chapter, we develop the control techniques that will later be applied to atom-cavity systems. In particular, we consider how decoherence can be used as a control mechanism. As a very broad description, we are interested in a system that contains a finite dimensional subspace that we wish to control coupled to an infinite dimensional environment.

Quantum control techniques that manipulate finite-dimensional Hilbert spaces have been shown to be very successful in engineering specific Hamiltonians [71, 72, 73]. However, this class of system is only a small subset of problems where quantum control could be applied. In general, quantum control requires the control of systems that have an infinite dimensional state space. Our system of interest is one of these - an atom-cavity system coupled to an infinite dimensional bosonic reservoir.

There are many ways to protect a finite dimensional subspace from the leakage of population (cf. Fig. 3.1). The general idea is to take advantage of mechanisms that restrict the time evolution of the system effectively onto the finite dimensional subspace, taking advantage of the resulting evolution to produce appropriate control
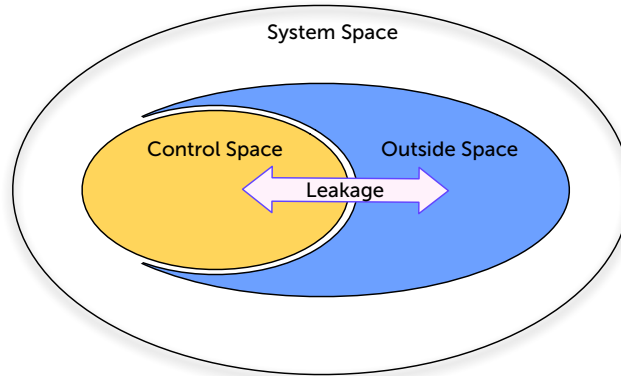
Figure 3.1: Illustration of the control problem. We wish to control the system evolution within a subspace (yellow) of the total space (white) whilst there is coupling to an external subspace (blue).

sequences [89, 90]. The most theoretically simple approach is to use a Hamiltonian that only acts on the desired subspace, thus allowing the time evolution of the system to remain only within this subspace. An example of this technique is in ion trap quantum computing where required interactions are applied in successive steps to perform gate operations [91]. The purpose here is to prevent the excitation of coherent phonon states as the number of phonons in the system can increase by at most one in each time step. At the end of the control sequence, the ions are returned into a state with zero phonon excitations [92, 93].

Alternative tools for protecting subspaces are based around specially shaped laser pulses applied to the system states. One instance of this technique was developed to minimise radiation damage when exciting specific ground-state vibrational modes of molecules [70]. The best known control strategy in quantum optical systems is probably that of stimulated Raman adiabatic passages (STIRAP) [68, 69]. STIRAP employs the adiabatic theorem to transfer populations between two states without a direct coupling between them and without any excited states ever becoming significantly populated. In composite quantum systems, like atoms which move slowly through an optical cavity, STIRAP can create ground state entanglement without populating excited electronic states and without creating photons inside the resonator [94]. A generalisation of both strategies is to simply use numerical

simulations which impose state dependent constraints to design optimal control sequences [95].

In this chapter, we discuss a strategy that relies on strong interaction outside the control subspace, rather than imposing well defined dynamics within it. If the strong interactions act *only* on the outside, they induce a timescale that is much shorter than the system evolution timescale. In particular, this timescale is shorter than the timescale on which population would normally leak out of the controlled subspace. When this is the case, one can show that these unwanted transitions become strongly inhibited [96, 97, 98]. This approach has many similarities with bang-bang and its generalisation dynamical decoupling [74, 75, 76] which also interrupt a relatively slow evolution with strong interactions.

The first half of this chapter considers systems where the strong interactions on the outside take the form of strong coherent coupling to auxiliary states. The second half adds strong dissipation on outside states as the strong interaction. This is to illustrate how dissipation can be used constructively to protect the controlled subspace against population leakage. We describe the dynamics of the system using rapidly-repeated measurements on whether the system remains in the controlled subspace or not [94, 99, 100, 101, 102, 103]. Using this description, the resulting protection of the population in the controlled subspace can be understood in terms of the quantum Zeno effect [77, 78, 79]. We note also that, when it is possible to register a spontaneous emission, a built-in error detection mechanism is included in this scheme.

The similarities between bang-bang, dynamical decoupling and protection using dissipation have been analysed in Refs. [104, 105]. The authors conclude that all these approaches are equivalent and can all be understood in some sense as the quantum Zeno effect [77]. In this chapter, we analyse the underlying processes with relatively simple toy models. This allows us to quantitatively compare the effectiveness of protection using strong coherent interactions and dissipation as well as gaining a more concrete understanding of how this technique applies later to

atom-cavity systems.

This chapter is organized in five sections. In the following section, we consider a two-level system with resonant coherent coupling. This represents the unprotected subspace scenario to which later schemes may be compared. In Section 3.3, we extend the outside space and show how strong interactions acting on the outside space can be used to protect the controlled subspace against leakage error - and how this can fail. Section 3.4 analyses the same level schemes but with the addition of non-zero spontaneous decay rates. The final example illustrates how dissipation provides a more foolproof protection where the strong coherent interaction scheme failed. We finally summarise our findings in Section 3.5.

3.2   An unprotected subspace

Let us first consider a case where no effort is made to protect a controlled subspace from leaking population into outside states. For simplicity, we assume that the controlled subspace contains only a single state $|0\rangle$. As shown in Fig. 3.2, there is moreover only one relevant state outside the controlled subspace which we denote by $|1\rangle$. The leakage of population from level 0 into level 1 could be due to resonant interactions (like a laser field). Although this is an almost trivial case, the analysis of the time evolution of this level scheme introduces the relevant time scales of the system. This will enable us later to characterise and to compare the effectiveness of different strategies for the protection of controlled subspaces against leakage errors.

In the following, we assume that the laser is in resonance with the 0–1 transition and denote its (real) Rabi frequency by ξ. Moreover, $\hbar\omega_i$ denotes the energy of states $|i\rangle$. The system Hamiltonian in the usual rotating wave and dipole approximation can be written as

$$H \quad = \quad \hbar\xi \, e^{i\omega_\xi t} \, |0\rangle\langle 1| + \text{h.c.} + \sum_{i=0}^{1} \hbar\omega_i \, |i\rangle\langle i| \tag{3.1}$$

with $\omega_\xi \equiv \omega_1 - \omega_0$. To solve the corresponding time evolution, we first change into

38
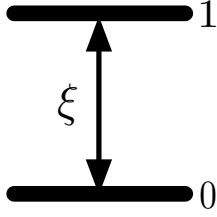
Figure 3.2: Toy model illustrating the leakage of population from an un-protected controlled subspace (represented by $|0\rangle$) with coupling strength ξ into an outside space (represented by $|1\rangle$).

an interaction picture with respect to $H_0 = \sum_{i=0}^{1} \hbar\omega_i |i\rangle\langle i|$. This transforms the Hamiltonian (3.1) into the interaction Hamiltonian

$$H_{\mathrm{I}} = \hbar\xi\,|0\rangle\langle 1| + \mathrm{h.c.} \tag{3.2}$$

To estimate the leakage rate of the controlled subspace in this case, we now calculate the population P_0 in $|0\rangle$ at time t, given that the system was initially in $|0\rangle$.

One way of doing this is to consider the usual Pauli operators σ_2 and σ_3,

$$\sigma_2 = -\mathrm{i}\,(\,|0\rangle\langle 1| - |1\rangle\langle 0|\,)\quad\text{and}\quad \sigma_3 = |0\rangle\langle 0| - |1\rangle\langle 1|\,, \tag{3.3}$$

and to use the relation

$$\frac{\mathrm{d}}{\mathrm{d}t}\langle A\rangle = -\frac{\mathrm{i}}{\hbar}\,\langle [A, H_{\mathrm{I}}]\rangle \tag{3.4}$$

for the time evolution of the expectation value of an operator A in the interaction picture to obtain a closed set of rate equations. This yields the differential equations

$$\frac{\mathrm{d}}{\mathrm{d}t}\begin{pmatrix} \langle\sigma_2\rangle \\ \langle\sigma_3\rangle \end{pmatrix} = 2\xi\begin{pmatrix} 0 & -1 \\ 1 & 0 \end{pmatrix}\begin{pmatrix} \langle\sigma_2\rangle \\ \langle\sigma_3\rangle \end{pmatrix} \tag{3.5}$$

which can be solved easily analytically.

39

A more straightforward way of solving the time evolution of the system is to write its state vector as $|\psi\rangle = \sum_{i=0,1} c_i |i\rangle$ and to use the Schrödinger equation to obtain differential equations for the complex coefficients c_i. However, the above approach of deriving rate equations for expectation values is more efficient, since we are only interested in the leakage of population out of the controlled subspace. Moreover, this approach can be extended easily to include more complex level schemes as well as the effect of spontaneous photon emission.

Since σ_3 commutes with H_0, we can calculate the population of the $|0\rangle$ state, $P_0 = \langle |0\rangle\langle 0| \rangle$, using the relation

$$P_0(t) = \frac{1}{2}(1 + \langle \sigma_3(t) \rangle).$$ (3.6)

Solving Eq. (3.5) for time-independent coupling constants ξ and for the case where the system is initially in $|0\rangle$, we find that the population in the initial state changes according to

$$P_0(t) = \frac{1}{2}(1 + \cos(2\xi t)) = \cos^2(\xi t).$$ (3.7)

This means, in the absence of any protection, the system remains inside the controlled subspace only on a time scale which is short compared to $1/\xi$.

3.3 Protecting a subspace with strong interactions

One way to protect the controlled subspace against errors is to involve the relevant outside states into a relatively fast time evolution. Indeed it has been found that strong interactions can have the same effect as rapidly repeated measurements whether the system remains in its initial subspace or not [104, 105]. In good agreement with the predictions of the quantum Zeno effect [77], these measurements strongly inhibit transitions out of the controlled subspace. In the following, we illustrate this approach with the help of the two toy models shown in Fig. 3.3. The purpose of the interactions with amplitude Ω is to induce fast oscillations of the
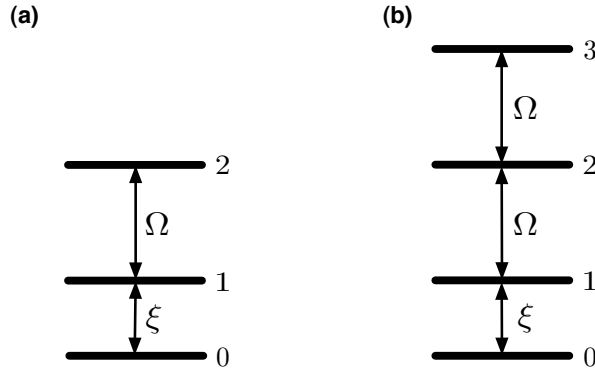
Figure 3.3: Toy models to illustrate the possible protection of a controlled subspace (represented by $|0\rangle$) with strong interactions with coupling strength Ω in the outside space. Here the outside space contains either the two states $|1\rangle$ and $|2\rangle$ (a) or the three states $|1\rangle$, $|2\rangle$, and $|3\rangle$ (b).

amplitude of the state $|1\rangle$. These cause $\langle\sigma_2\rangle$ in Eq. (3.3) to oscillate rapidly in time, such that $\frac{\mathrm{d}}{\mathrm{d}t}\langle\sigma_3\rangle$ in Eq. (3.5) becomes zero on average and the system remains approximately in $|0\rangle$.

As we shall see below, this strategy works well for the level scheme in Fig. 3.3(a). However, strong interactions acting on the outside space do not always protect the controlled subspace against leakage errors. Problems arise for example in the level scheme in Fig. 3.3(b). There the interactions in the outside space are more complex than the interactions which cause the leakage. The result is that the generation of approximate dark states in the outside space. These are zero eigenvectors of the fast system dynamics. Transitions between dark states and the controlled subspace are hence not protected by time scale separation, even when Ω becomes very large.

3.3.1   Single-coupling case

We begin with an analysis of the three-level system shown in Fig. 3.3(a). Again, the controlled subspace contains only a single state, $|0\rangle$, while the outside subspace contains the two states $|1\rangle$ and $|2\rangle$. In order to maximise the effect of the applied interactions, we assume resonant couplings. As before, ξ is the coupling constant for the 0–1 transition, while Ω denotes the coupling constant for the 1–2 transition.

Here we are especially interested in the case, where $\xi \ll \Omega$. Again we have a closer look at the time evolution of the population P_0 in the controlled subspace.

As in Section 3.2, we denote the energy of level i by $\hbar\omega_i$. The Hamiltonian for the level configuration in Fig. 3.3(a) can then be written as

$$H \quad = \quad \hbar\xi\,\mathrm{e}^{\mathrm{i}\omega_\xi t}\,|0\rangle\langle 1| + \hbar\Omega\,\mathrm{e}^{\mathrm{i}\omega_\Omega t}\,|1\rangle\langle 2| + \mathrm{h.c.} + \sum_{i=0}^{2}\hbar\omega_i\,|i\rangle\langle i| \tag{3.8}$$

with $\omega_\xi \equiv \omega_1 - \omega_0$ and $\omega_\Omega \equiv \omega_2 - \omega_1$. Transforming this Hamiltonian into the interaction picture with respect to $H_0 = \sum_{i=0}^{2}\hbar\omega_i\,|i\rangle\langle i|$, we obtain

$$H_\mathrm{I} \quad = \quad \hbar\xi\,|0\rangle\langle 1| + \hbar\Omega\,|1\rangle\langle 2| + \mathrm{h.c.} \tag{3.9}$$

This interaction Hamiltonian is time independent and contains only the weak coupling between $|0\rangle$ and $|1\rangle$ and the strong coupling between $|1\rangle$ and $|2\rangle$.

In order to obtain a closed system of rate equations, we now consider the expectation values of the Gell-Mann matrices [106]

$$\sigma_2 = -\mathrm{i}\,(|0\rangle\langle 1| - |1\rangle\langle 0|)\,,\quad \sigma_7 = -\mathrm{i}\,(|1\rangle\langle 2| - |2\rangle\langle 1|)\,,\quad \sigma_4 = |0\rangle\langle 2| + |2\rangle\langle 0|\,,$$

$$\sigma_3 = |0\rangle\langle 0| - |1\rangle\langle 1|\,,\quad \sigma_8 = \frac{1}{\sqrt{3}}\,(|0\rangle\langle 0| + |1\rangle\langle 1| - 2\,|2\rangle\langle 2|)\,. \tag{3.10}$$

These are generalisations of the Pauli operators used in Section 3.2. Overall there are eight Gell-Mann matrices which can be used to model the time evolution of coupled three-level systems in a convenient way. However, due to the specific form of the interactions in the level scheme in Fig. 3.3(a), we need to consider only five of them. Using relation (3.4), we find the following closed system of differential

42
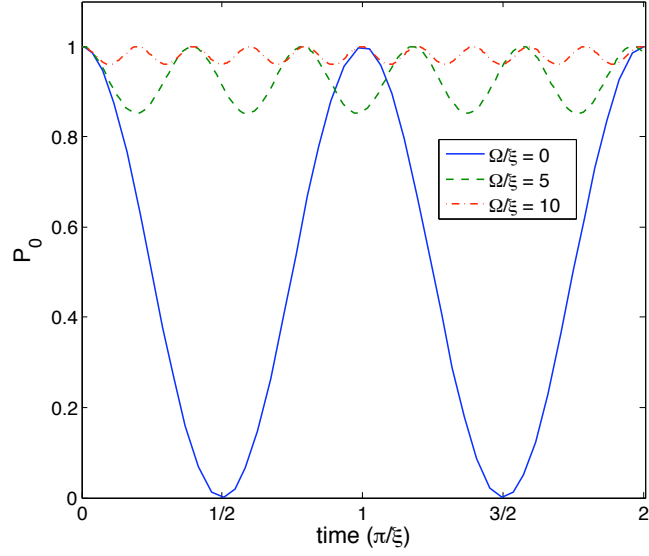
Figure 3.4: Time dependence of P_0 for the level scheme shown in Fig. 3.3(a) for different ratios of Ω/ξ. The system is initially in $|0\rangle$. For $\Omega = 0$, the system leaves its initial state space on a time scale given by $1/\xi$. For $\Omega > 10\,\xi$, the system remains there with a fidelity above 95 % which constitutes an effective protection of the initial state space.

equations

$$
\frac{\mathrm{d}}{\mathrm{d}t}
\begin{pmatrix}
\langle \sigma_2 \rangle \\
\langle \sigma_3 \rangle \\
\langle \sigma_4 \rangle \\
\langle \sigma_7 \rangle \\
\langle \sigma_8 \rangle
\end{pmatrix}
=
\begin{pmatrix}
0 & -2\xi & -\Omega & 0 & 0 \\
2\xi & 0 & 0 & -\Omega & 0 \\
\Omega & 0 & 0 & -\xi & 0 \\
0 & \Omega & \xi & 0 & -\sqrt{3}\Omega \\
0 & 0 & 0 & \sqrt{3}\Omega & 0
\end{pmatrix}
\begin{pmatrix}
\langle \sigma_2 \rangle \\
\langle \sigma_3 \rangle \\
\langle \sigma_4 \rangle \\
\langle \sigma_7 \rangle \\
\langle \sigma_8 \rangle
\end{pmatrix}.
\tag{3.11}
$$

These differential equations can be solved for example by calculating analytical expressions for the eigenvalues of this matrix.

From Eq. (3.10) we see that the population in the controlled subspace equals

$$
P_0 \;=\; \frac{1}{3} + \frac{1}{2}\langle \sigma_3 \rangle + \frac{1}{2\sqrt{3}}\langle \sigma_8 \rangle. \tag{3.12}
$$

Substituting the solution of the above rate equations into this equation, we find that

43

the population in $|0\rangle$ at time t evolves according to

$$P_0(t) \quad = \quad \frac{2\Omega^4 + \xi^4}{2\mu^4} + \frac{2\Omega^2\xi^2}{\mu^4}\cos(\mu t) + \frac{\xi^4}{2\mu^4}\cos(2\mu t) \qquad (3.13)$$

with $\mu^2 \equiv \Omega^2 + \xi^2$, if the system was initially in $|0\rangle$. For $\xi \ll \Omega$, Eq. (3.13) simplifies to

$$P_0(t) \quad = \quad 1 - \frac{2\xi^2}{\Omega^2}\left[1 - \cos\left(\Omega t\right)\right] \qquad (3.14)$$

which holds up to first order in ξ^2/Ω^2. As shown in Fig. 3.4, the system remains to a very good approximation, i.e. up to variations with an amplitude proportional to ξ^2/Ω^2, in $|0\rangle$. This means, for $\xi^2 \ll \Omega^2$, the controlled subspace is effectively protected against leakage errors.

3.3.2 Double-coupling case

Using the same notation as in the previous subsection, the Hamiltonian for the level configuration in Fig. 3.3(b) in the Schrödinger picture equals

$$H \quad = \quad \hbar\xi\,\mathrm{e}^{\mathrm{i}\omega_\xi t}|0\rangle\langle 1| + \hbar\Omega\,\mathrm{e}^{\mathrm{i}\omega_\Omega t}\left(|1\rangle\langle 2| + |2\rangle\langle 3|\right) + \mathrm{h.c.} + \sum_{i=0}^{3}\hbar\omega_i\,|i\rangle\langle i|. \quad (3.15)$$

Again we first simplify this Hamiltonian by changing into the interaction picture with respect to the free Hamiltonian $H_0 = \sum_{i=0}^{3}\hbar\omega_i\,|i\rangle\langle i|$. This yields

$$H_\mathrm{I} \quad = \quad \hbar\xi\,|0\rangle\langle 1| + \hbar\Omega\left(|1\rangle\langle 2| + |2\rangle\langle 3|\right) + \mathrm{h.c.} \qquad (3.16)$$

Instead of solving the corresponding Schrödinger equation, we apply again Eq. (3.4) to obtain a closed set of rate equations.

To predict the time evolution of the population P_0 in the controlled subspace,

44

we now have to consider nine generalised Gell-Mann matrices [106]. These are

$$\sigma_2 = -\mathrm{i}\,(|0\rangle\langle 1| - |1\rangle\langle 0|)\,, \quad \sigma_7 = -\mathrm{i}\,(|1\rangle\langle 2| - |2\rangle\langle 1|)\,,$$

$$\sigma_{10} = -\mathrm{i}\,(|0\rangle\langle 3| - |3\rangle\langle 0|)\,, \quad \sigma_{14} = -\mathrm{i}\,(|2\rangle\langle 3| - |3\rangle\langle 2|)\,,$$

$$\sigma_4 = |0\rangle\langle 2| + |2\rangle\langle 0|\,, \quad \sigma_{11} = |1\rangle\langle 3| + |3\rangle\langle 1|\,,$$

$$\sigma_3 = |0\rangle\langle 0| - |1\rangle\langle 1|\,, \quad \sigma_8 = \frac{1}{\sqrt{3}}\,(|0\rangle\langle 0| + |1\rangle\langle 1| - 2\,|2\rangle\langle 2|)\,,$$

$$\sigma_{15} = \frac{1}{\sqrt{6}}\,(|0\rangle\langle 0| + |1\rangle\langle 1| + |2\rangle\langle 2| - 3\,|3\rangle\langle 3|)\,. \tag{3.17}$$

Moreover, we notice that the interaction Hamiltonian (3.16) can be written as

$$H_{\mathrm{I}} = \hbar\xi\,\sigma_1 + \hbar\Omega\,(\sigma_6 + \sigma_{13}) \tag{3.18}$$

with

$$\sigma_1 = |0\rangle\langle 1| + |1\rangle\langle 0|\,, \quad \sigma_6 = |1\rangle\langle 2| + |2\rangle\langle 1|\,, \quad \sigma_{13} = |2\rangle\langle 3| + |3\rangle\langle 2|\,. \tag{3.19}$$

Substituting Eqs. (3.17)–(3.19) into Eq. (3.4) and evaluating the relevant commutators, we see that the expectation of the operators in Eq. (3.17) evolve according to

$$\frac{\mathrm{d}}{\mathrm{d}t}\begin{pmatrix} \langle\sigma_2\rangle \\ \langle\sigma_3\rangle \\ \langle\sigma_4\rangle \\ \langle\sigma_7\rangle \\ \langle\sigma_8\rangle \\ \langle\sigma_{10}\rangle \\ \langle\sigma_{11}\rangle \\ \langle\sigma_{14}\rangle \\ \langle\sigma_{15}\rangle \end{pmatrix} = \begin{pmatrix} 0 & -2\xi & -\Omega & 0 & 0 & 0 & 0 & 0 & 0 \\ 2\xi & 0 & 0 & -\Omega & 0 & 0 & 0 & 0 & 0 \\ \Omega & 0 & 0 & -\xi & 0 & \Omega & 0 & 0 & 0 \\ 0 & \Omega & \xi & 0 & -\sqrt{3}\Omega & 0 & -\Omega & 0 & 0 \\ 0 & 0 & 0 & \sqrt{3}\Omega & 0 & 0 & 0 & -\frac{2}{\sqrt{3}}\Omega & 0 \\ 0 & 0 & -\Omega & 0 & 0 & 0 & \xi & 0 & 0 \\ 0 & 0 & 0 & \Omega & 0 & -\xi & 0 & -\Omega & 0 \\ 0 & 0 & 0 & 0 & \frac{2}{\sqrt{3}}\Omega & 0 & \Omega & 0 & -\frac{2\sqrt{2}}{\sqrt{3}}\Omega \\ 0 & 0 & 0 & 0 & 0 & 0 & 0 & \frac{2\sqrt{2}}{\sqrt{3}}\Omega & 0 \end{pmatrix}\begin{pmatrix} \langle\sigma_2\rangle \\ \langle\sigma_3\rangle \\ \langle\sigma_4\rangle \\ \langle\sigma_7\rangle \\ \langle\sigma_8\rangle \\ \langle\sigma_{10}\rangle \\ \langle\sigma_{11}\rangle \\ \langle\sigma_{14}\rangle \\ \langle\sigma_{15}\rangle \end{pmatrix}.$$

$$\tag{3.20}$$

Figure 3.5: Time dependence of P_0 for the level scheme shown in Fig. 3.3(b) for different ratios of Ω/ξ. Here the controlled subspace is no longer protected against leakage, even when Ω becomes as large as $100\,\xi$. The reason is the leakage of population into the dark state $|\lambda_0\rangle$ which is illustrated in Fig. 3.7.

This system of linear differential equations can, in principle, be solved analytically. However, for simplicity, we restrict ourselves to the presentation of a numerical solution.

Using the Gell Mann matrices defined in Eq. (3.17), the population in the initial state P_0 can now be written as

$$P_0 \;\;=\;\; \frac{1}{4} + \frac{1}{2}\,\langle\sigma_3\rangle + \frac{1}{2\sqrt{3}}\,\langle\sigma_8\rangle + \frac{1}{2\sqrt{6}}\,\langle\sigma_{15}\rangle. \tag{3.21}$$

The time evolution of P_0 obtained from substituting the numerical solution of the differential equation (3.20) into Eq. (3.21) is shown in Fig. 3.5. Comparing the result for different values of Ω/ξ with the time evolution in the $\Omega = 0$ case, we see that the controlled subspace is not protected, even when Ω is much larger than ξ. Leakage of population out of the controlled subspace happens on the same time scale as in the unprotected case.

Why does the protection of the controlled subspace work in the level scheme shown in Fig. 3.3(a) but not in the very similar level scheme shown in Fig. 3.3(b)?
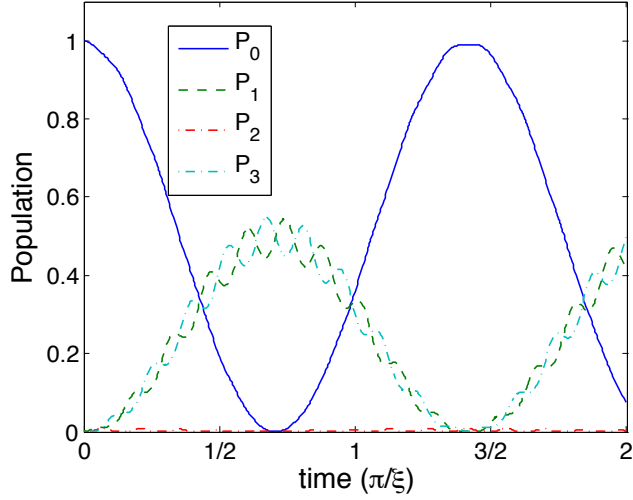
Figure 3.6: Time dependence of all four of the levels in the scheme shown in Fig. 3.3(b) for a ration of $\Omega/\xi = 10$. This highlights that the $|0\rangle$ state is no longer protected as population leaks into the $|1\rangle$ and $|3\rangle$ states.

To see some further details of the time evolution, a plot of the populations of all the states of the system is shown in Fig. 3.6 for a choice of $\Omega/\xi = 100$. In this figure, it is clear that the populations in the $|1\rangle$ and $|3\rangle$ states are not prevented from increasing.

The reason for this becomes clear when we rewrite the Hamiltonian in Eq. (3.16) in terms of the states

$$|0\rangle, \quad |\lambda_0\rangle \equiv \frac{1}{\sqrt{2}}(|1\rangle - |3\rangle), \quad |\lambda_1\rangle \equiv \frac{1}{\sqrt{2}}(|1\rangle + |3\rangle) \quad \text{and} \quad |2\rangle. \quad (3.22)$$

Using this notation, H_{I} becomes

$$H_{\mathrm{I}} = \frac{1}{\sqrt{2}}\hbar\xi\,|0\rangle\langle\lambda_0| + \frac{1}{\sqrt{2}}\hbar\xi\,|0\rangle\langle\lambda_1| + \sqrt{2}\hbar\Omega\,|\lambda_1\rangle\langle2| + \text{h.c.} \quad (3.23)$$

The effect of this Hamiltonian is illustrated in Fig. 3.7. It shows that the system is only protected against leakage into the $|\lambda_1\rangle$ state, since this state experiences a strong interaction. However, the system is not protected against leakage into $|\lambda_0\rangle$, since $|\lambda_0\rangle$ is a zero eigenstate of the Ω terms in Eq. (3.23). This means, $|\lambda_0\rangle$ is not
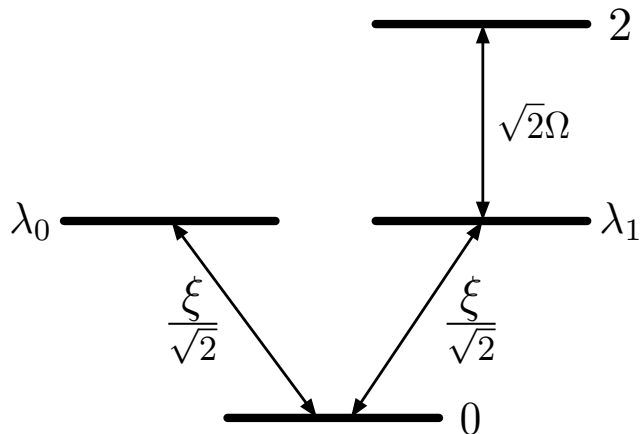
Figure 3.7: Illustration of the effect of the Hamiltonian (3.23) onto the states involved in the time evolution of the system. This level scheme is identical to the one shown in Fig. 3.3(b) but now we clearly see why the initial state $|0\rangle$ is no longer protected against leakage errors.

involved in a fast evolution and the transfer from $|0\rangle$ to $|\lambda_0\rangle$ occurs on the same time scale as in the unprotected case. In the final section, we show that dissipation is able to remove such dark states from the system so that the controlled subspace becomes protected again.

3.4 Protecting a subspace with dissipation

In this section we analyse three examples (cf. Fig. 3.8) which illustrate the possible protection of the controlled subspace *using dissipation*. The controlled subspace contains again only the $|0\rangle$ state, while the outside space contains one, two or three states. The only difference to the examples discussed in Sections 3.2 and 3.3 is the presence of a non-zero spontaneous decay rate Γ. As we shall see below, the controlled subspace is well protected against leakage in all three scenarios, when the interactions in the outside space described by Ω and the spontaneous decay rate Γ are sufficiently larger than ξ.
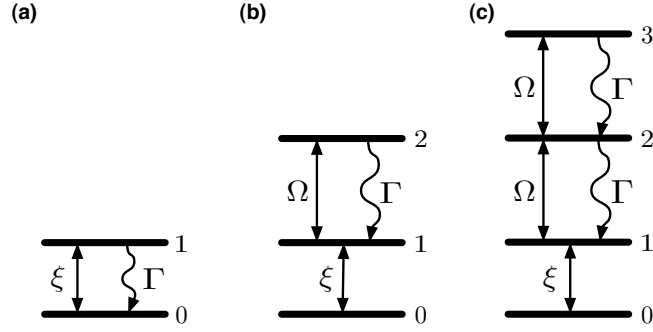
Figure 3.8: Toy models to illustrate the possible protection of the controlled subspace (represented by $|0\rangle$) with a non-zero spontaneous decay rate Γ and strong interactions with coupling strength Ω in the outside space.

3.4.1 Single-coupling case with dissipation

Let us first have a look at the three-level system shown in Fig. 3.8(b). To describe its time evolution, we go again into the interaction picture with respect to the free evolution and analyse the master equation

$$\dot{\rho} = -\frac{\mathrm{i}}{\hbar}[H_{\mathrm{I}}, \rho] + \frac{\Gamma}{2}\Big[2\,|1\rangle\langle2|\,\rho\,|2\rangle\langle1| - \rho\,|2\rangle\langle2| - |2\rangle\langle2|\,\rho\Big] . \tag{3.24}$$

The interaction Hamiltonian H_{I} is the same as in Eq. (3.9). In order to predict the time evolution of the population in the controlled subspace, we derive again a closed system of rate equations. The time derivative of the expectation value of an operator A is now given by

$$\frac{\mathrm{d}}{\mathrm{d}t}\langle A\rangle = \mathrm{Tr}\,(A\dot{\rho}) . \tag{3.25}$$

Figure 3.9: Time dependence of P_0 for the level scheme shown in Fig. 3.8(b) for $\Gamma = \Omega$ and different ratios of Ω/ξ. On average, the protection of the controlled subspace is more or less the same as in Fig. 3.4 which corresponds to the same level scheme but with $\Gamma = 0$ (cf. Fig. 3.3(a)).

Taking this into account, we find that the Gell Mann matrices in Eq. (3.10) evolve according to

$$
\frac{\mathrm{d}}{\mathrm{d}t}
\begin{pmatrix}
\langle \sigma_2 \rangle \\
\langle \sigma_3 \rangle \\
\langle \sigma_4 \rangle \\
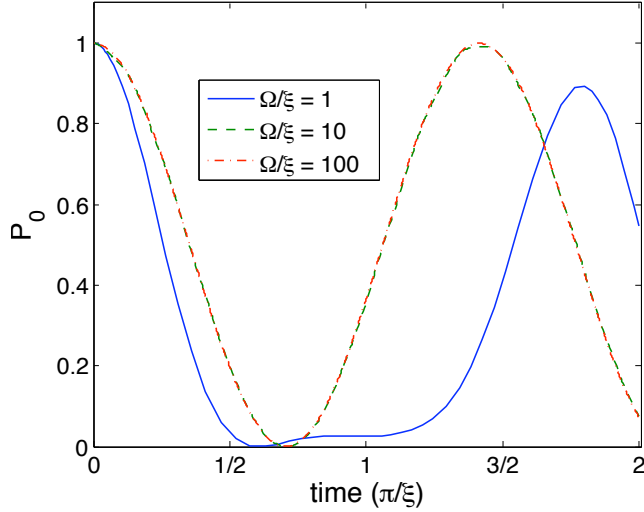\langle \sigma_7 \rangle \\
\langle \sigma_8 \rangle
\end{pmatrix}
=
\begin{pmatrix}
0 & -2\xi & -\Omega & 0 & 0 \\
2\xi & 0 & 0 & -\Omega & \frac{1}{\sqrt{3}}\Gamma \\
\Omega & 0 & -\frac{1}{2}\Gamma & -\xi & 0 \\
0 & \Omega & \xi & -\frac{1}{2}\Gamma & -\sqrt{3}\Omega \\
0 & 0 & 0 & \sqrt{3}\Omega & -3\Gamma
\end{pmatrix}
\begin{pmatrix}
\langle \sigma_2 \rangle \\
\langle \sigma_3 \rangle \\
\langle \sigma_4 \rangle \\
\langle \sigma_7 \rangle \\
\langle \sigma_8 \rangle
\end{pmatrix}
+
\begin{pmatrix}
0 \\
-\frac{1}{3}\Gamma \\
0 \\
0 \\
\sqrt{3}\Gamma
\end{pmatrix}.
$$

(3.26)

These equations resemble the ones shown in Eq. (3.11). The additional Γ terms take the effect of dissipation into account.

The population in the controlled subspace can be obtained by substituting for example the numerical solution of these equations into Eq. (3.12). The result is shown in Fig. 3.9. For simplicity we assumed $\Gamma = \Omega$. For $\Omega = 0$, we see again the Rabi oscillations of the unprotected case. However, when Ω becomes sufficiently larger than ξ, then the system remains to a very good approximation in its initial

state. On average, the protection of the controlled subspace is more or less the same as in Section 3.3.1, where we had $\Gamma = 0$ (cf. Fig. 3.4). There seems to be no advantage of having a non-zero spontaneous decay rate in the system! Notice that having $\Gamma \neq 0$ in the level scheme in Fig. 3.8(b) is only advantageous when someone actually observes whether the system emits photons or not. Indeed, one can show that the system remains in its initial state $|0\rangle$ with a very high fidelity under the condition of *no* photon emission [107]. If a photon emission is detected, then the system has left the controlled subspace and the anticipated control experiment needs to be restarted.

Comparing the level scheme in Fig. 3.8(b) with the level scheme analysed in Refs. [107, 62, 108], we see that its dynamics exhibits so-called macroscopic light and dark periods. Indeed, for ξ much smaller than Ω and Γ, the initial state $|0\rangle$ is an approximate zero eigenstate of the system dynamics. The absence of photon emissions hence confirms that the system is in this state. As a consequence of the quantum Zeno effect, it therefore remains there for a relatively long time. On average, this time equals $\Omega^2 / \Gamma \xi^2$ which is much larger than $1/\xi$ [107]. In other words, the system exhibits a macroscopic dark period. The system may eventually drop out of the controlled subspace, thereby entering a so-called macroscopic light period and causing fluorescence at a rate which depends on Ω and Γ. This behaviour is not reflected in Fig. 3.9, since the density matrix description used here does not allow us to distinguish the different trajectories of the system.

3.4.2 Single-state outside

Let us now have a look at the simple level configuration in Fig. 3.8(a). Its time evolution is given by the master equation

$$\dot{\rho} = -\frac{\mathrm{i}}{\hbar} [H_{\mathrm{I}}, \rho] + \frac{\Gamma}{2} \Big[2 |0\rangle\langle 1| \rho |1\rangle\langle 0| - \rho |1\rangle\langle 1| - |1\rangle\langle 1| \rho \Big]. \tag{3.27}$$

In the interaction picture with respect to the free evolution, the interaction Hamiltonian H_{I} is the same as in Eq. (3.2). To predict the time evolution of P_0 we proceed as
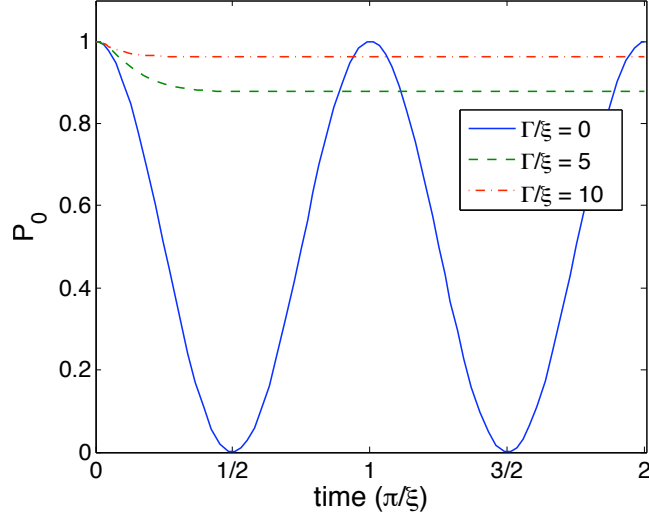
Figure 3.10: Time dependence of P_0 for the level scheme shown in Fig. 3.8(a) for different ratios of Γ/ξ. For $\Gamma \gg \xi$, the system remains in the controlled subspace with a very high fidelity.

in Section 3.2 and consider again the Pauli operators in Eq. (3.3). Their expectation values evolve now according to

$$
\frac{\mathrm{d}}{\mathrm{d}t}
\begin{pmatrix} \langle \sigma_2 \rangle \\ \langle \sigma_3 \rangle \end{pmatrix}
=
\begin{pmatrix} -\frac{1}{2}\Gamma & -2\xi \\ 2\xi & -\Gamma \end{pmatrix}
\begin{pmatrix} \langle \sigma_2 \rangle \\ \langle \sigma_3 \rangle \end{pmatrix}
+
\begin{pmatrix} 0 \\ \Gamma \end{pmatrix} .
\tag{3.28}
$$

Combining the result of this equation with Eq. (3.6) yields the time dependence of the population P_0 in the controlled subspace.

Fig. 3.10 shows a numerical solution of the time dependence of P_0 for different ratios Γ/ξ. For $\Gamma = 0$, we observe the Rabi oscillations in and out of the initial subspace which occur in the unprotected case. For $\Gamma \gg \xi$, the state vector becomes $|0\rangle$ with a very high fidelity. But even for relatively modest values for Γ/ξ, the density matrix ρ settles quickly into a steady state with the system predominantly in $|0\rangle$. The reason for this very strong protection of the controlled subspace is that, even when it leaves, the system returns very rapidly via the spontaneous emission of a photon.
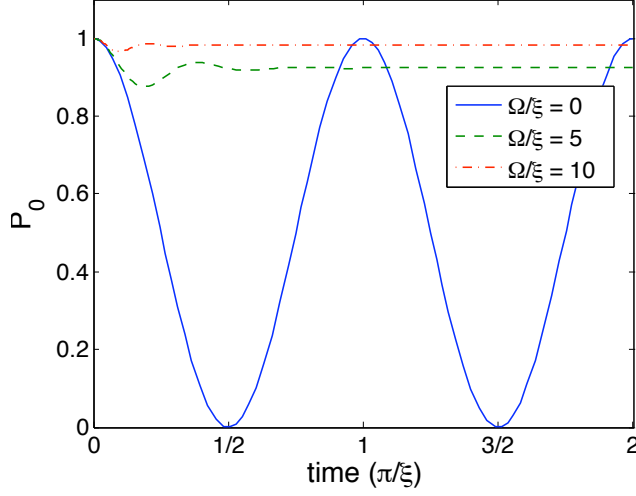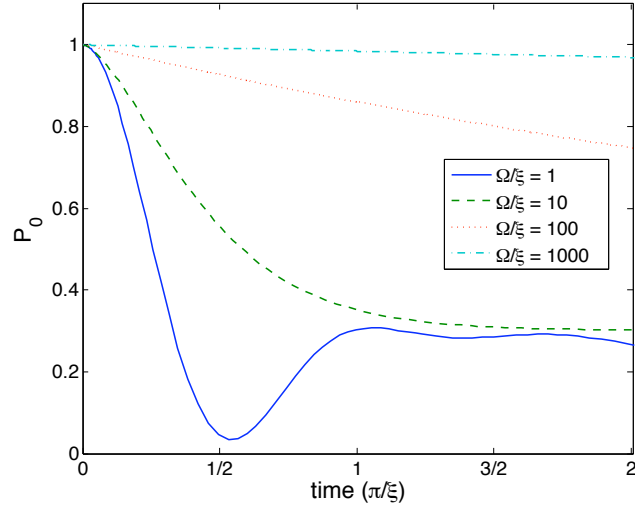
Figure 3.11: Time dependence of P_0 for the level scheme shown in Fig. 3.8(c) for $\Gamma = \Omega$ and different ratios of Ω/ξ. Compared to Fig. 3.5, we now observe an increasing effectiveness of protection of the controlled subspace with increasing values of Ω.

3.4.3 Double-coupling case with dissipation

This final subsection analyses the time evolution of the four-level system shown in Fig. 3.8(c). The only difference to the level scheme in Fig. 3.3(b) is the presence of the non-zero spontaneous decay rate Γ. To calculate the time evolution of the population in the controlled subspace, we now consider the master equation

$$
\begin{aligned}
\dot{\rho} &= -\frac{\mathrm{i}}{\hbar}[\,H_\mathrm{I}, \rho\,] + \frac{\Gamma}{2}\Big[\,2\,|1\rangle\langle 2|\,\rho\,|2\rangle\langle 1| - \rho\,|2\rangle\langle 2| - |2\rangle\langle 2|\,\rho\,\Big] \\
&\quad + \frac{\Gamma}{2}\Big[\,2\,|2\rangle\langle 3|\,\rho\,|3\rangle\langle 2| - \rho\,|3\rangle\langle 3| - |3\rangle\langle 3|\,\rho\,\Big]\,,
\end{aligned}
\tag{3.29}
$$

whose interaction Hamiltonian H_I can be found in Eq. (3.16). Proceeding as above, we find that the time evolution of the Gell Mann matrices (3.17) is now given by

53

the differential equations

$$\frac{\mathrm{d}}{\mathrm{d}t} \left(\langle\sigma_2\rangle, \langle\sigma_3\rangle, \langle\sigma_4\rangle, \langle\sigma_7\rangle, \langle\sigma_8\rangle, \langle\sigma_{10}\rangle, \langle\sigma_{11}\rangle, \langle\sigma_{14}\rangle, \langle\sigma_{15}\rangle \right)^{\mathrm{T}}$$

$$= M \left(\langle\sigma_2\rangle, \langle\sigma_3\rangle, \langle\sigma_4\rangle, \langle\sigma_7\rangle, \langle\sigma_8\rangle, \langle\sigma_{10}\rangle, \langle\sigma_{11}\rangle, \langle\sigma_{14}\rangle, \langle\sigma_{15}\rangle \right)^{\mathrm{T}}$$

$$+ \left(0, -\frac{1}{4}\Gamma, 0, 0, \frac{1}{4\sqrt{3}}\Gamma, 0, 0, 0, \frac{1}{\sqrt{6}}\Gamma \right)^{\mathrm{T}} \tag{3.30}$$

with

$$M = \begin{pmatrix}
0 & -2\xi & -\Omega & 0 & 0 & 0 & 0 & 0 & 0 \\
2\xi & 0 & 0 & -\Omega & \frac{1}{\sqrt{3}}\Gamma & 0 & 0 & 0 & -\frac{1}{2\sqrt{6}}\Gamma \\
\Omega & 0 & -\frac{1}{2}\Gamma & -\xi & 0 & \Omega & 0 & 0 & 0 \\
0 & \Omega & \xi & -\frac{1}{2}\Gamma & -\sqrt{3}\Omega & 0 & -\Omega & 0 & 0 \\
0 & 0 & 0 & \sqrt{3}\Omega & -\Gamma & 0 & 0 & -\frac{2}{\sqrt{3}}\Omega & \frac{3}{2\sqrt{2}}\Gamma \\
0 & 0 & -\Omega & 0 & 0 & -\frac{1}{2}\Gamma & \xi & 0 & 0 \\
0 & 0 & 0 & \Omega & 0 & -\xi & -\frac{1}{2}\Gamma & -\Omega & 0 \\
0 & 0 & 0 & 0 & \frac{2}{\sqrt{3}}\Omega & 0 & \Omega & -\Gamma & -\frac{2\sqrt{2}}{\sqrt{3}}\Omega \\
0 & 0 & 0 & 0 & 0 & 0 & 0 & \frac{2\sqrt{2}}{\sqrt{3}}\Omega & -\Gamma
\end{pmatrix} \tag{3.31}$$

Fig. 3.11 shows the time dependence of P_0 for the case where the system is initially in the controlled subspace and has been obtained by substituting the numerical solution of these equations into Eq. (3.21).

Comparing Figs. 3.5 and 3.11, we see that the presence of a sufficiently large spontaneous decay rate Γ combined with the presence of a relatively large coupling constant Ω now results in an effective protection of the controlled subspace against leakage errors. There are different ways of seeing how this protection (which was not there before) has been achieved. One way is to have a closer look at the above master equation and to notice that the state $|\lambda_0\rangle$ is no longer a zero eigenstate of the system dynamics. Whenever population accumulates in this state, the system returns (either via the emission of a photon or as a result of its no-photon evolution) on the time scale given by Γ into $|1\rangle$, where it experiences fast driving with Ω.
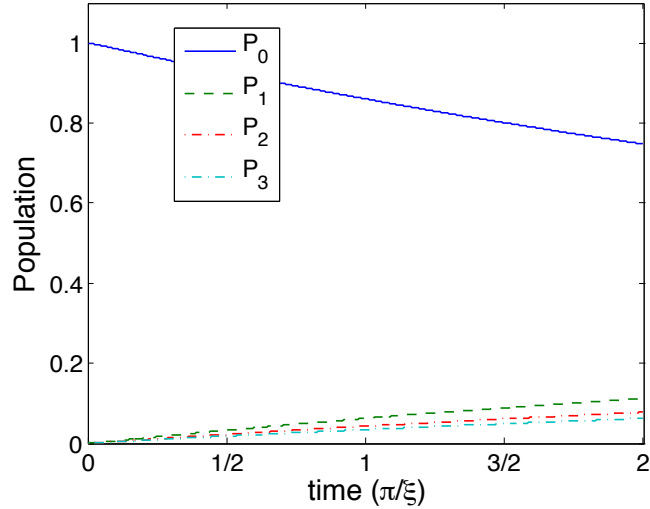
Figure 3.12: Time dependence of all four states of the level scheme shown in Fig. 3.8(c) for $\Gamma = \Omega$ and a ratios of $\Omega/\xi = 100$. Compared to Fig. 3.6, we now observe the effectiveness of protection of the controlled subspace as the $|1\rangle$ and $|3\rangle$ states no longer become populated rapidly.

Fig. 3.12 shows the effect of this on the populations of all four states of the system for a ratio of $\Omega/\xi = 100$. It is obvious in this figure that the dark state that was clearly still populated in Fig. 3.6 is now also eliminated. This example confirms that dissipation can provide a very efficient tool for restricting the time evolution of a system onto a controlled subspace.

Another way to gain an intuition into the behaviour of the level scheme in Fig. 3.8(c) is to compare it to the level scheme in Fig. 3.8(b) which we analysed in Section 3.4.1. Observing whether the system emits photons or not, one would notice again two very distinct phases of operation. The system either emits photons at a high rate or it remains dark for a relatively long time. A macroscopic light period, on one hand, indicates that the state vector lies entirely outside the controlled subspace. A macroscopic dark period, on the other hand, indicates that the system is in $|0\rangle$. In other words, if the system is initially in the controlled subspace, it remains there on average much longer than in the unprotected case. The result is the protection of the system against leakage errors which, when they occur, are heralded by an easy-to-detect fluorescence signal.

55

3.5   Summary

This chapter illustrates two methods to protect a controlled subspace against the leakage of population into the outside space: one using strong interactions in the outside space and one using dissipation. This is done with the help of relatively simple toy models whose time evolution can be analysed relatively easily. For simplicity, we assume that the controlled subspace consists only of one state, namely $|0\rangle$. The outside space contains either one, two or three states denoted $|1\rangle$, $|2\rangle$, and $|3\rangle$ (cf. Figs. 3.3 and 3.8). Section 3.2 discusses the unprotected case and shows that unwanted transitions from $|0\rangle$ to $|1\rangle$ (due to resonant coupling) occur on a time scale given by a relatively small parameter ξ (cf. Fig. 3.2).

In Section 3.3, the decoherence time of the system is increased to one which scales as ξ^2 by applying relatively fast interactions with coupling strength Ω to the outside space. However, these strong interactions are not always sufficient for protecting a controlled subspace against leakage errors. While it works well for the level scheme shown in Fig. 3.3(a), no protection occurs for the level scheme shown in Fig. 3.3(b). The reason is the existence of an approximate zero eigenstate outside the controlled subspace. This state does not experience fast driving and therefore behaves as the state $|1\rangle$ in the unprotected case.

Section 3.4 considers three scenarios where a spontaneous decay rate Γ has been added to the level schemes analysed in Sections 3.2 and 3.3. All the level schemes shown in Fig. 3.8 exhibit a strong protection of the controlled subspace. One way to understand the mechanism which inhibits the population transfer out of the controlled subspace is to interpret the behaviour of the system in terms of the quantum Zeno effect [77, 78, 79]. Suppose being outside the controlled subspace results necessarily in the spontaneous emission of a photon. Then, observing whether a photon emission takes place or not is equivalent to performing a measurement on whether the system is in the controlled subspace or not. If these measurements occur on a sufficiently short time scale, then a system initially in the controlled subspace remains there much longer than in an unobserved case. A similar interpretation ap-

plies to the protection of the controlled subspace with a strong interaction illustrated in Fig. 3.3(a) [104, 105].

For the purposes of the remainder of this thesis, a further aspect should be remarked upon. The suppression of decoherence as described in this chapter in general results in an effective time evolution which can be described by an effective Hamiltonian [96, 74, 100, 109]

$$H_{\text{eff}} \quad = \quad \mathbf{P}_{\text{CS}}\, H\, \mathbf{P}_{\text{CS}}\,, \tag{3.32}$$

where $\mathbf{P}_{\text{CS}}$ denotes the projector onto the controlled subspace and H is the total system Hamiltonian. Once the protection is in place, the interactions contained in H_{eff} can be tailored to a desirable control task. In quantum information processing, applications of this technique could be on preparation of entangled states or more general gate operations. Our particular use of it relates to the former.

Chapter 4

Reservoir Engineering

4.1 Introduction

The previous two chapters have both been focused on developing the theoretical tools we require for this one. We now turn to the task of applying this to cavity QED systems that can be used to perform useful quantum information processing tasks. The motivation for us here thus comes from limitations of current experiments with optical cavities. Recent progress in experiments with these optical cavities has mainly been motivated by potential applications in quantum information processing. These applications often require the simultaneous trapping of at least two atomic qubits inside a single resonator field mode. It has been shown that the common coupling to a quantised mode can be used to implement quantum gate operations [110, 100, 111, 101, 112] and the controlled generation of entanglement [113, 94, 114, 51, 115]. However, the practical realisation of these schemes with current technologies is experimentally challenging. The reason is that strong atom-cavity interactions require relatively small mode volumes and high quality mirrors; aims that are difficult to reconcile with the placement of several atoms or ions into the same cavity.

To solve this problem, it has been proposed to couple distant cavities via linear optics networks [116, 117, 12]. Under realistic conditions, this strategy allows at least

for the probabilistic build up of highly entangled states. Alternatively, atoms can be shuttled successively in and out of the resonator [118, 119, 120]. In this chapter we propose another alternative which uses fibre-coupled cavities. The basic idea is to employ reservoir engineering based on the reservoir manipulation that can be derived from the methods in chapter 2 and control techniques of chapter 3 to make two cavities behave effectively as one. Quantum computing schemes designed for several qubits placed into the same resonator can, using this reservoir engineering, be applied to a much wider range of experimental scenarios. Such schemes are no longer restricted to atomic qubits but can also be implemented with quantum dots [121, 122], NV color centers [123, 124], and superconducting flux qubits [45]. Another possible application of the two fibre-coupled optical cavities described here could be the transfer of quantum information from one cavity to another which means performing a SWAP operation between two qubits coupled to a common field mode [125, 57, 58].

This chapter is organised into five sections. The first details the basic idea behind reservoir engineering to turn two coupled cavities effectively into a single common cavity mode. This includes a derivation of the single mode behaviour that we later recreate. The second and third section detail two proposals for the actual reservoir engineering using interference on detector screens and direct fibre coupling respectively. Section 4.3.3 describes two different scenarios for the fibre-coupling scheme where one of the common modes decouples effectively from the system dynamics with one of them being especially robust against parameter fluctuations. Finally the findings are summarised in section 4.5.

4.2 Basic Idea

The basic goal of this chapter is to demonstrate how one can engineer a system of two cavities that, through some coupling between them, behave as though they have only a single common cavity mode between them. In this section, we outline the theoretical framework for how two coupled cavities may be described by common

cavity modes such that the elimination of one of these results in a single common cavity mode. Then, to give a blueprint for what the dynamics of a single cavity mode actually looks like, we present in this section a description of a single cavity coupled to a reservoir and driven continuously by a resonant laser. This analysis is simply the derivation of chapter 2 without the presence of an atom in the cavity.

4.2.1 Reservoir Engineering

The effect of the reservoir engineering described in this chapter should be to have two qubits placed into the two cavities behave as though they where in the same cavity. This means, there should exist a single common cavity mode that has a component in both of the physical cavities. We should begin with a closer look at the creation of a non-local cavity field mode via reservoir engineering from a more quantum optical point of view. First we point out that given two cavities with fixed polarisation, there are two quantised cavity field modes. For example, one could describe the setup using the individual cavity modes with annihilation operators c_1 and c_2. But there is also the possibility of describing the cavities by two common (i.e. non-local) field modes. Their cavity photon annihilation operators are of the general form

$$
\begin{aligned}
c_a &= \frac{1}{\xi} \left(\xi_2^* \, c_1 - \xi_1^* \, c_2 \right) , \\
c_b &= \frac{1}{\xi} \left(\xi_1 \, c_1 + \xi_2 \, c_2 \right) ,
\end{aligned}
\tag{4.1}
$$

where ξ_1 and ξ_2 are complex coefficients and

$$
\xi \equiv \sqrt{|\xi_1|^2 + |\xi_2|^2} \, .
\tag{4.2}
$$

One can easily check that, if c_1 and c_2 obey the usual boson commutator relations for independent field modes, then so do c_a and c_b, i.e.

$$
[\, c_a, c_a^\dagger \,] = [\, c_b, c_b^\dagger \,] \;\; = \;\; 1 \;\; \text{and} \;\; [\, c_a, c_b^\dagger \,] = 0 \, .
\tag{4.3}
$$

In general, an atomic qubit placed into one of the two cavities interacts simultaneously with the c_a and with the c_b mode, since both are non-local.

The next step in generating an effective single cavity is to eliminate one of the two common modes from the dynamics of the system. To do this, we first have to separate the evolution of these two common modes. This can be done by getting the two common modes to couple to different reservoir modes. In this chapter we will describe two alternative ways of achieving this coupling. One of these methods is considered the more experimentally realisable so most of this chapter will be devoted to the details of this scheme. The other method will be presented as an alternative in the final section of this chapter.

For both of these methods, the next step is to eliminate one of the common modes from the system dynamics. As is suggested by the analysis in chapter 3 and as we shall see below in this chapter, if one of the two common cavity modes experiences a much stronger coupling to the environment than the other one and is hence damped away by a much larger spontaneous decay rate, it effectively decouples from the system dynamics. By separating the reservoir for the two common cavity modes, it is possible to give them different decay rates. The details of how this is achieved varies between the two implementations and will be described for each of them individually. We now move on to defining the dynamics of a single cavity mode as the blueprint for what we are trying to engineer out of two cavities.

4.2.2   A single cavity in a reservoir

As stated above, the system we consider here is the same as that of chapter 2 without the atoms, as shown in Fig. 4.1. There is no need to rehash the full derivation so we will simply state the useful results of this derivation here. The non-interacting parts of the Hamiltonian describing the cavity system are

$$H_0 = H_{\text{cavity}} + H_{\text{field}} \,, \tag{4.4}$$
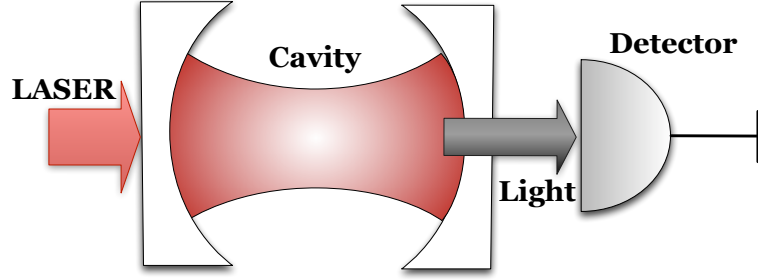
Figure 4.1: Experimental setup of a single cavity driven by a laser field. The photons leaking out through the cavity mirrors are monitored by a detector.

where

$$
\begin{aligned}
H_{\text{cavity}} &= \hbar\omega_c c^\dagger c \ \text{ and} \\
H_{\text{field}} &= \sum_{\mathbf{k}\lambda} \hbar\omega_k a^\dagger_{\mathbf{k}\lambda} a_{\mathbf{k}\lambda} \,,
\end{aligned}
\tag{4.5}
$$

with all notation having the same meaning as in chapter 2. The Hamiltonian in an interaction picture with respect to this H_0 is

$$
H_{\text{I}} = \frac{1}{2}\hbar\left(\Omega\, c + \Omega^* \, c^\dagger\right) + \sum_k \hbar\left(g_{\mathbf{k}\lambda}\, \mathrm{e}^{\mathrm{i}(\omega_k-\omega_c)t}\, c a^\dagger_{\mathbf{k}\lambda} + g^*_{\mathbf{k}\lambda}\, \mathrm{e}^{-\mathrm{i}(\omega_k-\omega_c)t}\, c^\dagger a_{\mathbf{k}\lambda}\right) \,, \tag{4.6}
$$

where the laser driving of frequency Ω is now on the cavity mode rather than the atomic driving of chapter 2. From here on, we assume that the polarisation of the laser is fixed and not altered anywhere in the system such that there is only one polarisation of light present and the λ subscript can be dropped.

Proceeding as in chapter 2, the conditional Hamiltonian and reset operator for this system can be derived. The conditional Hamiltonian describing the time evolution when no photon is emitted by the cavity is

$$
H_{\text{cond}} = \frac{1}{2}\hbar\left(\Omega c + \Omega^* c^\dagger\right) - \frac{\mathrm{i}}{2}\hbar\kappa c^\dagger c \,, \tag{4.7}
$$

where the cavity decay rate κ is the same as in Eq. 2.46. The reset operator describ-

ing the event of a photon emission from the cavity is

$$R_c = \sqrt{\kappa} c \, . \tag{4.8}$$

Inserting these into the master equation definition of Eq. 2.37 gives the master equation

$$\dot{\rho} = -\frac{i}{\hbar} \left[H_{\text{cond}} \rho - \rho H_{\text{cond}}^\dagger \right] + R \rho R^\dagger \, . \tag{4.9}$$

This is the standard master equation for the quantum optical description of the field inside an optical cavity. The only assumption made in the derivation of this equation is that the environment constantly absorbs photons from the free radiation field on a time scale Δt so that, once emitted, they cannot re-enter the cavity field.

If we are for example interested in the time evolution of the mean number of photons n inside the cavity, then there is no need to solve the whole master equation (4.9). Instead, we use this equation to get a closed set of rate equations with n being one of its variables. More concretely, considering the expectation values

$$
\begin{aligned}
n &\equiv \langle c^\dagger c \rangle \, , \\
k &\equiv \frac{i}{|\Omega|} \langle \Omega c - \Omega^* c^\dagger \rangle \, ,
\end{aligned}
\tag{4.10}
$$

we find that their time evolution is given by a closed set of differential equations,

$$
\begin{aligned}
\dot{n} &= \frac{1}{2} |\Omega| \, k - \kappa \, n \, , \\
\dot{k} &= |\Omega| - \frac{1}{2} \kappa \, k \, .
\end{aligned}
\tag{4.11}
$$

Setting the right hand sides of these equations equal to zero, we find that the stationary state of the laser-driven cavity corresponds to $n = |\Omega|^2 / \kappa^2$. Since the steady state photon emission rate is the product of n with the decay rate κ, this yields

$$I = |\Omega|^2 / \kappa \, . \tag{4.12}$$

Measurements of the parameter dependence of this intensity can be used to determine $|\Omega|$ and κ experimentally and to verify single-mode behaviour.

4.2.3 Outlook for two cavities

The general extension of the description above to two cavities is also fairly straightforward. The starting non-interacting Hamiltonian now has a cavity component given by

$$H_{\text{cavity}} = \sum_{i=1,2} \hbar\omega_c c_i^\dagger c_i \,, \tag{4.13}$$

where we assume that the two cavities are as identical as possible and share the same frequency ω_c. The significant difference comes in the parts of the interacting Hamiltonian describing the cavity-reservoir interaction. These terms now depend on the form of the reservoir. The goal we are aiming towards is that the final conditional Hamiltonian takes the form

$$H_{\text{cond}} = \frac{1}{2}\hbar \sum_{i=1,2} \left(\Omega_i c_i + \Omega_i^* c_i^\dagger \right) - \frac{\text{i}}{2}\hbar\kappa_a c_a^\dagger c_a - \frac{\text{i}}{2}\hbar\kappa_b c_b^\dagger c_b \,, \tag{4.14}$$

where $c_{i=1,2}$ are the annihilation operators for cavity modes of cavities 1 and 2 and $c_{i=a,b}$ are these modes written in a common mode basis as in Eq. 4.1. The separate decay terms for the two common modes are the essential feature of this Hamiltonian. They also correspond to two separate reset operators

$$R_a = \sqrt{\kappa_a}c_a \quad \text{and} \quad R_b = \sqrt{\kappa_b}c_b \tag{4.15}$$

that describe the emission of photons from the two common modes. It is this feature that we use reservoir engineering to create. Setting the condition

$$\kappa_b \quad \gg \quad \kappa_a\,, \Omega_i \,, \tag{4.16}$$

where κ_a is the relevant decay rate of the c_a mode, κ_b is the decay rate of c_b and Ω_i represents relevant system dynamics such as laser driving frequency; the c_b mode can be eliminated by overdamping. Following this elimination, the effective conditional Hamiltonian for the two cavity system becomes

$$H_{\text{eff}} = \frac{1}{2}\hbar\left(\Omega_a c_a + \Omega_a^* c_a^\dagger\right) - \frac{\mathrm{i}}{2}\hbar\kappa_a c_a^\dagger c_a\,, \tag{4.17}$$

where Ω_a is a combination of Ω_1 and Ω_2. This Hamiltonian is identical to that for a single cavity in Eq. 4.7 indicating that this two cavity system now behaves as a single mode cavity.

In the following, we show the two methods for arranging a reservoir that produces the desired Hamiltonian description.

4.3 Reservoir Engineering with a Single Fibre

The first method we describe for separating the common cavity modes is to use a single-mode fibre directly connecting the two cavities, as shown in Fig. 4.2. The idea is that the fibre creates a reservoir which only one common cavity mode can couple to. Given the boundary conditions imposed where the fibre couples to the cavities at either end, a quantisation condition is imposed on the modes of the fibre. This condition restricts the fibre mode to only coupling to one of the common cavity modes and not the orthogonal one. One way to understand this is that populations from the individual cavities c_1 and c_2 coupling into the fibre interfere constructively if they are in one common cavity mode and destructively if they are in the other.

Fibre coupled optical cavities, as proposed here, with applications in quantum information processing have already been widely discussed in the literature (see e.g. Refs. [59, 126, 57, 58, 125, 127]). The main difference of the cavity coupling scheme presented here is that it does not rely on coherent time evolution. Instead it actively uses dissipation in order to achieve its task. We therefore expect that the proposed scheme is more robust against errors. For example, the fibre considered
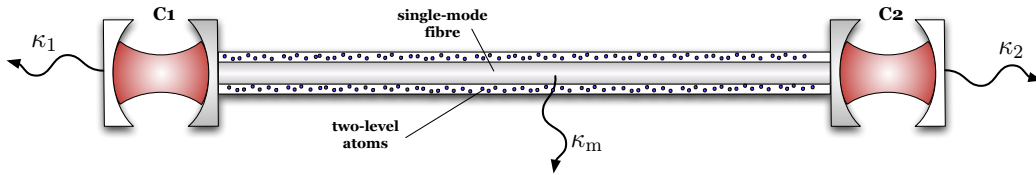
Figure 4.2: Experimental setup of two optical cavities coupled via a single-mode fibre. Photons can leak out through the outer mirrors with the spontaneous decay rate κ_1 and κ_2, respectively. The connection between both cavities constitutes a third reservoir with spontaneous decay rate κ_m for a common non-local resonator field mode.

here which is coated with two-level atoms acts as a reservoir for the cavity photons and supports a more continuous range of frequencies than should be allowed for the cavity description employed in Refs. [59, 126, 57, 58]. We also expect that the setup considered here is more robust against fibre losses [125, 127].

In this scheme, all the detail of the reservoir engineering is in the behaviour of the single mode fibre that connects the two cavities. For this reason, we will completely derive the master equation for this system using the methodology of chapter 2.

4.3.1 Experimental Setup and Basic Idea

The experimental setup proposed in this section consists of two cavities with the same frequency ω_{cav}. As illustrated in Fig. 4.2, the cavities should be coupled via an optical single-mode fibre which is coated with two-level atoms. There are three separate spontaneous decay channels in the system. Both cavities emit photons into adjacent reservoirs through an outcoupling mirror - in the following, we denote the corresponding decay rates for this by κ_1 and κ_2. In addition, light can leak into the optical fibre. The purpose of the coating of atoms on this fibre is to measure the evanescent electric field of the fibre destructively. In other words, the optical fibre with atomic coating constitutes an additional reservoir for the cavity photons with κ_m denoting the respective decay rate. As above, we are aiming to separate two orthogonal common modes by giving them very different decay rates. However, for this scheme, it is convenient to stipulate this difference in decay rates from the beginning. Thus, we are here especially interested in the parameter regime, where

κ_m is much larger than κ_1 and κ_2 as well as being much larger than any other coupling constants, like the laser driving frequencies Ω_1 and Ω_2 of applied laser fields, i.e.

$$\kappa_\mathrm{m} \quad \gg \quad \kappa_i, \Omega_i. \qquad (4.18)$$

Most importantly, the decay channel provided by the optical fibre should not be seen by all cavity photons but only by some of them, since the aim of this section is to create a setup where two common cavity modes have very different spontaneous decay rates.

To achieve this, we pose several conditions on the optical fibre coupling illustrated in Fig. 4.2:

1. Different from Ref. [59, 126], we do not treat the fibre between the cavities as a resonant cavity. Instead, we consider a fibre which supports a standing wave field with a broadened optical frequency due to the width of the fibre, the imperfection of the mirrors and the presence of atoms around the fibre [128]. Our description is thus of a continuum of field modes with frequencies which include the cavity frequency ω_cav.

2. In addition, the frequency range supported by the fibre should not be too broad. More concretely, the fibre needs to be short and thin enough to have a well defined optical path length for each frequency supported by the fibre. At the optical frequency ω_cav, there should be only one standing wave which fulfils the boundary condition of vanishing electric field amplitudes at the surface of the adjacent cavity mirrors. Waves which are half a wave length λ_cav shorter or longer should not fit into the fibre.

3. The purpose of the atoms which surround the optical single-mode fibre is similar to their purpose in Ref. [129] by Franson *et al.*, namely to measure evanescent electric field modes. In the following, we assume that the atoms have a transition frequency ω_0 which is relatively close to the frequency ω_cav of

the resonators and a sufficiently large spontaneous decay rate Γ. This means, the atoms can absorb light traveling through the fibre and dispose of it via spontaneous emission into the environment.

4. The atoms should measure electric field amplitudes on a time scale which is long compared to the time it takes a photon to travel from one resonator to the other. In this way, the atoms measure only relatively long living photons inside the fibre, i.e. the field amplitudes of the electromagnetic standing waves with vanishing amplitudes at the fibre ends, and cannot gain information about the source of a photon.

5. At the same time we assume that the environment-induced photon measurements on the fibre photons occur on a much shorter time scale than the measurement in the reservoir outside the outcoupling mirrors in order to assure that Eq. (4.18) holds, i.e. κ_{m} is indeed much larger than κ_1 and κ_2.

Suppose there is initially only one photon in cavity 1 and none in cavity 2. In this case, some light will travel from cavity 1 to cavity 2. However, when there is excitation in both cavities, some of the light can no longer leave its respective cavity, since it does not couple to the standing wave light mode inside the fibre with vanishing amplitudes at the fibre ends. However, other waves leak more easily into the fibre, since their efforts are met by waves with the same amplitude coming from the other side. The above conditions assume that the photons are measured on a relatively slow time scale and that the atoms in the evanescent field of the fibre cannot distinguish photons traveling left or right. They are therefore only able to absorb light from the standing waves which can exist inside the fibre for a relatively long time. In the specific example discussed in this paragraph, there is a probability $\frac{1}{2}$ that the initial photon remains inside the setup and another probability $\frac{1}{2}$ that it gets absorbed.

Although this chapter mainly makes reference to optical cavities and single-mode fibre connection, any implementation which meets the above requirements would work equally well. For example, a specific alternative to coupling the cavities with
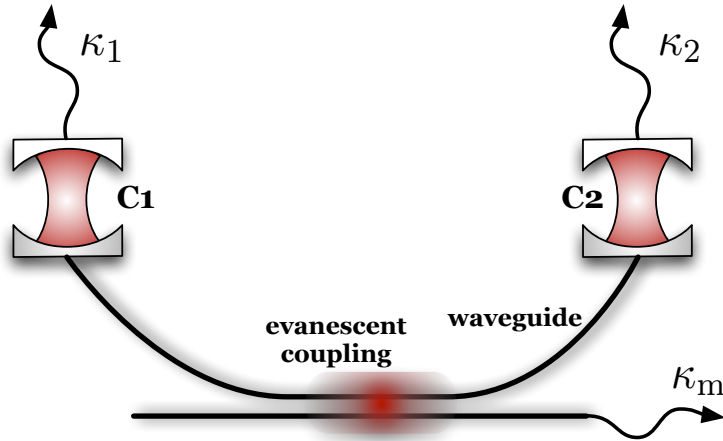
Figure 4.3: Schematic view of an alternative experimental setup. If the cavities are mounted on an atom chip, the could be coupled via a waveguide etched onto the chip. To emulate environment-induced measurements of the field amplitude within the waveguide, a second waveguide should be placed into its evanescent field which constantly damps away any eletromagnetic field amplitudes.

an optical single-mode fibre (c.f. Fig. 4.2) is shown in Fig. 4.3. If the cavities are mounted on an atom chip, a similar connection between them could be created with the help of a waveguide etched onto the chip. Such a connection too supports only a single electromagnetic field mode. To detect its field amplitude, a second waveguide connected to a detector should be placed into its evanescent field, thereby constantly removing any field amplitude from the nanowire between the cavities.

4.3.2 Open system approach for two laser-driven fibre-coupled cavities

In this section, we derive the master equation for the two fibre-coupled optical cavities shown in Fig. 4.2. We proceed as in the single cavity section 4.2.2 and first present the equations which describe the no-photon time evolution of the cavities. To obtain the master equation, we average again over a subensemble with and a subensemble without photon emission. A discussion of the behaviour predicted by this equation for certain interesting parameter regimes can be found later in Section 4.3.3.

70

System Hamiltonian

The experimental setup considered in this section contains two optical cavities coupled via an optical single-mode fibre or a waveguide (c.f. Figs. 4.2 and 4.3). The total system Hamiltonian H in the Schrödinger picture is of exactly the same form as the Hamiltonian in section 4.2.2. Again, H_{cav} and H_{res} denote the energy of the system and its reservoirs, while H_{dip} models the cavity-environment couplings and the effect of applied laser fields. In the following, we denote the annihilation operators of the two cavities by c_1 and c_2, respectively, while

$$\omega_{\text{c},1} = \omega_{\text{c},2} = \omega_{\text{cav}} \tag{4.19}$$

is the corresponding frequency which should be for both cavities the same. The energy of the resonators is hence given by

$$H_{\text{cav}} = \sum_{i=1,2} \hbar\omega_{\text{cav}}\, c_i^\dagger c_i \,. \tag{4.20}$$

The reservoir of the system now consists of three components. Its Hamiltonian can be written as

$$H_{\text{res}} = \sum_{i=1,2}\sum_k \hbar\omega_k\, a_{k,i}^\dagger a_{k,i} + \sum_k \hbar\omega_k\, b_k^\dagger b_k \,, \tag{4.21}$$

where ω_k denotes the frequency of the free field radiation modes with wavenumber k. The annihilation operators $a_{k,i}$ describe the free radiation field modes on the unconnected side of each cavity with k being the respective wavenumber and i indicating which cavity the field interacts with. The annihilation operators b_k describe the continuum of quantised light modes of the central waveguide on the connected side of both cavities with vanishing electric field amplitudes at the fibre ends. For each wave number k, these modes correspond to a single standing light wave with contributions traveling in different directions through the fibre. As in the previous section, we restrict ourselves to the polarisation of the applied laser field. Since there

is no mode mixing, this is the only polarisation which needs to be considered which is why the index λ has been omitted.

The only term still missing is the interaction Hamiltonian H_{dip} which describes the coupling of the two cavities to any laser fields present and to their respective reservoirs. We add two lasers in Fig. 4.2 that drive both of the cavities from the outside. Assuming that both of these lasers are in resonance with the cavity fields and applying the usual dipole and rotating wave approximation, H_{dip} can in analogy to Eq. (4) in Ref. [57], be written as

$$
\begin{aligned}
H_{\mathrm{dip}} \;=\; & \sum_{i=1,2} \sum_{k} \hbar s_{k,i}\, c_i a_{k,i}^{\dagger} + \hbar g_{k,i}\, c_i b_k^{\dagger} \\
& + \sum_{i=1,2} \frac{1}{2} \hbar \Omega_i \, \mathrm{e}^{-\mathrm{i}\omega_{\mathrm{cav}} t} \, c_i + \mathrm{H.c.}\,,
\end{aligned}
\tag{4.22}
$$

where $s_{k,i}$ and $g_{k,i}$ are system-reservoir coupling constants and where Ω_i is the laser driving frequency (similar to the Rabi frequency for an atomic system) of the laser driving cavity i.

In order to be able to calculate the photon and the no-photon time evolution of the cavities over a time interval Δt with the help of second order perturbation theory, we proceed as in Section 4.2.2 and transform the Hamiltonian H of the system into the interaction picture relative to H_0 in Eq. (4.4). This finally yields

$$
\begin{aligned}
H_{\mathrm{I}} \;=\; & \sum_{i=1,2} \sum_{k} \hbar s_{k,i}\, \mathrm{e}^{\mathrm{i}(\omega_k - \omega_{\mathrm{cav}})t}\, c_i a_{k,i}^{\dagger} \\
& + \hbar g_{k,i}\, \mathrm{e}^{\mathrm{i}(\omega_k - \omega_{\mathrm{cav}})t} c_i b_k^{\dagger} + \frac{1}{2} \hbar \Omega_i \, c_i + \mathrm{H.c.}
\end{aligned}
\tag{4.23}
$$

which describes the interaction of the cavities with their reservoirs and the two lasers.

No-photon time evolution

As in the single-cavity case, we assume that the unconnected mirrors of the res- onators leak photons into free radiation fields, where they are continuously mon-

itored by the environment or actual detectors (cf. Fig. 4.2). In addition, there is now a continuous monitoring of the photons which can leak into the single-mode fibre (or waveguide) connecting both cavities. Again, it is not crucial whether an external observer actually detects these photons or not, as long as the effect on the system is the same as if the photon has actually been measured. Important is only that photons within the three reservoirs, the surrounding free radiation fields and the single-mode fibre, are constantly removed from the system and cannot re-enter the cavities.

In principle, there are now three different response times Δt of the environment, i.e. one for each reservoir. For simplicity and since it does not affect the resulting master equation we consider only one of them. Denoting this response time of the environment again by Δt, we assume in the following that

$$\frac{1}{\omega_{\mathrm{cav}}} \ll \Delta t \;\; \mathrm{and} \;\; \Delta t \ll \frac{1}{\kappa_{\mathrm{m}}}, \, \frac{1}{\kappa_1}, \, \frac{1}{\kappa_2} \,, \tag{4.24}$$

where κ_{m} is a characteristic spontaneous decay rate for the leakage of photons from the cavities into the optical fibre (or waveguide), while κ_i denotes the decay rate of cavity i with respect to its outcoupling mirror. This condition allows us to proceed as in section 4.2.2 and to calculate the time evolution of the system within a time interval Δt using second order perturbation theory. The first condition in Eq. (4.24) assures that there is sufficient time between measurements for photon population to build up within the reservoirs (otherwise, there would not be any spontaneous emissions). This is also consistent with the fast decay of any system-environment correlations which provide a lower bound for Δt. The second condition in Eq. (4.24) is necessary to avoid the return of photons from the reservoirs into the cavities.

Proceeding as in the previous section and using again Eq. (2.33), we find that the conditional Hamiltonian describing the time evolution of the two cavities under

73

the condition of no photon emission in Δt into any of the three reservoirs equals

$$
\begin{aligned}
U_{\text{cond}}(\Delta t, 0) = \\
\mathbb{I} - \frac{\text{i}}{2} \sum_{i=1,2} \left(\Omega_i\, c_i + \Omega_i^*\, c_i^\dagger\right)\Delta t \\
- \int_0^{\Delta t} \text{d}t \int_0^t \text{d}t' \sum_{i=1,2} \sum_k \text{e}^{\text{i}(\omega_k - \omega_{\text{cav}})(t'-t)} |s_{k,i}|^2\, c_i^\dagger c_i \\
- \int_0^{\Delta t} \text{d}t \int_0^t \text{d}t' \sum_k \text{e}^{\text{i}(\omega_k - \omega_{\text{cav}})(t'-t)} (g_{k,1}^*\, c_1^\dagger + g_{k,2}^*\, c_2^\dagger) \\
\times (g_{k,1}\, c_1 + g_{k,2}\, c_2).
\end{aligned} \tag{4.25}
$$

The first three terms of this evaluate to

$$
\begin{aligned}
\mathbb{I} - \frac{\text{i}}{2} \sum_{i=1,2} \left(\Omega_i\, c_i + \Omega_i^*\, c_i^\dagger\right)\Delta t \\
- \frac{1}{2}\kappa_1 \Delta t\, c_1^\dagger c_1 - \frac{1}{2}\kappa_2 \Delta t\, c_2^\dagger c_2.
\end{aligned} \tag{4.26}
$$

Using exactly the same approximations as described in detail in chapter 2 and the notation

$$
\xi_i \equiv \sum_k g_{k,i} \tag{4.27}
$$

with ξ defined as in Eq. (4.2), the final term in Eq. (4.25) can be written as

$$
-\frac{1}{2\xi^2}\kappa_{\text{m}}\Delta t \left(\xi_1^*\, c_1^\dagger + \xi_2^*\, c_2^\dagger\right)\left(\xi_1\, c_1 + \xi_2\, c_2\right). \tag{4.28}
$$

Here κ_1, κ_2, and κ_{m} are the spontaneous decay rates already mentioned in Eq. (4.24). The corresponding conditional Hamiltonian equals

$$
\begin{aligned}
H_{\text{cond}} &= \sum_{i=1,2} \frac{1}{2}\hbar\Omega_i\, c_i + \text{H.c.} - \frac{\text{i}}{2}\hbar\kappa_i\, c_i^\dagger c_i \\
&\quad - \frac{\text{i}}{2\xi^2}\hbar\kappa_{\text{m}} \left(\xi_1^*\, c_1^\dagger + \xi_1^*\, c_2^\dagger\right)(\xi_1\, c_1 + \xi_2\, c_2)
\end{aligned} \tag{4.29}
$$

and describes the no-photon time evolution of cavity 1 and cavity 2.

Effect of photon emission

Proceeding as in Section 2.4.4, assuming that the respective reservoir is initially in its vacuum state, using first order perturbation theory, and calculating the state of the system under the condition of a photon detection, we find that photon emission into the individual reservoir of cavity i is described by

$$R_i \;=\; \sqrt{\kappa_i}\, c_i \,. \tag{4.30}$$

The leakage of a photon through the waveguide reservoir changes the system according to

$$R_\mathrm{m} \;=\; \frac{1}{\xi}\sqrt{\kappa_\mathrm{m}}\,(\xi_1\, c_1 + \xi_2\, c_2)\,. \tag{4.31}$$

The normalisation of these operators has again been chosen such that the probability for an emission in Δt into one of the reservoirs equals $\|R_\mathrm{x}\,|\varphi(0)\,\rangle\|^2\,\Delta t$ with x $=$ $1, 2, \mathrm{m}$ and with $|\varphi(0)\rangle$ being the initial state of the two cavities.

Master equation

Averaging again over the possibilities of both no-photon evolution and photon emission events, we arrive at the master equation

$$\begin{aligned}
\dot{\rho} \;=\; & -\frac{\mathrm{i}}{\hbar}\,[\,H_\mathrm{cond}, \rho\,] + R_1\,\rho\, R_1^\dagger + R_2\,\rho\, R_2^\dagger \\
& + R_\mathrm{m}\,\rho\, R_\mathrm{m}^\dagger
\end{aligned} \tag{4.32}$$

which is analogous to Eq. (3.27) and where ρ is the density matrix of the two cavity fields.

This master equation fulfils the condition of having potentially different decay rates for different common modes. The elimination of one of the common modes

from the system dynamics using this decay rate difference was simply assumed for the previous system. In this case, as we take the scheme more seriously as an experimental possibility, the details of using dissipation as a control mechanism are shown in more detail.

4.3.3 Single-mode behaviour of two fibre-coupled cavities

In this section, we discuss how to decouple one of the common cavity field modes in Eq. (4.1) from the system dynamics of the fibre-coupled cavities. The physics behind this kind of control strategy was the focus of chapter 3. Here we apply the theory developed in that chapter to our reservoir engineering scheme. After introducing a certain convenient common mode representation, we see that there are two interesting parameter regimes: The first one is defined by a careful alignment of the laser driving frequencies Ω_1 and Ω_2, whilst the second one is defined by the condition that κ_m is much larger than all other spontaneous decay rates and laser driving frequencies in the system, as assumed in Eq. (4.18). In this second parameter regime, one of the common modes can be adiabatically eliminated from the system dynamics, analogously to the control strategy of chapter 3. Consequently, this case does not require any alignment and is much more robust against parameter fluctuations. As we shall see below, the resulting master equation and its stationary state photon emission rate are formally the same as those obtained in Section 4.2.2 for the single-cavity case.

Common mode representation

Looking at the conditional Hamiltonian in Eq. (4.29), it is easy to see that κ_m is the spontaneous decay of a certain single non-local cavity field mode. Adopting the notation introduced in Section 4.1, we see that this mode is indeed the c_b mode defined in Eq. (4.1). As already mentioned in the introduction of this chapter, the c_b mode is the only common cavity field which interacts with the optical fibre connecting both cavities. The fibre provides an additional reservoir into which the

photons in this mode can decay with κ_{m} being the corresponding spontaneous decay rate. Photons in the c_a mode do not see the fibre and decay only via κ_1 and κ_2.

It is hence natural to replace the annihilation operators c_1 and c_2 by the common mode operators c_a and c_b. Doing so, Eq. (4.29) becomes

$$
\begin{aligned}
H_{\mathrm{cond}} \;=\; & \frac{1}{2}\hbar(\Omega_a\,c_a + \Omega_b\,c_b) + \mathrm{H.c.} - \frac{\mathrm{i}}{2}\hbar\kappa_{\mathrm{m}}\,c_b^\dagger c_b \\
& - \frac{\mathrm{i}}{2\xi^2}\hbar\Big[\left(\kappa_1|\xi_2|^2 + \kappa_2|\xi_1|^2\right) c_a^\dagger c_a \\
& + \left(\kappa_1|\xi_1|^2 + \kappa_2|\xi_2|^2\right) c_b^\dagger c_b \\
& + (\kappa_1 - \kappa_2)\left(\xi_1\xi_2\,c_b^\dagger c_a + \xi_1^*\xi_2^*\,c_a^\dagger c_b\right)\Big]
\end{aligned}
\tag{4.33}
$$

with the effective laser driving frequencies

$$
\begin{aligned}
\Omega_a &\equiv \frac{1}{\xi}(\Omega_1\xi_2 - \Omega_2\xi_1)\,, \\
\Omega_b &\equiv \frac{1}{\xi}(\Omega_1\xi_1^* + \Omega_2\xi_2^*)\,.
\end{aligned}
\tag{4.34}
$$

The last term in Eq. (4.33) describes a mixing of the c_a mode and the c_b mode which occurs when the decay rates κ_1 and κ_2 are not of the same size. Finally, we find that the reset operators in Eqs. (4.30) and (4.31) become

$$
\begin{aligned}
R_1 &= \frac{1}{\xi}\sqrt{\kappa_1}\left(\xi_2\,c_a + \xi_1^*\,c_b\right), \\
R_2 &= -\frac{1}{\xi}\sqrt{\kappa_2}\left(\xi_1\,c_a - \xi_2^*\,c_b\right), \\
R_{\mathrm{m}} &= \sqrt{\kappa_{\mathrm{m}}}\,c_b
\end{aligned}
\tag{4.35}
$$

in the common mode representation.

Single-mode behaviour due to careful alignment

Let us first have a look at the case where the single-mode behaviour of the two cavities in Fig. 4.2 is due to a careful alignment of the laser driving frequencies Ω_1

and Ω_2 and both cavity decay rates being the same, i.e.

$$\kappa \equiv \kappa_1 = \kappa_2 \tag{4.36}$$

which sets $\kappa_1 - \kappa_2$ equal to zero. When two fibre-coupled cavities are driven by two laser fields with a fixed phase relation, the result is always the driving of only one common cavity field mode. If the cavities are therefore driven such that the driven mode is identical to the c_a mode, an initially empty c_b mode remains empty. As one can easily check using the definitions of the laser driving frequencies Ω_a and Ω_b in Eq. (4.34), this applies when

$$\frac{\Omega_1}{\Omega_2} = -\frac{\xi_2^*}{\xi_1^*}, \tag{4.37}$$

as it results in $\Omega_a \neq 0$ and $\Omega_b = 0$.

The question that now immediately arises is how to choose Ω_1 and Ω_2 in an experimental situation where ξ_1 and ξ_2 are not known. We therefore remark here that the sole driving of the c_a mode can be distinguished easily from the sole driving of the c_b mode by actually measuring the photon emission from the waveguide. In the first case, the corresponding stationary state photon emission rate assumes its minimum, while it assumes its maximum in the latter. Variations of the laser driving frequency Ω_1 with respect to Ω_2 in a regime where both of them are of comparable size as κ_{m} can hence be used to determine ξ_1/ξ_2 experimentally.

Neglecting all terms which involve the annihilation operator c_b, as there are no c_b modes to annihilate, results in the effective master equation

$$
\begin{aligned}
\dot{\rho} &= -\frac{\mathrm{i}}{\hbar}\left[H_{\mathrm{cond}}, \rho\right] + \kappa\, c_a\, \rho\, c_a^\dagger, \\
H_{\mathrm{cond}} &= \frac{1}{2}\hbar\Omega_a\, c_a + \mathrm{H.c.} - \frac{\mathrm{i}}{2}\hbar\,\kappa\, c_a^\dagger c_a.
\end{aligned}
\tag{4.38}
$$

This master equation is equivalent to Eqs. (4.7), (4.8), and (4.9) in Section 4.2.2 which describes a single cavity. However, it is important to remember that the

above equations are only valid when the alignment of the laser driving frequencies and cavity decay rates is *exactly* as in Eqs. (4.37) and (4.36). Any fluctuation forces us to reintroduce the c_b mode into the description of the system dynamics.

Robust decoupling of one common mode

To overcome this problem, let us now have a closer look at the parameter regime in Eq. (4.18), where the laser driving frequencies Ω_a and Ω_b, and the spontaneous decay rates κ_1 and κ_2 are much smaller than κ_{m}. To do so, we write the state vector of the system under the condition of no photon emission as

$$|\varphi^0(t)\rangle \quad = \quad \sum_{i,j=0}^{\infty} \zeta_{i,j}(t) \, |i,j\rangle \,, \tag{4.39}$$

where $|i,j\rangle$ denotes a state with i photons in the c_a mode and j photons in the c_b mode and the $\zeta_{i,j}(t)$ are the corresponding coefficients of the state vector at time t. Using Eqs. (4.38), (4.33), and (4.35) one can then show that the time evolution coefficients $\zeta_{i,0}$ and $\zeta_{i,1}$ are given by

$$
\begin{aligned}
\dot{\zeta}_{i,0} \quad = \quad & -\frac{\mathrm{i}}{2}\left[\sqrt{i+1}\,\Omega_a\zeta_{i+1,0} + \sqrt{i}\,\Omega_a^*\zeta_{i-1,0} + \Omega_b\zeta_{i,1}\right] \\
& -\frac{1}{2\xi^2}\kappa_1\left[i|\xi_2|^2\zeta_{i,0} + \sqrt{i}\,\xi_1^*\xi_2^*\zeta_{i-1,1}\right] \\
& -\frac{1}{2\xi^2}\kappa_2\left[i|\xi_1|^2\zeta_{i,0} + \sqrt{i}\,\xi_1^*\xi_2^*\zeta_{i-1,1}\right]
\end{aligned}
\tag{4.40}
$$

and

$$
\begin{aligned}
\dot{\zeta}_{i,1} \quad = \quad & -\frac{\mathrm{i}}{2}\Big[\sqrt{i+1}\,\Omega_a\zeta_{i+1,1} + \sqrt{i}\,\Omega_a^*\zeta_{i-1,1} + \sqrt{2}\,\Omega_b\zeta_{i,2} \\
& +\Omega_b^*\zeta_{i,0}\Big] - \frac{1}{2\xi^2}\kappa_1\Big[\left(|\xi_1|^2 + i|\xi_2|^2\right)\zeta_{i,1} \\
& +\sqrt{i+1}\,\xi_1\xi_2\zeta_{i+1,0} + \sqrt{2i}\,\xi_1^*\xi_2^*\zeta_{i-1,2}\Big] \\
& -\frac{1}{2\xi^2}\kappa_2\Big[\left(|\xi_2|^2 + i|\xi_1|^2\right)\zeta_{i,1} - \sqrt{i+1}\,\xi_1\xi_2\zeta_{i+1,0} \\
& -\sqrt{2i}\,\xi_1^*\xi_2^*\zeta_{i-1,2}\Big] - \frac{1}{2}\kappa_m\zeta_{i,1}\,.
\end{aligned}
\tag{4.41}
$$

In the parameter regime given by Eq. (4.18), states with photons in the c_b mode evolve on a much faster time scale than states with population only in the c_a mode. Consequently, the coefficients $\zeta_{i,j}$ with $j > 1$ can be eliminated adiabatically from the system dynamics. Doing so and setting the right hand side of Eq. (4.41) equal to zero, we find that

$$\zeta_{i,1} = -\frac{1}{\kappa_{\mathrm{m}}}\left[i\Omega_b^*\zeta_{i,0} - \sqrt{i+1}\,\frac{\xi_1\xi_2}{\xi^2}\Delta\kappa\zeta_{i+1,0}\right] \tag{4.42}$$

with $\Delta\kappa$ defined as

$$\Delta\kappa \equiv \kappa_1 - \kappa_2. \tag{4.43}$$

Substituting Eq. (4.42) into Eq. (4.40), we find that the effective conditional Hamiltonian of the two cavities is now given by

$$H_{\mathrm{cond}} = \frac{1}{2}\hbar\Omega_{\mathrm{eff}}\,c_a + \mathrm{H.c.} - \frac{i}{2}\hbar\kappa_{\mathrm{eff}}\,c_a^\dagger c_a. \tag{4.44}$$

Up to first order in $1/\kappa_{\mathrm{m}}$, the effective laser driving frequency Ω_{eff} and the effective decay rate κ_{eff} of the c_a mode are given by

$$\begin{aligned}
\Omega_{\mathrm{eff}} &\equiv \Omega_a + \frac{\xi_1\xi_2\Delta\kappa}{\xi^2\kappa_m}\Omega_b, \\
\kappa_{\mathrm{eff}} &\equiv \frac{1}{\xi^2}\left[\kappa_1|\xi_2|^2 + \kappa_2|\xi_1|^2 - \frac{|\xi_1\xi_2|^2\Delta\kappa^2}{\xi^2\kappa_m}\right].
\end{aligned} \tag{4.45}$$

The decay rate κ_{eff} lies always between κ_1 and κ_2. If both cavities couple in the same way to their individual reservoirs, i.e. when $\xi_1 = \xi_2$ and $\kappa_1 = \kappa_2$, then we have $\Omega_{\mathrm{eff}} = \Omega_a$ and $\kappa_{\mathrm{eff}} = \kappa_1$.

Eq. (4.42) shows that any population in the c_a mode always immediately causes a small amount of population in the c_b mode. Taking this into account, the reset

operators in Eq. (4.35) become

$$
\begin{aligned}
R_1 &= \sqrt{\kappa_1}\,\frac{\xi_2}{\xi}\left[1 - \frac{|\xi_1|^2\Delta\kappa}{\xi^2\kappa_m}\right]c_a\,, \\
R_2 &= -\sqrt{\kappa_2}\,\frac{\xi_1}{\xi}\left[1 + \frac{|\xi_2|^2\Delta\kappa}{\xi^2\kappa_m}\right]c_a\,, \\
R_{\mathrm{m}} &= -\sqrt{\kappa_m}\,\frac{\xi_1\xi_2\Delta\kappa}{\xi^2\kappa_{\mathrm{m}}}\,c_a\,.
\end{aligned}
\tag{4.46}
$$

Substituting these and Eq. (4.44) into the master equation (3.27) we find that it indeed simplifies to the master equation of a single cavity. Analogous to Eq. (4.9) we now have

$$
\dot{\rho} = -\frac{\mathrm{i}}{\hbar}\left[H_{\mathrm{cond}},\rho\right] + \kappa_{\mathrm{eff}}\,c_a\,\rho\,c_a^\dagger\,,
\tag{4.47}
$$

while Eqs. (4.44) and (4.46) are analogous to Eqs. (4.7) and (4.8). The only difference to Section 4.2.2 is that the single mode c is now replaced by the non-local common cavity field mode c_a, while Ω and κ are replaced by Ω_{eff} and κ_{eff} in Eq. (4.45). The c_b mode no longer participates in the system dynamics and remains to a very good approximation in its vacuum state.

Finally, let us remark that one way of testing the single-mode behaviour of the two fibre-coupled cavities is to measure their stationary state photon emission rate I. Since their master equation is effectively the same as in the single-cavity case, this rate is under ideal decoupling conditions, i.e. in analogy to Eq. (4.12), given by

$$
I = |\Omega_{\mathrm{eff}}|^2/\kappa_{\mathrm{eff}}\,.
\tag{4.48}
$$

If the decay rates κ_1 and κ_2 and the laser driving frequencies Ω_1 and Ω_2 are known, then the only unknown parameters in the master equation are the relative phase between ξ_1 and ξ_2, the ratio $|\xi_1/\xi_2|$, and the spontaneous decay rate κ_{m}. These can, in principle be determined experimentally, by measuring I for different values of Ω_1 and Ω_2 [1].

---

[1] The dependence of I on the modulus squared of Ω_{eff} means that it is not possible to measure

Effectiveness of the c_b mode decoupling

To conclude this section, we now have a closer look at how small κ_{m} can be with respect to the κ_i and Ω_i whilst still decoupling the c_b mode from the system dynamics. To have a criterion for how well the above described decoupling mechanism works we calculate in the following, the relative amount of population in the c_b mode when the laser-driven cavities have reached their stationary state with $\dot{\rho} = 0$. This means, we now consider the mean photon numbers of the two common cavity modes

$$n_a \equiv \langle c_a^\dagger c_a \rangle \quad \text{and} \quad n_b \equiv \langle c_b^\dagger c_b \rangle \tag{4.49}$$

and use the master equation to obtain rate equations which predict their time evolution. In order to obtain a closed set of differential equations, we need to consider the expectation values

$$
\begin{aligned}
k_a &\equiv \frac{\mathrm{i}}{|\Omega_a|} \langle \Omega_a c_a - \Omega_a^* c_a^\dagger \rangle \,, \\
k_b &\equiv \frac{\mathrm{i}}{|\Omega_b|} \langle \Omega_b c_b - \Omega_b^* c_b^\dagger \rangle \,, \\
m &\equiv \frac{1}{\xi^2} \langle \xi_1 \xi_2 c_b^\dagger c_a + \xi_1^* \xi_2^* c_a^\dagger c_b \rangle \,, \\
l_a &\equiv \frac{\mathrm{i}}{|\Omega_b| \xi^2} \langle \xi_1 \xi_2 \Omega_b c_a - \xi_1^* \xi_2^* \Omega_b^* c_a^\dagger \rangle \,, \\
l_b &\equiv \frac{\mathrm{i}}{|\Omega_a| \xi^2} \langle \xi_1 \xi_2 \Omega_a c_b - \xi_1^* \xi_2^* \Omega_a^* c_b^\dagger \rangle
\end{aligned}
\tag{4.50}
$$

in addition to n_a and n_b. Physically, k_a, k_b, l_a and l_b describe field quadratures of the common cavity modes whilst m describes transitions between them. Using these

---

the absolute values of ξ_1 and ξ_2 but this is exactly as one would expect it to be. Also in the single optical cavity, the overall phase factor of its field mode is not known a priori and has in general no physical consequences.

expectation values and Eqs. (4.32), (4.33), and (4.35), we find that

$$
\begin{aligned}
\dot{n}_a &= \frac{|\Omega_a|}{2} k_a - \frac{1}{2}\Delta\kappa\, m - \kappa_a n_a\,, \\
\dot{n}_b &= \frac{|\Omega_b|}{2} k_b - \frac{1}{2}\Delta\kappa\, m - (\kappa_b + \kappa_m) n_b\,, \\
\dot{k}_a &= |\Omega_a| - \frac{1}{2}\Delta\kappa\, l_b - \frac{1}{2}\kappa_a k_a\,, \\
\dot{k}_b &= |\Omega_b| - \frac{1}{2}\Delta\kappa\, l_a - \frac{1}{2}(\kappa_b + \kappa_m) k_b\,, \\
\dot{m} &= \frac{|\Omega_b|}{2} l_a + \frac{|\Omega_a|}{2} l_b - \frac{|\xi_1\xi_2|^2}{\xi^4}\Delta\kappa\,[n_a + n_b] \\
&\quad - \frac{1}{2}(\kappa_1 + \kappa_2 + \kappa_m) m\,, \\
\dot{l}_a &= \frac{1}{2\xi^2|\Omega_a|}[\xi_1\xi_2\Omega_b\Omega_a^* + \xi_1^*\xi_2^*\Omega_b^*\Omega_a] - \frac{|\xi_1\xi_2|^2}{2\xi^4}\Delta\kappa\, k_b \\
&\quad - \frac{1}{2}\kappa_a l_a\,, \\
\dot{l}_b &= \frac{1}{2\xi^2|\Omega_b|}[\xi_1\xi_2\Omega_b\Omega_a^* + \xi_1^*\xi_2^*\Omega_b^*\Omega_a] - \frac{|\xi_1\xi_2|^2}{2\xi^4}\Delta\kappa\, k_a \\
&\quad - \frac{1}{2}\kappa_b l_b\,, \tag{4.51}
\end{aligned}
$$

where

$$
\begin{aligned}
\kappa_a &\equiv \frac{1}{\xi^2}(\kappa_1|\xi_2|^2 + \kappa_2|\xi_1|^2)\,, \\
\kappa_b &\equiv \frac{1}{\xi^2}(\kappa_1|\xi_1|^2 + \kappa_2|\xi_2|^2) \tag{4.52}
\end{aligned}
$$

are the spontaneous decay rates of the c_a and the c_b mode, respectively.

The stationary state of the system can be found by setting the right hand sides of the above rate equations equal to zero. However, the analytic solution of these equations is complicated and not very instructive. We therefore restrict ourselves in the following to the case, where both cavities are driven by laser fields with identical laser driving frequencies and where both couple identically to the environment, i.e. where

$$
\Omega = \Omega_1 = \Omega_2 \quad \text{and} \quad \xi = |\xi_1| = |\xi_2|\,. \tag{4.53}
$$

83
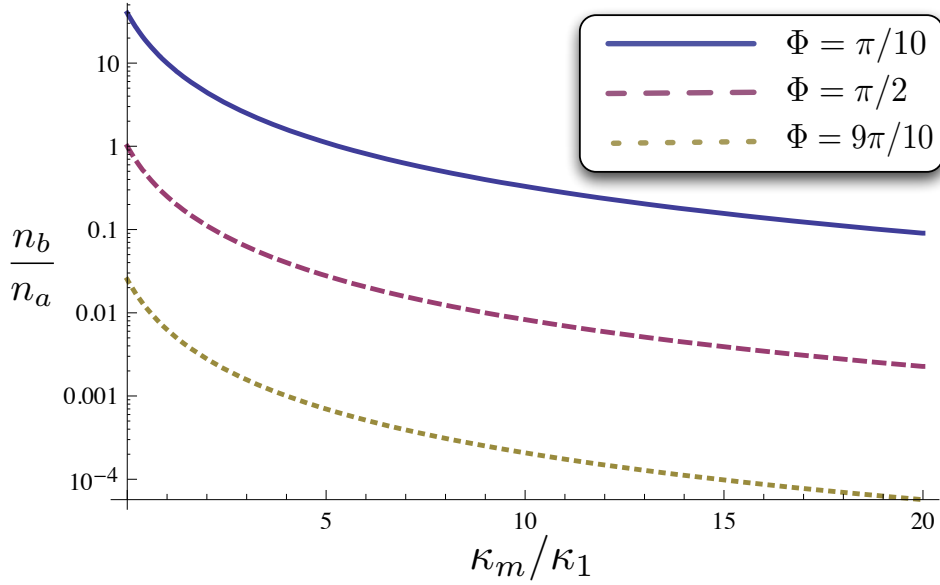
Figure 4.4: Stationary state value of n_b/n_a as a function of κ_{m} for $\xi_1 = \xi_2$ and $\Omega_1 = \Omega_2 = \kappa_1 = \kappa_2$ for three different values of Φ obtained from Eq. (4.57).

The remaining free parameters are a phase factor Φ between ξ_1 and ξ_2 defined by the equation

$$\xi_2 = \mathrm{e}^{\mathrm{i}\Phi}\,\xi_1 \tag{4.54}$$

and the cavity decay rates κ_1, κ_2, and κ_{m}. The reason that we restrict ourselves here to the case where the relative phase between the laser driving frequencies Ω_1 and Ω_2 equals zero, is that varying this phase has the same effect as varying the phase Φ.

Identical decay rates κ_1 and κ_2

To illustrate how these free parameters affect the robustness of the c_b mode decoupling, we now analyse some specific choices of parameters. The first and simplest choice of parameters is to set the decay rates for both cavities the same. As in

Eq. (4.36) we define

$$\kappa \equiv \kappa_1 = \kappa_2 \tag{4.55}$$

which implies $\Delta \kappa = 0$ and $\kappa_a = \kappa_b = \kappa$. Moreover, the rate equations in Eq. (4.51) simplify to the four coupled equations

$$
\begin{aligned}
\dot{n}_a &= \frac{|\Omega|}{\sqrt{2}}(1 - \cos \Phi)^{\frac{1}{2}} k_a - \kappa n_a \,, \\
\dot{n}_b &= \frac{|\Omega|}{\sqrt{2}}(1 + \cos \Phi)^{\frac{1}{2}} k_b - (\kappa + \kappa_m) n_b \,, \\
\dot{k}_a &= \sqrt{2}|\Omega|(1 - \cos \Phi)^{\frac{1}{2}} - \frac{1}{2} \kappa k_a \,, \\
\dot{k}_b &= \sqrt{2}|\Omega|(1 + \cos \Phi)^{\frac{1}{2}} - \frac{1}{2}(\kappa + \kappa_m) k_b \,.
\end{aligned}
\tag{4.56}
$$

The stationary state of these equations can be calculated by setting these derivatives equal to zero. Doing so, we find that the mean number of photons in the c_a and in the c_b mode approach the values

$$
\begin{aligned}
n_a &= (1 - \cos \Phi) \frac{\Omega^2}{\kappa^2} \,, \\
n_b &= (1 + \cos \Phi) \frac{\Omega^2}{(\kappa + \kappa_{\mathrm{m}})^2}
\end{aligned}
\tag{4.57}
$$

after a certain transition time. A measure for the effectiveness of the decoupling of the c_b mode is given by the final ratio n_b/n_a which is given by

$$\frac{n_b}{n_a} = \frac{1 + \cos \Phi}{1 - \cos \Phi} \cdot \frac{\kappa^2}{(\kappa + \kappa_{\mathrm{m}})^2} \,. \tag{4.58}$$

In general, this ratio tends to zero when κ_{m} becomes much larger than κ. There is only one exceptional case, namely the case where $\cos \Phi = 1$. This case corresponds to sole driving of the c_b mode, where the stationary state of the c_a mode corresponds to $n_a = 0$.

This behaviour is confirmed by Fig. 4.4 which shows the steady state value of n_b/n_a in Eq. (4.57) as a function of κ_{m} for three different values of Φ. In all three

Figure 4.5: Stationary state value of n_b/n_a as a function of κ_m for $\xi_1 = \xi_2$, $\Omega_1 = \Omega_2 = \kappa_1$, and $\kappa_2 = 0.5\,\kappa_1$. As in Fig. 4.4, we observe a very rapid drop of the relative population in the c_b mode as κ_m increases.

cases, the mean photon number in the c_b mode decreases rapidly as κ_m increases. This is an indication of the robustness of decoupling of the c_b mode. It shows that this decoupling does not require phase-locking of the driving lasers. However, as already mentioned above, one should avoid sole driving of the c_b mode. Indeed we find relatively large values for n_b/n_a when the angle Φ is relatively small. The case $\Phi = \pi/2$ corresponds to equal driving of both common modes. In this case we have $n_b/n_a < 0.01$ when κ_m is at least eight times larger than κ which is a relatively modest decoupling condition. Close to the perfect alignment case (with $\Phi = \pi$) which we discussed in detail in the previous subsection, n_b/n_a is even smaller than in the other two cases. For $\Phi = 0.9\,\pi$ and $\kappa_\mathrm{m} > 8\,\kappa$, we now already get $n_b/n_a \ll 0.001$.

Different decay rates κ_1 and κ_2

In the above case with $\Delta\kappa = 0$, there is no transfer of photons between the two modes. To show that this is not an explicit requirement for the decoupling of the c_b mode, we now have a closer look at the case where $\Delta\kappa \neq 0$ and where mixing
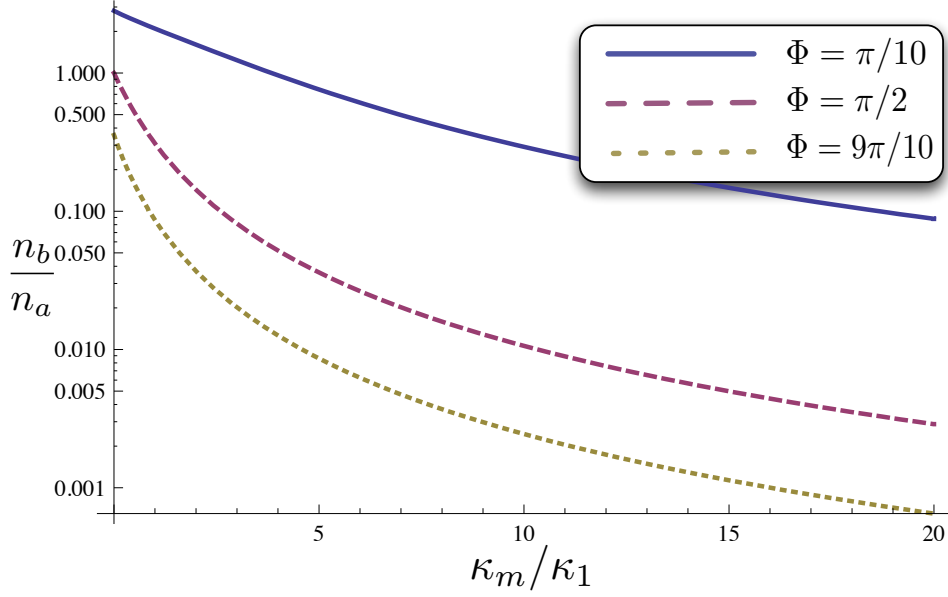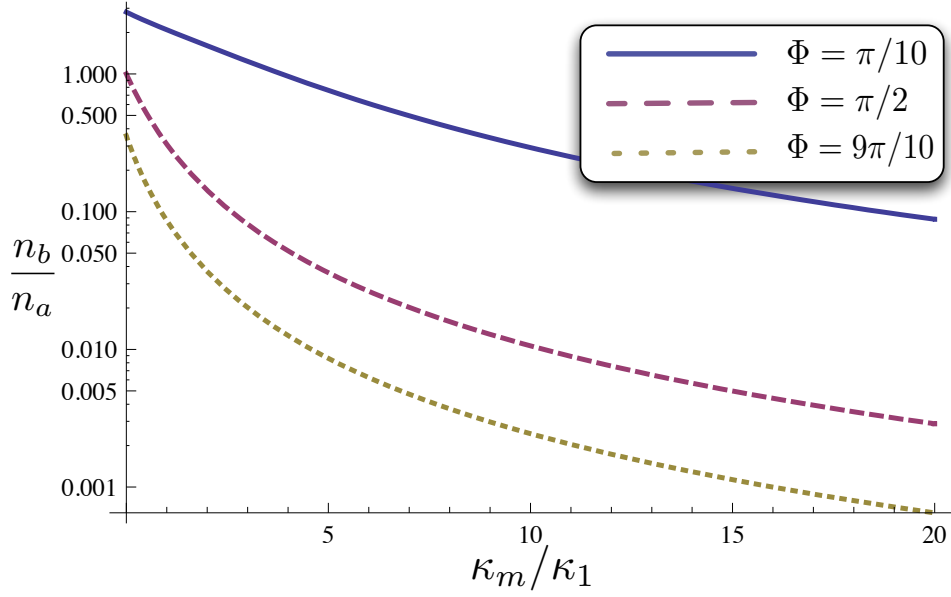
Figure 4.6: Stationary state value of n_b/n_a as a function of κ_m for $\xi_1 = \xi_2$, $\Omega_1 = \Omega_2 = \kappa_1$, and $\kappa_2 = 1.5\,\kappa_1$. As in Figs. 4.4 and 4.5, n_b/n_a decreases rapidly as κ_m increases. The main difference to Fig. 4.5 is that we now have $\Delta\kappa < 0$ instead of having $\Delta\kappa > 0$.

between both common cavity modes occurs. Let us first have a look at the case where $\Phi = 0$ and where only the c_b mode is driven. In this case, we expect $\Delta\kappa$ to result in an enhancement of the single mode behaviour compared to the $\Delta\kappa = 0$ case. The reason is that the effective laser driving frequency Ω_eff in Eq. (4.45) is now always larger than zero such that n_a no longer tends to zero when $\Phi \to 0$. Different from this, we expect the stationary state value of n_b/n_a to increase when $\Phi = \pi$. The reason for this is that this case now no longer corresponds to perfect alignment which required $\Delta\kappa = 0$ (c.f. Eq. (4.36)). This behaviour of the two fibre-coupled cavities is confirmed by Figs. 4.5 and 4.6 which have been obtained by setting the time derivatives of the original rate equations (4.51) equal to zero. For the parameters considered here, the introduction of $\Delta\kappa$ has no effect on the effectiveness of the decoupling of the c_b mode when $\Phi = \pi/2$ and both modes are equally driven by laser fields.

Before we move on to discuss the second method of reservoir engineering, we will consider the importance of having the cavity frequencies in resonance with each other

and the connecting fibre. This issue is also related to the interferometric stability of the setup. An instability would have the effect of lengthening or shortening the fibre and changing the frequency of the field it supports. We note that the common cavity modes that is eliminated is defined in Eq. 4.1 with reference only to ξ_1 and ξ_2, which represent the coupling between the cavities and the fibre. An interferometric instability could have the effect of changing the frequency matching between the cavities and the fibre. In the case where both cavities are identical, this would not change the relative amplitude of ξ_1 and ξ_2 as long as the frequency shift is not so great that a higher harmonic of the fibre field comes close to resonance. In this case there would be a π phase flip between ξ_1 and ξ_2.

If the cavities have different frequencies, then a shifting of the fibre frequency could bring one of the cavities closer to resonance while the other drifts out. In this case the relative amplitude of ξ_1 and ξ_2 would change with the instability causing a different common cavity mode to be eliminated. If the instability only changes the the fibre frequency on a slow time scale this would still not be a major problem as the elimination of one common cavity mode would still persist.

4.4 Reservoir Engineering with Interference

The second method we propose as an alternative implementation, is explicitly based on interference of photons emitted by the two cavities in a setup as shown in Fig. 4.7.

In this setup, two cavities couple individually to an optical single-mode fibre. These fibres guide the photons from each cavity onto a single photon detector which cannot resolve the origin of the incoming photons. If the light coupling out of the two fibre tips onto the detector surface is perfectly overlapping and of a narrow enough focus, then only photons emitted by one precisely defined common cavity mode reaches each detector. By splitting the fibre modes with a polarising beam splitter and placing a phase plate into one of the outcoupling paths, it is possible to align the setup such that orthogonal common modes couple to the two detectors separately. In this section, we carefully analyse the physical requirements for implementing this

88
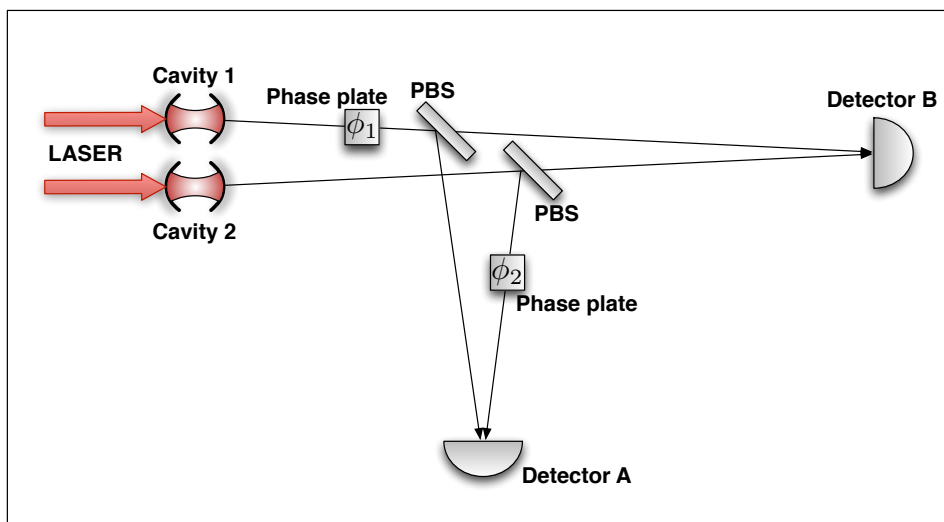
Figure 4.7: Experimental setup with two cavities emitting photons into fibres. By using polarising beam splitters and phase plates, the emissions are separated such that photons from orthogonal common modes reach different detectors. Interference on the detectors means the detectors can only measure photons from one common mode.

scheme and show that it would require subwavelength fibre tips at the detectors. These are relatively hard to realise experimentally although it is feasible with current technology [130].

The main aspect of interest in this setup is thus the interference on the detector surface and it is to this that we will pay special attention. For this purpose, we first consider a simplified setup with just a single detector and no polarising beam splitters, shown in Fig. 4.8.

The first condition we have to stipulate is that the light coming out of the two fibre tips overlaps exactly on the surface of the detector. This requires choosing the angle 2ξ between the fibres as a function of the fibre radius R, the opening angle β, the distance D between the fibres and their distance L from the screen (cf. Fig. 4.9). Overlapping light cones mean that every photon arriving on the screen contains a contribution from both fibres and there is in general no information about its origin. This results in an interference pattern. Suppose the light in the two fibres is exactly in phase and of exactly the same wavelength - in this case, we expect maximum
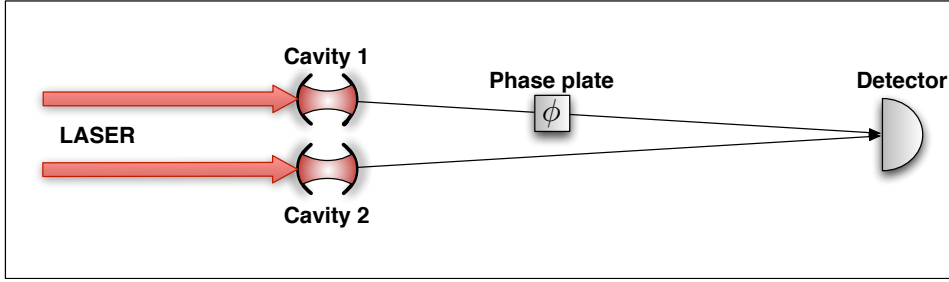
Figure 4.8: Experimental setup showing two single mode fibres coupling to two cavities at one end with the out-coupling light fields at the other ends overlapping on a detector surface.

intensity in the middle of the screen due to the symmetry of the above described setup. Other points on the screen are in general of lower intensity.

Let us describe the light mode with wave number k in fibre i by the photon annihilation operator $a_{\mathbf{k},i}$ (for simplicity we assume one fixed polarisation). Then the above interference effect can be described by saying that each point on the screen measures photons in a certain common mode. The annihilation operators of these modes are given by

$$b_{\mathbf{k}}(\varphi) \;\;=\;\; \left(a_{\mathbf{k},1} + \mathrm{e}^{\mathrm{i}\varphi}\, a_{\mathbf{k},2}\right)/\sqrt{2}\,, \tag{4.59}$$

where φ depends on the location of the respective point on the screen. For example, the centre of the screen only measures the common photon mode defined by $(a_{\mathbf{k},1} + a_{\mathbf{k},2})/\sqrt{2}$. This is due to the fact that every photon contribution from one fibre has an equal photon contribution with the same path length from the other fibre. As already mentioned above, this leads to an interference maximum, if the light in both fibres is in phase and of the same wavelength. If the light in the $\mathbf{k}$ mode of both fibres has a π phase difference, then there is no population in the $(a_{\mathbf{k},1} + a_{\mathbf{k},2})/\sqrt{2}$ and the centre of the screen becomes an interference minimum with respect to $\mathbf{k}$.

In the following, we want to take advantage of this interference effect by arranging the photon detection such that a large majority of the points on the screen detects
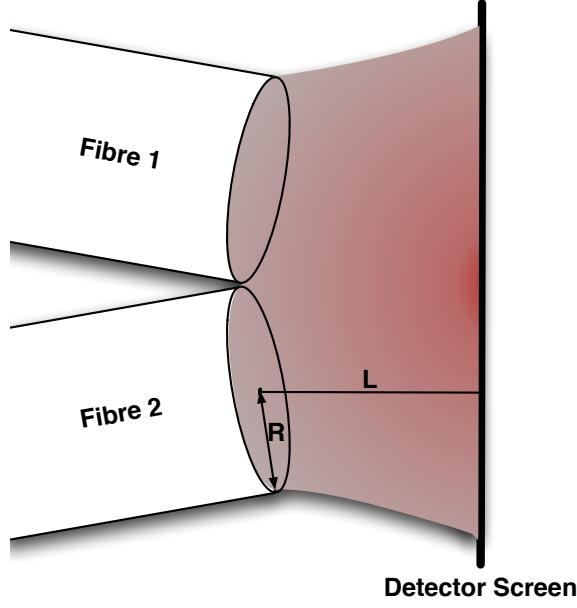
Figure 4.9: Experimental setup showing the two fibre tips and the outcoming light cones which should overlap on a close by screen. Here ξ is the angle between the two fibre tips with respect to the normal of the screen at a distance D from each other and L from the screen.

common photon modes of the form

$$b_{\mathbf{k},1} \;\; = \;\; (a_{\mathbf{k},1} + a_{\mathbf{k},2})/\sqrt{2}\,, \tag{4.60}$$

while the orthogonal modes which are given by

$$b_{\mathbf{k},2} \;\; = \;\; (a_{\mathbf{k},1} - a_{\mathbf{k},2})/\sqrt{2} \tag{4.61}$$

remain undetected. This requires that the maximum path differences remain small compared to the wavelength λ of the light traveling inside the fibre. In the following, we therefore use geometric optics based on the assumption that the light traveling in both fibres is exactly in phase and of the same frequency and estimate the maximum path difference of the two wave fronts on the screen. To maximise constructive interference of the $a_{\mathbf{k},1}$ and the $a_{\mathbf{k},2}$ mode, we arrange the fibres such that there is no gap between the fibre tips.

First, we consider standard single mode fibres which can be described by a Gaus-

91

sian beam analysis. This is only possible, if the diameter of the fibres, $2R$, is comparable or larger than λ. As we shall see below, in this case there are always areas of constructive interference as well as areas of destructive interference. This is a consequence of energy conservation. It guarantees that all the light in the $b_{\mathbf{k},1}$ mode *and* all the light in the $b_{\mathbf{k},2}$ mode is detected on the screen. Afterwards, we apply the same classical wave analysis to optical fibres with sub-wavelength diameter fibre tips with $R \ll \lambda$. It is shown that it is possible to arrange the fibres such that the screen detects only the $b_{\mathbf{k},1}$ mode. The light in the $b_{\mathbf{k},2}$ mode interferes destructively at the detector surface. This means, the light in this mode does not arrive at the detector but is reflected back to be reabsorbed by the cavities or absorbed by the fibre glass.

4.4.1 Estimation of maximum path differences by geometric optics

In the following, we use geometric optics to obtain an estimation of the maximum path difference of the light arriving on the detector surface. As already pointed out above, the light arriving in the middle of the screen can come from every possible point on the surface of the fibre tips, as illustrated in Fig. 4.10. If we assume that the wave fronts of the light arriving at the two fibre tips are exactly in phase, then each possible path from one fibre has an equal length path from the other fibre. Hence all incoming light interferes constructively. However, here we are only interested in single mode fibres, where the only supported mode has a Gaussian profile. Most importantly, the light cone created at the tip of each fibre has an opening angle of a finite size. We denote this angle in the following by β, as shown in Fig. 4.10(c). Consequently, most points outside the centre of the screen are reached only from parts of the fibre surface as illustrated in Fig. 4.10(b). At these points, the light from the two fibres no longer interferes constructively. The largest difference in path length occurs at the edges of the light cone (cf. Fig. 4.10(c)). In this case, the only light arriving on the screen comes from the edges of the fibres. In the following, we estimate this maximum path difference by having a closer look at Figs. 4.9 and 4.10.
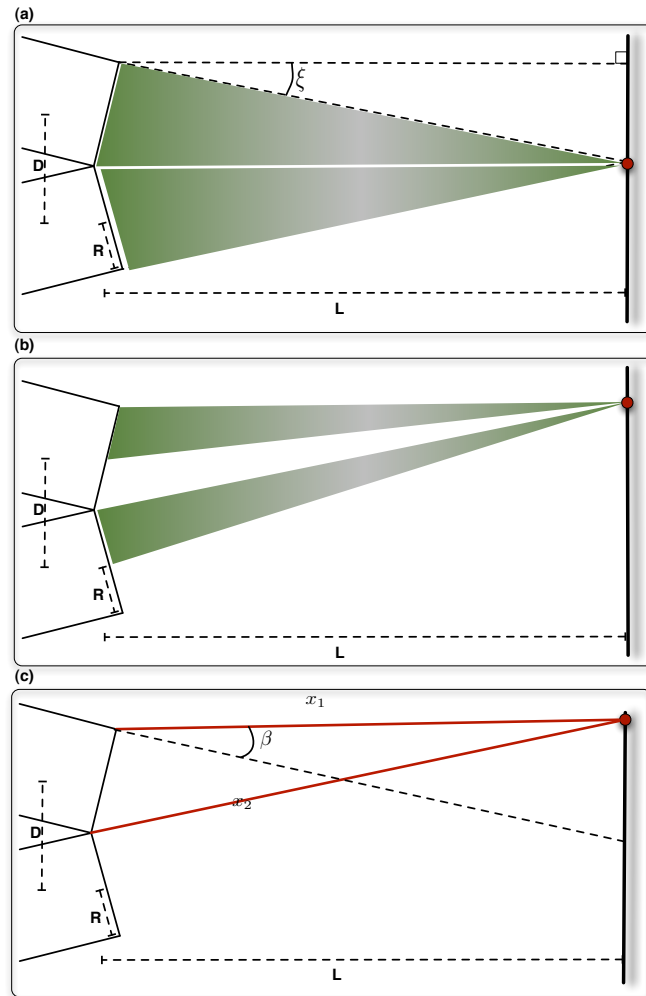
Figure 4.10: Ray diagram for the two fibre tips shown in Fig. 4.9. The figure indicates the proportion of light and possible paths that can reach three specific points on the detector screen.

Let us denote the path lengths which contribute to the interference at the edge of the light cone by x_1 and x_2. Simple trigonometry lets us write x_1 and x_2 as

$$x_1 = \frac{L - R \sin \xi}{\cos(\beta - \xi)} \quad \text{and} \quad x_2 = \frac{L + R \sin \xi}{\cos(\beta + \xi)} . \tag{4.62}$$

Moreover, we notice that the distance between the centres of the optical fibres D is equal to

$$D = 2R \cos \xi , \tag{4.63}$$

since the fibre tips are in direct contact in order to minimise the path difference, defined as

$$\Delta x = x_2 - x_1 \,. \tag{4.64}$$

In order for the light from the two fibres to overlap fully, the following condition must be fulfilled

$$D + x_1 \sin(\beta - \xi) = x_2 \sin(\beta + \xi) \,. \tag{4.65}$$

We now use these equations to obtain an expression for Δx as a function of R, β, and ξ only. This is possible, since fixing these parameters determines the distance L of the fibre tips from the screen.

To eliminate L, we substitute Eqs. 4.62 and 4.63 into Eq. 4.65 and obtain

$$\frac{L}{R} = \frac{1 - \sin^2 \beta - \sin^2 \xi}{\sin \xi} - \frac{\sin \beta \cos \beta}{\cos \xi} \,. \tag{4.66}$$

Combining this expression for L with $x_2 - x_1$ obtained from Eq. 4.62 results in

$$\Delta x = 2R \left[\sin \beta + \tan \xi \cos \beta \right] \tag{4.67}$$

which depends indeed only on R, β, and ξ. The ξ dependence clearly minimises Δx when ξ goes to zero. Practically, ξ cannot equal zero as in this case, the distance to the detector must go to infinity however, ξ can go arbitrarily close to zero. This simplifies Eq. 4.67 to a simple sin dependence on β. Remember that β is the angle at which light emitted by the fibre tips diverges. We have not yet discussed what determines the value of β and it is to this that we now turn our attention. For an estimate of the value of beta, we must consider a more detailed description of the form of the light beam emitted by the fibres.
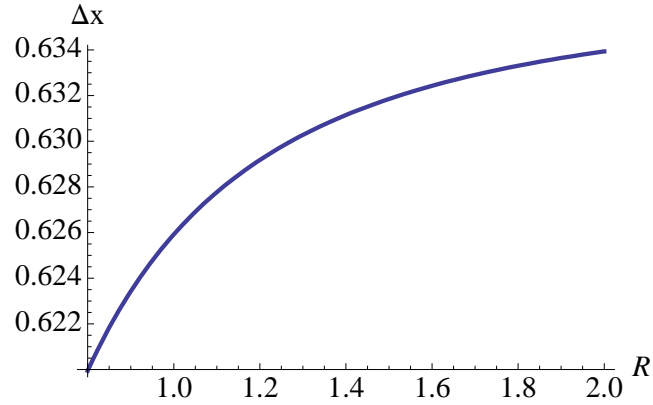
Figure 4.11: Plot of Δx against the fibre tip diameter R for a Gaussian beam emission with divergence angle β given by Eq. 4.68. All units are in λ.

4.4.2 Gaussian Beam Analysis for standard single mode fibres

A single mode fibre with a diameter larger than the wavelength of light travelling through it supports a Gaussian mode profile. The light emitted by such a fibre has the same gaussian profile. The divergence of such a beam is a well known result in classical optics [131] and, in the $L \gg \lambda$ limit, it is

$$\beta = \lambda/\pi R. \tag{4.68}$$

Since single mode fibres have a radius which is comparable to the wavelength λ, there is always a finite opening angle β. Assuming, that ξ is made as small as possible and thus the greater contribution to Δx in Eq 4.67 comes from the first term, we can now plot the value of Δx against a varying fibre tip diameter R with β given by Eq 4.68.

From the plot of Δx against R shown in Fig. 4.68 it is clear that the path difference is always greater than $\lambda/2$ for a fibre tip of diameter comparable to λ. This means it is not possible, in this type of system, with the assumptions we have made, to produce an interference pattern where only the constructive interference at the centre is seen.

The assumptions made in this analysis are that geometric optics is applicable to

the single mode fibre tip emissions and no account has been taken of the Gaussian intensity profile of the Gaussian beam emitted by the fibre tips. A more complete description may be derived by treating the light emissions as two propagating Gaussian beams and numerically calculating the interference pattern when these two light fields overlap on a detector screen. A Gaussian beam is defined as a beam whose transverse electric field and intensity is described by a Gaussian distribution.

The complex electric field amplitude of such a beam propagating along the z-axis is given by

$$
\begin{aligned}
E(r, z) &= \frac{E_0 w_0}{w(z)} \exp\left(-\frac{r^2}{w^2(z)}\right) \\
&\times \exp\left[-\mathrm{i}kz - \mathrm{i}\frac{kr^2}{2R(z)} + \mathrm{i}\zeta(z)\right],
\end{aligned} \tag{4.69}
$$

where r is the radial distance from the axis of the beam, z is the axial distance from the beams narrowest point, k is the wave number and w_0 is the waist size, and where

$$
\begin{aligned}
w(z) &\equiv w_0\sqrt{1 + \left(\frac{z}{z_R}\right)^2} \\
R(z) &\equiv z\left[1 + \left(\frac{z_R}{z}\right)^2\right] \\
\zeta(z) &\equiv \arctan\left(\frac{z}{z_R}\right)
\end{aligned} \tag{4.70}
$$

with $z_R \equiv \pi w_0^2/\lambda$. Considering the setup show in Fig. 4.9, we are interested in beams propagating at an angle ξ to the z-axis and meeting at centre of the screen. By taking this rotation to be around the y-axis and displacing the origin of the beam in the x-direction, we can achieve this by simply rotating the x and z co-ordinates in the equations above such that

$$
\begin{aligned}
z &\rightarrow z\cos\xi - (x + x_0)\sin\xi \qquad \text{and} \\
x &\rightarrow (x + x_0)\cos\xi + z\sin\xi.
\end{aligned} \tag{4.71}
$$

where x_0 is the new position for the origin. In order for the centre of the beams to

Figure 4.12: Gaussian beam intensity on a screen from a beam incident at angle $\xi = \pi/270$ with initial beam width $w_0 = 1$ and wavelength $\lambda = 1$.

be at $x = 0$ on the screen, the z-position of the screen must be $z = x_0/\tan\xi$.

The second beam is simply found by a rotation of $-\xi$ and a displacement of $-x_0$ at the origin. The result of adding the two electric fields and plotting the resulting intensity is shown in Fig. 4.12. This figure very clearly shows the interference pattern expected, although it is confined only to the area on the screen that the individual Gaussian beams would be illuminating.

A more interesting and relevant scenario is the case where the Gaussian beams are π out of phase at their origins. This leads to destructive interference at the centre of the detector screen. Plotting this in the limit of a very small angle ξ, a large distance L and a small separation D puts us in the regime we considered in the previous section. If it were indeed possible to eliminate photon emissions by interference of this kind, then there should not be much of the pattern visible in this plot.

Fig. 4.13 clearly shows that a significant part of the interference pattern is still visible. In fact, it is possible numerically to show that the total intensity of this interference pattern is still exactly equal to the total intensity of the two separate beams where they originate at the fibre tips. This total intensity does in fact decrease as the fibres are moved very close together but this is due to the fact that the evanescent fields of the Gaussian beams begin to overlap already before they leave
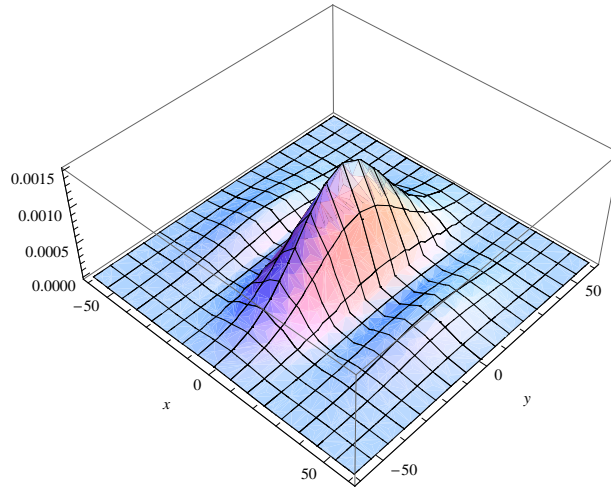
97
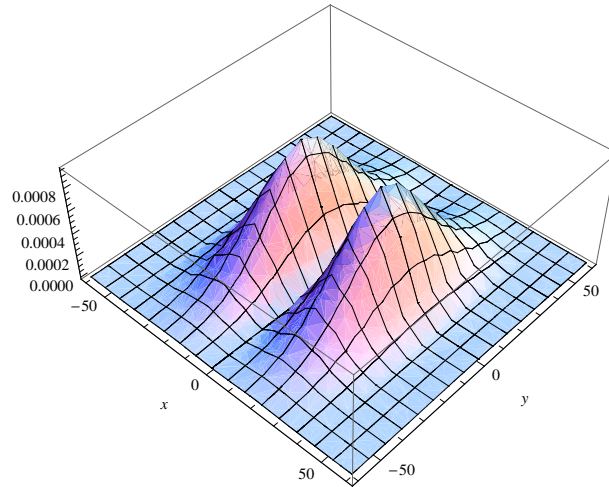
Figure 4.13: Gaussian beam intensity on a screen from a beam incident at angle $\xi = \pi/270$ with initial beam width $w_0 = 1$ and wavelength $\lambda = 1$. The beams are π out of phase leading to destructive interference at the origin.

the fibres.

4.4.3 Sub-wavelength fibre tips

Given that it is not possible to achieve the interference effect we seek with standard single mode fibre tips, we now turn to sub-wavelength fibre tips. Work on sub-wavelenth diameter fibres and tapered fibres has attracted recent interest as the large amplitude evanescent fields may be used to trap or interact with atomic vapours around the fibre [132]. In this field, the fibre is thinned for a short section but the fibre ends remain their normal thickness so results from this field are not really useful to us in our current analysis. Sub-wavelength fibre tips have been studied extensively for use in scanning near-field optical microscopy [133, 134, 135, 136, 137]. The purpose of this field is to use light fields at the tips of probes for high resolution microscopy. fibre tips that are tapered and coated in a layer of aluminium are used to generate light fields around the fibre tip that are focused to a point on the scanned surface which is much smaller that the wavelength of the light used. In this way, the resolution achieved by this technique can far exceed what is possible with diffraction limited far-field microscopy.

In order to optimise tapered fibre tips for microscopy, research has gone into

analysing the form of fields inside tapered optical waveguides. Optimisation is focused on minimising the spot sized produced by the fibre tips whilst maximising the amount of light that is transmitted through the fibre tip. Novotny and Hafner calculated the mode structure in a metallic waveguide at optical frequencies [138]. They found that as the fibre is increasingly tapered, all modes but the HE_{11} are progressively cut off. At a wavelength of 488nm an aluminium coated waveguide supports the HE_{11} mode for a core diameter between ≈ 250 and $160nm$. Up to this point, the transmission rate is determined mainly by the proportion of light travelling in this mode relative to modes that are cut off. The magnitude of this effect is likely related to the angle of the taper and as yet poorly understood. Light that is not transmitted up to this point is either reflected or absorbed by the aluminium cladding.

Beyond the $160nm$ cutoff, the HE_{11} mode also runs into cutoff and light transmission decays exponentially. The larger distance between the cutoff point and the aperture, the less light is transmitted. Novotny *et al* [139] predict that a large taper angle could be used to drastically improve the transmission of light through the aperture which is otherwise extremely low. In Ref. [136] show that it is possible to achieve a spot size as small as $20nm$ with an aperture radius $R = 10nm$ and a taper angle around 30 to 50 degrees. The transmission of light through the aperture relative to the amount of light input to the fibre is around 10^{-4}.

To put this into context, we should consider what spot size we would require for the symmetric light emission (with a maximum of intensity at the centre of the detector) to outweigh the antisymmetric light emission (with maxima out at a path difference of $\lambda/2$) by a factor of 10^3. This can be calculated by taking the ratio of total power of each of the signals as a function of the spot size radius r and solving for r when this ratio is equal to 10^{-3}, ie.

$$
\begin{aligned}
\frac{I_s}{I_a} &= \frac{\int_{-r}^{r} \sin^2 x\, dx}{\int_{-r}^{r} \cos^2 x\, dx} \equiv 10^{-3} \\
&= \frac{r - \frac{1}{2}\sin(2r)}{r + \frac{1}{2}\sin(2r)} \equiv 10^{-3}.
\end{aligned}
\tag{4.72}
$$

99

The solution to this is $r \approx 0.5$. Hence a spot size of around $\lambda/10$ would give this magnitude of amplitude difference. It should thus be possible to substantially improve the transmission of light through the aperture of the fibre tip by sacrificing a larger spot size than Novotny *et al* show to be possible.

The above analogy to experimental and theoretical results from the field of microscopy suggest it may be possible to implement an interference scheme from two fibres where the emission of one common mode is blocked. What is not discussed in microscopy is what happens to the light that does not emerge from the fibre tip. For the functioning of our scheme, we would like it to be reflected and reabsorbed by the cavities. The alternative is that this light is absorbed or otherwise scattered by the fibres resulting in no difference in decay rates from the two common cavity modes. Without this difference in decay rates, the effect of creating a single common cavity mode is not possible.

4.4.4 Final Scheme

We assume for the remainder of this section that the interference does work as we hope and thus each detector provides a decay channel for only one common cavity mode of the form

$$c(\varphi) = (c_1 + e^{i\varphi}c_2)/\sqrt{2}\,, \tag{4.73}$$

where φ is a set constant that defines which common mode is measured and depends on the coupling constant between the cavity modes and the fibre modes and the path differences between each cavity and the detector.

We now return to considering the full setup in Fig. 4.7. If we again denote the cavity modes in cavity 1 and 2 by c_1 and c_2 and the fibre mode measured by detectors a and b by $b_{\mathbf{k},a}$ and $b_{\mathbf{k},b}$ then the Hamiltonian describing coupling between these modes can be written as

$$H_{\text{int}} = \sum_{\mathbf{k}} \left[g_{\mathbf{k},a} \left(e^{i\mathbf{k}\cdot\mathbf{r}+\phi_1}c_1 + c_2 \right) b_{\mathbf{k},a}^{\dagger} + g_{\mathbf{k},b} \left(e^{i\mathbf{k}\cdot\mathbf{r}+\phi_1}c_1 + e^{i\phi_2}c_2 \right) b_{\mathbf{k},b}^{\dagger} \right] + \text{H.c.} \tag{4.74}$$

where $\phi_{1,2}$ represent the phase plates, r is the path length difference between the two fibres to the detector and the couplings between the two cavities and fibres $g_{\mathbf{k},(a,b)}$ are determined by the cavity fibre coupling and the alignment of the polarising beam splitters. The polarising beam splitters could be arranged such that an equal amount of light goes to each detector or such that more goes to one than the other. It is assumed that the cavity-fibre coupling is the same for both cavities.

By tuning the phase plates such that

$$\phi_1 = \mathbf{k} \cdot \mathbf{r} \quad \text{and} \quad \phi_2 = \pi \,, \tag{4.75}$$

this interaction Hamiltonian can be simplified to

$$H_{\text{int}} = \sum_{\mathbf{k}} \left[g_{\mathbf{k},a} c_a b_{\mathbf{k},a}^\dagger + g_{\mathbf{k},b} c_b b_{\mathbf{k},b}^\dagger \right] + \text{H.c.}\,, \tag{4.76}$$

where

$$c_a = (c_1 + c_2) \quad \text{and} \quad c_b = (c_1 - c_2) \,. \tag{4.77}$$

Applying the quantum jump approach to this Hamiltonian results in a conditional Hamiltonian

$$H_{\text{cond}} = -\frac{\mathrm{i}}{2} \hbar \kappa_a c_a^\dagger c_a - \frac{\mathrm{i}}{2} \hbar \kappa_b c_b^\dagger c_b \,, \tag{4.78}$$

and two reset operators

$$R_a = \sqrt{\kappa_a} c_a \quad \text{and} \quad R_b = \sqrt{\kappa_b} c_b \,. \tag{4.79}$$

These are precisely the Hamiltonian and reset operators that we were aiming for from section 4.2.3. The absolute size of the decay rates κ_a and κ_b are determined by the actual decay rates of the individual cavities. However, their relative size can be altered by rotating the polarising beam splitters in Fig. 4.7 relative to the

polarisation of the emitted light such that more light is reflected than transmitted (or vice versa). Thus we have achieved our aim of engineering a bath that enables two common cavity modes to have different decay channels and couple to them with different decay rates.

The detailed analysis of how one of the common cavity modes decouples from the system dynamics is the same as for the previous scheme analysed in section 4.3. For the sake of brevity, we thus omit the rehashing of this analysis here.

4.5   Summary

In conclusion, this chapter detailed two possible schemes for reservoir engineering that make two separate cavities behave effectively as one. The first scheme, depicted in Fig. 4.2, couples two cavities with a single-mode fibre coated with two-level atoms or a waveguide (c.f. Fig. 4.3). The second scheme, depicted in Fig. 4.7, explicitly uses interference on the surface of a detector to achieve this reservoir engineering. This scheme has very stringent experimental requirements regarding the fibre tips being of sub-wavelength diameter and aluminium coated. Hence most of the analysis of this chapter focused on the first scheme.

Since there are two cavities, the description of the fibre-coupled system in Fig. 4.2 requires two orthogonal cavity field modes. These could be the individual cavity modes with the annihilation operators c_1 and c_2 or common modes with the annihilation operators c_a and c_b in Eq. (4.1). Here we consider the case where the connection between the cavities constitutes a reservoir for only one common cavity field mode but not for both. If this mode is the c_b mode, it can have a much larger spontaneous decay rate than the c_a mode which does not see this reservoir. A non-local resonator is created, when operating the system in the parameter regime given by Eq. (4.18), where the c_b mode can be adiabatically eliminated from the system dynamics, thereby leaving behind only the c_a mode.

The purpose of the atoms which coat the fibre is similar to their purpose in Ref. [129], namely to measure its evanescent electric field destructively, although

here there is no need to distinguish between one and two photon states. These measurements should occur on a time scale which is long compared to the time it takes a photon to travel from one resonator to the other. One can easily check that this condition combined with Eq. (4.18) poses the following upper bound on the possible length R of the fibre:

$$\frac{R}{c} \ll \frac{1}{\kappa_{\mathrm{m}}} \ll \frac{1}{\kappa_1}, \frac{1}{\kappa_2}\,. \tag{4.80}$$

Here κ_1, κ_2, and κ_{m} are the spontaneous cavity decay rates through the outcoupling mirrors of cavity 1 and cavity 2 and through the fibre reservoir, respectively, while c denotes the speed of light. This means, the possible length R of the fibre depends on how good the cavities are. For good cavities, R could be of the order of several meters. However, the upper bound for R depends also on the fibre diameter and the quality of the mirrors. The reason is that the fibre should not support a too wide range of optical frequencies, i.e. the fibre should support only one standing wave with frequency ω_{cav} and not two degenerate ones.

There are different ways of seeing how the coated fibre removes one common cavity field mode from the system dynamics. One way is to compare the setup in Fig. 4.2 with the two-atom double-slit experiment by Eichmann *et al.* [67] which has been analysed in detail for example in Refs. [81, 66]. In this experiment, two atoms are simultaneously (i.e. in phase) driven by a single laser field and emit photons into different spatial directions. The emitted photons are collected on a photographic plate which shows intensity maxima as well as completely dark spots. A dark spot corresponds to a direction of light emission where the atomic excitation does not couple to the free radiation field between the atoms and the screen due to destructive interference. The setup in Fig. 4.2 creates an analog situation: The photons inside the two resonators are the sources for the emitted light, thereby replacing the atomic excitation. Moreover, the light inside the fibre is equivalent to a single-mode (i.e. one wave vector $\mathbf{k}$) of the free radiation field in the double slit experiment. There is hence one common resonator mode – the c_b mode – which does not couple to the fibre.

This chapter describes the setups in Figs. 4.2 and 4.3 in a more formal way. Starting from the Hamiltonian as in Ref. [110] for the cavity-fibre coupling but considering the radiation field inside the fibre as a reservoir we derive the master equations for the time evolution of the photons in the optical cavities. After the adiabatic elimination of one common cavity mode, namely the c_b mode, due to overdamping of its population, we arrive at a master equation which is equivalent to the master equation of a single laser-driven optical cavity.

A concrete measure for the quality of the decoupling of the c_b mode is the stationary state value of n_b/n_a, where n_a and n_b are the mean numbers of photons in the c_a and the c_b mode, respectively, when both cavities are driven by a resonant external laser field. Our calculations show that this ratio can be reduced significantly by a careful alignment of the driving lasers. However, even when both cavity modes couple equally to two external laser fields, n_b/n_a can be as small as 0.01 even when κ_m is only one order of magnitude larger than κ_1, κ_2, and the laser driving frequencies of the driving lasers. This parameter regime consequently does not require any alignment and is very robust against parameter fluctuations.

Possible applications of this setup become apparent when one places for example atomic qubits, single quantum dots, or NV color centers into each cavity. These would feel only a common cavity field mode and interact as if they were sitting in the same resonator. Such a scenario has applications in quantum information processing, since it allows to apply quantum computing schemes like the ones proposed in Refs. [51, 115] which would otherwise require the shuttling of qubits in and out of an optical resonator to spatially separated qubits. This application using quantum dots is the focus of the next chapter of this thesis.

Chapter 5

Entanglement using Reservoir Engineering

This chapter is ostensibly about an entanglement scheme for two qubits located in separate cavities that are coupled by a single mode optical fibre. In fact, the purpose of this chapter is to act as an example of how the fibre coupling reservoir engineering scheme proposed in the previous chapter may be applied to a quantum information processing task. This may bring us closer to using the reservoir engineering proposed in this thesis towards implementing a scalable measurement based quantum computing architecture for qubits in optical cavities.

The strength of measurement-based quantum computing is that its performance is independent of the experimental parameters. Whenever a certain measurement outcome is obtained, the system is projected onto a well-defined state with a very high fidelity. This is useful when the final state is highly entangled or differs from the initial one only by a desired quantum gate operation. One example of measurement-based quantum computing is linear optics schemes based on the detection of single photons [9]. Further examples are the processing of atomic qubits via the detection of single or no photons [116, 100, 11, 12] and the manipulation of the electron-spin states of quantum dots via charge detection [140]. However, the scalability of these approaches depends strongly on the respective measurement efficiency.
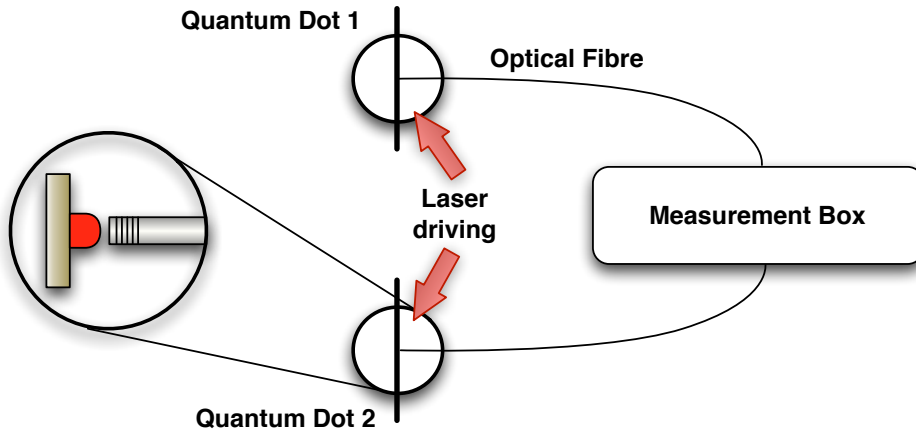
Figure 5.1: Experimental setup to entangle two distant quantum dots via the observation of macroscopic quantum jumps.

The entangling scheme by Metz *et al.* [51] alleviates the detection problem via the observation of macroscopic quantum jumps [62]. This means, the interactions in the system are engineered such that it emits a random telegraph signal of long periods of intense fluorescence (light periods) interrupted by long periods of no photon emission (dark periods). The successful state preparation is heralded by a macroscopic dark period. Ref. [51] describes a scheme that prepares two laser driven atoms inside an optical cavity in a maximally entangled state. The same authors have shown that electron shelving techniques allow even for the build up of large cluster states [115]. However, this requires the shuttling of atomic qubits in and out of an optical cavity, which is time consuming and susceptible to additional decoherence in the form of heating.

In this chapter, by applying the reservoir engineering from the previous chapter, we propose a scheme for distributed entanglement preparation with inherent scalability. We require neither the transport of qubits from one interaction zone to another nor the detection of single photons. This is achieved with the direct fibre coupling scheme from the previous chapter. Qubits placed in the cavities of this scheme experience only one common resonator mode, sometimes also called a bus mode [141]. They thus behave effectively as though they were placed in the same
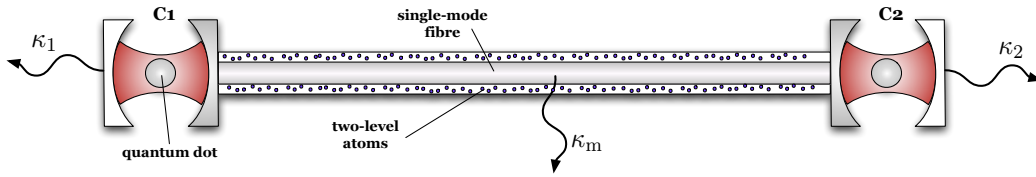
Figure 5.2: Possible implementation of the measurement box in Fig. 5.1 using the direct fibre-coupling scheme in chapter 4.

cavity.

Consequently, it is now possible to generalise ideas for the generation of scalable entanglement in atom-cavity systems to solid state systems. As in previous quantum dot schemes (see e.g. Refs. [121, 122, 142, 143]), we encode information in electron-spin states. Each dot is driven by a laser field and placed inside an optical cavity. This is feasible with current technology [144, 145, 146, 147, 148]. The light coming from the outside mirrors of the cavities is continuously measured by detectors. (c.f. Figs. 5.1 and 5.2).

The detected fluorescence signal exhibits macroscopic quantum jumps such that a dark period indicates the shelving of the qubits in a maximally entangled state. Transitions from one fluorescence period into another are now caused by spin-bath couplings, parameter fluctuations, or the spontaneous emission of photons into free space. These jumps play a vital role in the proposed state preparation scheme and make it relatively robust against experimental imperfections. We require only that the cavities experience the same system-bath interaction. The quantum dots do not have to be identical.

5.1 Theoretical Model

As was already mentioned above, the experimental setup for the entanglement scheme is as shown in Fig. 5.1, with two quantum dots placed into the cavities of the single fibre-coupled reservoir engineering scheme described in the previous chapter. Thus, as well as the cavity mode terms and their interaction with the environment, the full system Hamiltonian must now also contain terms that describe the quantum dots and their interaction with the cavity modes and the environment.
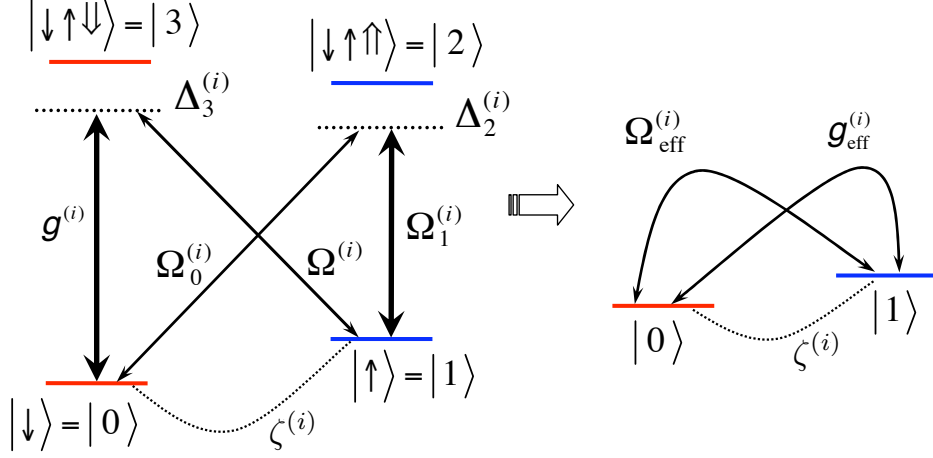
Figure 5.3: Level configuration and effective level scheme of a single quantum dot.

Essentially, we are simply replacing the cavities from the previous chapter, with a composite quantum dot-cavity system [144, 145, 146, 147, 148]. The internal level configuration of each quantum dot is shown in Fig. 5.3 and should be as in a recent experiment by Atatüre et $al.$ [149] on spin-state preparation with near-unity fidelity. In the ground states $|0\rangle = |\downarrow\rangle$ and $|1\rangle = |\uparrow\rangle$, the dot contains one spin up or one spin down electron with angular momentum projection $m_z = -1/2$ and $m_z = +1/2$. In the excited states $|2\rangle = |\downarrow\uparrow\Downarrow\rangle$ and $|3\rangle = |\downarrow\uparrow\Uparrow\rangle$, the dot contains two electrons in a singlet state and a heavy hole with spin projections $m_z = -3/2$ and $m_z = +3/2$. The 1–2 dipole transition of dot i is driven by a circularly polarised laser with Rabi frequency $\Omega_1^{(i)}$ and detuning $\Delta_2^{(i)}$. Additional laser fields drive the quadrupole transitions 0–2 and 1–3 with Rabi frequency $\Omega_0^{(i)}$ and $\Omega^{(i)}$ and detuning $\Delta_2^{(i)}$ and $\Delta_3^{(i)}$. The 0–3 transition couples with detuning $\Delta_3^{(i)}$ and coupling constant $g^{(i)}$ to the quantised mode of cavity i.

In analogy to both chapter 2 and 4, the Hamiltonian for this system in an

appropriate interaction picture with the rotating wave approximation may be written

$$
\begin{aligned}
H_{\text{sys}} \;=\; & \sum_{i=1,2} \Big[\hbar g^{(i)} \, |0\rangle_{ii}\langle 3| \, c_i^\dagger + \sum_{j=0,1} \frac{1}{2}\hbar\Omega_j^{(i)} \, |j\rangle_{ii}\langle 2| \\
& + \frac{1}{2}\hbar\Omega^{(i)} \, |1\rangle_{ii}\langle 3| + \text{H.c.} + \sum_{j=2,3} \hbar\Delta_j^{(i)} \, |j\rangle_{ii}\langle j| \\
& + \frac{1}{2}\hbar\zeta^{(i)} \, |0\rangle_{ii}\langle 1| + \text{H.c.} \Big] .
\end{aligned}
\tag{5.1}
$$

The last term takes uncontrolled spin-bath interactions into account which mix the states $|0\rangle$ and $|1\rangle$ with coupling strength $\zeta^{(i)}$ [150]. Without restrictions, we can assume that $\Omega_j^{(i)}$, $\Omega^{(i)}$ and $g^{(i)}$ are real by including their phases in $|2\rangle$, $|3\rangle$ and the cavity photon states.

The reservoir coupling between the cavity modes and the reservoirs are as described in detail in the previous chapter. The results from there are combined with the system Hamiltonian in Eq. 5.1 to give a conditional Hamiltonian that describes the evolution of this system under the condition of no photon emissions

$$
\begin{aligned}
H_{\text{cond}} \;=\; & H_{\text{sys}} - \frac{\text{i}}{2}\hbar\kappa_i \, c_i^\dagger c_i - \frac{\text{i}}{2\xi^2}\hbar\kappa_{\text{m}} \, (\xi_1^* c_1^\dagger + \xi_1^* c_2^\dagger)(\xi_1 c_1 + \xi_2 c_2) \\
& - \frac{\text{i}}{2}\hbar\Gamma_j^{(i)} |j\rangle_{ii}\langle j| ,
\end{aligned}
\tag{5.2}
$$

where, as previously, $\kappa_{i=1,2}$ are the decay rates for photons leaking from the outside mirrors of cavities 1 and 2, κ_{m} is the decay rate for photons leaking into the connecting fibre reservoir and $\Gamma_j^{(i)}$ are the decay rates of the states $|2\rangle$ and $|3\rangle$.

This conditional Hamiltonian, along with corresponding reset operators that describe photon emission events is the basic theoretical model we require to describe the entanglement scheme.

5.2   Effective system dynamics

The next step we take is to apply adiabatic elimination and the robust decoupling approach to reservoir engineering described in section 4.3.3 to derive an effective

dynamics for a qubit subspace of the quantum dot states coupled to a single common cavity mode. We therefore consider a parameter regime in which the cavity a-mode and the excited states $|2\rangle$ and $|3\rangle$ evolve on a much faster time scale than all other states,

$$\Omega_j^{(i)}, \Omega^{(i)}, g^{(i)}, \kappa_b \ll \Delta_2^{(i)}, \Delta_3^{(i)}, \kappa_a \,. \tag{5.3}$$

This allows us to eliminated them adiabatically and the Hamiltonian (5.2) simplifies to

$$\begin{aligned}
H_{\text{cond}} &= -\sum_{i=1,2} \Big[\frac{1}{2}\hbar\big(\Omega_{\text{eff}}^{(i)} - \zeta^{(i)}\big) |0\rangle_{ii}\langle 1| \\
&\quad + \hbar g_{\text{eff}}^{(i)} |0\rangle_{ii}\langle 1| \, c_b^\dagger + \text{H.c.} + \hbar\Delta_{\text{eff;cav}}^{(i)} |0\rangle_{ii}\langle 0| \, c_b^\dagger c_b \\
&\quad + \sum_{j=0,1} \hbar\Delta_{\text{eff};j}^{(i)} |j\rangle_{ii}\langle j| \Big] - \frac{\mathrm{i}}{2}\hbar\kappa_b \, c_b^\dagger c_b \,,
\end{aligned} \tag{5.4}$$

with

$$\begin{aligned}
\Omega_{\text{eff}}^{(i)} &\equiv \Omega_0^{(i)}\Omega_1^{(i)}/2\Delta_2^{(i)}, \\
g_{\text{eff}}^{(i)} &\equiv g^{(i)}\Omega^{(i)}/2\sqrt{2}\Delta_3^{(i)}, \\
\Delta_{\text{eff};0}^{(i)} &\equiv \Omega_1^{(i)2}/4\Delta_2^{(i)}, \\
\Delta_{\text{eff};1}^{(i)} &\equiv \Omega_1^{(i)2}/4\Delta_2^{(i)} + \Omega^{(i)2}/4\Delta_3^{(i)} \quad \text{and} \\
\Delta_{\text{eff;cav}}^{(i)} &\equiv g^{(i)2}/2\Delta_3^{(i)} \,.
\end{aligned} \tag{5.5}$$

The situation described by this Hamiltonian is analogous to the situation considered in Ref. [51], where both qubits experience the same effective coupling constants, for small $\zeta^{(i)}$ and when

$$\frac{\Omega_0^{(1)}\Omega_1^{(1)}}{\Omega_0^{(2)}\Omega_1^{(2)}} = \frac{\Delta_2^{(1)}}{\Delta_2^{(2)}}, \quad \frac{g^{(1)2}}{g^{(2)2}} = \frac{\Omega^{(1)2}}{\Omega^{(2)2}} = \frac{\Delta_3^{(1)}}{\Delta_3^{(2)}} \,. \tag{5.6}$$

In this case, the common cavity mode decay rate κ_b is now larger than any of the other effective system parameters so this common cavity mode can also be adiabatically eliminated. The Hamiltonian in Eq. (5.4) then becomes, up to an overall
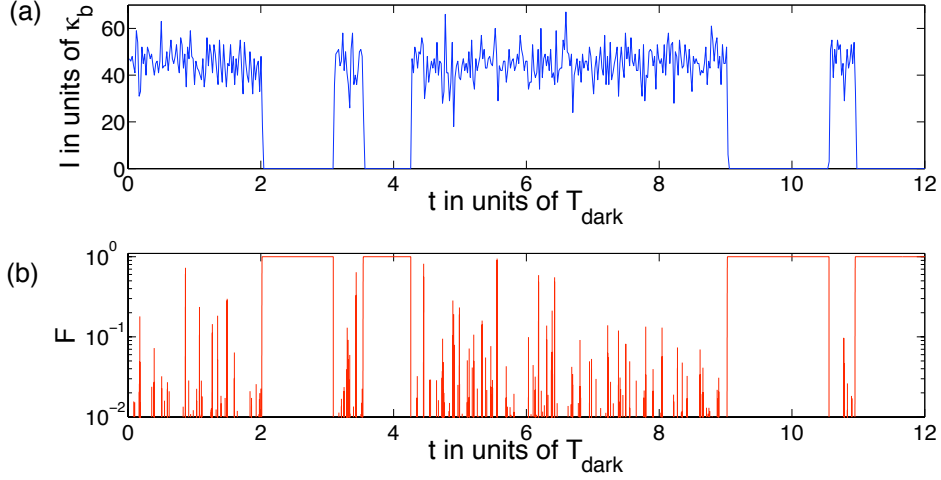
Figure 5.4: (a) Possible trajectory of the photon density $I(t)$ at detector b obtained from a quantum jump simulation with $\Omega_{\text{eff}}^{(1)} = \Delta_{\text{eff};0}^{(1)} = \frac{1}{2}\Delta_{\text{eff};1}^{(1)} = \frac{1}{4}\kappa_{\text{eff}}^{(1,1)}$ and with $\zeta^{(1)} = -\zeta^{(2)} = 0.005\,\kappa_b$. (b) Logarithmic plot of the corresponding fidelity F of the maximally entangled state $|a_{01}\rangle$.

energy shift,

$$
\begin{aligned}
H_{\text{cond}} &= -\frac{\hbar}{2\sqrt{2}}\Big[\Delta\zeta\left(|00\rangle\langle a_{01}| - |a_{01}\rangle\langle 11|\right) \\
&\quad + \left(2\Omega_{\text{eff}}^{(1)} - \zeta^{(1)} - \zeta^{(2)}\right)\left(|00\rangle\langle s_{01}| + |s_{01}\rangle\langle 11|\right) + \text{H.c.}\Big] \\
&\quad + \hbar\left(\Delta_{\text{eff};0}^{(1)} - \Delta_{\text{eff};1}^{(1)}\right)\left(|00\rangle\langle 00| - |11\rangle\langle 11|\right) \\
&\quad - \frac{\mathrm{i}}{2}\hbar\kappa_{\text{eff}}^{(1,1)}\left(|s_{01}\rangle\langle s_{01}| + |11\rangle\langle 11|\right)
\end{aligned}
\tag{5.7}
$$

with $\Delta\zeta \equiv \zeta^{(1)} - \zeta^{(2)}$ and defining the antisymmetric and symmetric qubit states

$$
|a_{01}\rangle \equiv (|01\rangle - |10\rangle)/\sqrt{2} \quad\text{and}\quad |s_{01}\rangle \equiv (|01\rangle + |10\rangle)/\sqrt{2}.
\tag{5.8}
$$

5.3 Heralding entangled states

For $\Delta\zeta = 0$, there are no transitions between the symmetric and antisymmetric subspace. Once in a symmetric state, the system emits photons via the c_b common cavity mode. However, when the qubits are in the only antisymmetric qubit state $|a_{01}\rangle$, *no* photons arrive at the detectors. The detector signal hence reveals informa-
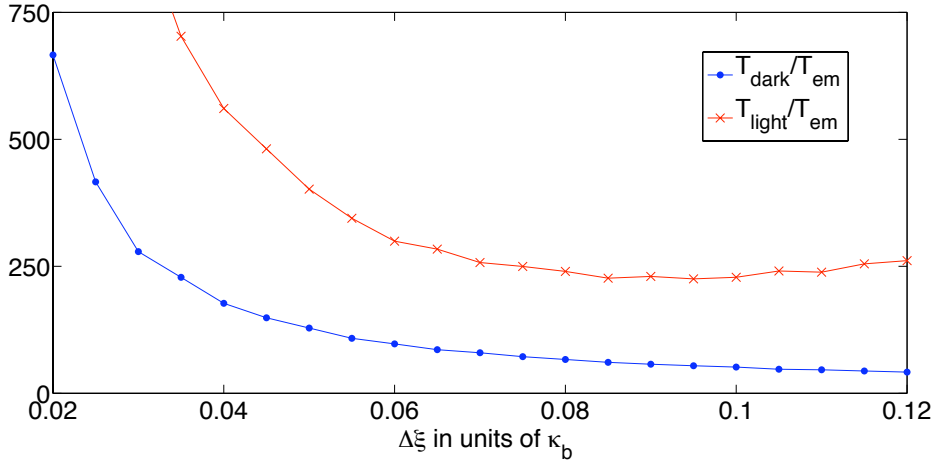
Figure 5.5: Quadratic dependence of the mean length of the light and dark periods, T_{dark} and T_{light}, on $\Delta\zeta$ obtained from a quantum jump simulation with $\Omega_{\text{eff}}^{(1)} = \Delta_{\text{eff};0}^{(1)} = \frac{1}{2}\Delta_{\text{eff};1}^{(1)} = \frac{1}{4}\kappa_{\text{eff}}^{(1,1)}$ and with $\zeta^{(1)} = -\zeta^{(2)}$.

tion about the state of the quantum dots. The overall effect of this is the continuous projection of the qubits either onto the symmetric subspace or onto $|a_{01}\rangle$.

In the case of small deviations $\Delta\zeta \neq 0$, macroscopic quantum jumps occur from one subspace into the other. The system exhibits long periods of intense photon emissions (light periods) interrupted by long periods of no emission (dark periods) [62], as shown in Fig. 5.4(a). The population in $|a_{01}\rangle$ is very close to unity during a dark period (c.f. Fig. 5.4(b)). A dark period hence prepares the qubits with a very high fidelity in a maximally entangled state. Identifying a successful state preparation is easy when the mean dark period length, T_{dark}, is long compared to the mean time between photon emissions within a light period, T_{em}. Due to the constant projection of the qubits, T_{dark} and T_{light} scale as $1/\Delta\zeta^2$ (c.f. Fig. 5.5) and can be very long.

Transitions between light and dark periods are also caused by parameter fluctuations violating condition (5.6) and the spontaneous emission of photons, which are not emitted to the detectors. The effect of these errors on the fidelity of the prepared state has already been studied in Ref. [50] for an analogous setup. The analysis there suggests that spontaneous emission from excited states can be toler-

ated, even if the system is operated in the vicinity of the bad-cavity limit. Moreover, random variations of the coupling constants up to 30% do not affect the fidelity of the prepared state. They only reduce the occurrence of relatively long dark periods.

The use of quantum dots for qubits in this scheme opens up the possibility of relatively long lived storage of the entangled state as a nuclear spin qubit. Whilst the coherence time for the qubits used in this scheme is long enough for them to be useful for quantum computing tasks, nuclear spins have been shown to have coherence times up to seconds, long enough to act as a quantum memory [151, 40].

5.4 Summary

In summary, we have shown that it is possible to entangle distant quantum dots with electron-spin qubits via the observation of a macroscopic fluorescence signal. This is achieved by applying the robust reservoir engineering scheme using a single-mode optical fibre directly coupling two cavities as described in chapter 4 of this thesis, to an entanglement scheme for two atoms in a single cavity [51]. Separating the qubits used for this entanglement scheme into two separate cavities also allows us to adapt to using quantum dots as qubits rather than the atomic qubits that this scheme was originally designed for.

The application of reservoir engineering to such an entanglement scheme is presented here as one example for possible quantum information processing architectures based on reservoir engineering. The generalisation of this scheme to the build up of large cluster states is, in principle, straightforward [115, 10, 11, 12]. This open up new possibilities in implementing the type of measurement based quantum computing schemes that where discussed in the introduction of this thesis using solid state qubits.

Chapter 6

Conclusion

In conclusion, this thesis proposes using reservoir engineering as the basis for scalable quantum information processing. This reservoir engineering is described by the quantum jump approach which predicts the effect of reservoir couplings on system dynamics. The specific coupling to the environment introduces a quantum control technique that restricts the time evolution of the system to a subspace. The particular systems we consider for implementation are based on qubits (atoms, ions or solid state) coupled to optical cavities, as these have seen very promising experimental results in recent years. In particular, we propose making use of the direct coupling of optical cavities to single mode optical fibres that is currently being considered by a number of experimental groups.

The methodology for applying the quantum jump approach to atom-cavity systems (or analogously solid state qubit-cavity systems) is developed in chapter 2. The emphasis here is on dealing with reservoirs that have a more complicated structure than usual and can affect the dynamics of the system involved in a non-trivial way.

Chapter 3 focuses on the possibility of using reservoir coupling as a quantum control technique and compares the effectiveness of this to a control technique that acts only inside the system. The basic idea of the control technique developed in this chapter is to use strong coupling to an environment to induce a faster time-scale on the evolution of the system subspace that is subject to this coupling. This effectively

decouples this subspace from the system dynamics. The effect is closely related to the quantum Zeno effect [79].

After developing the tools required for reservoir engineering, chapter 4 discusses a concrete example of reservoir engineering using two possible implementations. The simpler (and potentially easier to realise in an experiment) method uses as single-mode fibre directly coupling two cavities. This fibre is coated in Rubidium atoms that continuously measure its evanescent field. The fibre may thus be treated as another reservoir, though due to its boundary conditions, it couples to only one of two possible common cavity modes. In the parameter regime where the decay rate of the cavity modes into this reservoir is greater than the decay rate out of the other sides of the cavities, this common cavity is effectively eliminated from the system dynamics. The resulting effective dynamics of the cavity modes is such that it act as only a single common cavity mode that exists across both cavities.

The final chapter, applies the reservoir engineering technique of chapter 4 to an entanglement scheme that was originally designed for two atoms place into a single cavity. We show how this scheme can be implemented with two quantum dots placed in separate cavities thus representing a quantum information processing architecture that uses solid state qubits and is inherently scalable.

Bibliography

[1] RP Feynman, FJ Dyson, and J Robbins. *The pleasure of finding things out: the best short works of Richard P. Feynman* Penguin Books 2001.

[2] RP Feynman. Simulating physics with computers. *Int J Theor Phys*, 21(6):467–488 1982.

[3] D Deutsch. Quantum-theory, the church-turing principle and the universal quantum computer. *P Roy Soc Lond A Mat*, 400(1818):97–117 1985.

[4] P Shor. Polynomial time algorithms for discrete logarithms and factoring on a quantum computer. *Proc. 35th Ann. Sym. Found. Comp. Sci.* p. 124, 1994.

[5] L Grover. A fast quantum mechanical algorithm for database search. *Proc. ACM 28* 1996.

[6] D Deutsch and R Jozsa. Rapid solution of problems by quantum computation. *P Roy Soc Lond A Mat*, 439(1907):553–558 1992.

[7] PW Shor. Scheme for reducing decoherence in quantum computer memory. *Phys. Rev. A*, 52(4):2493–2496 (R) 1995.

[8] R Raussendorf and HJ Briegel. A one-way quantum computer. *Phys. Rev. Lett.*, 86(22):5188–5191 2001.

[9] E Knill, R Laflamme, and G Milburn. A scheme for efficient quantum computation with linear optics. *Nature*, 409(6816):46–52 2001.

Bibliography

[10] DE Browne and T Rudolph. Resource-efficient linear optical quantum computation. *Phys. Rev. Lett.*, 95(1):010501 2005.

[11] YL Lim, A Beige, and L Kwek. Repeat-until-success linear optics distributed quantum computing. *Phys. Rev. Lett.*, 95(3):4 2005.

[12] SD Barrett and P Kok. Efficient high-fidelity quantum computation using matter qubits and linear optics. *Phys. Rev. A*, 71(6):060310 2005.

[13] C Bennett and G Brassard. Quantum cryptography: Public key distribution and coin tossing. *Proc. of IEEE International Conference on Computers, Systems, and Signal Processing* 175, 1984.

[14] AK Ekert. Quantum cryptography based on bell theorem. *Phys. Rev. Lett.*, 67(6):661–663 1991.

[15] HJ Kimble. The quantum internet. *Nature*, 453(7198):1023–1030 2008.

[16] EM Purcell. Spontaneous emission probabilities at radio frequencies *Phys. Rev.* 69(11-1):681-681 1946.

[17] P Goy, JM Raimond, M Gross, and S Haroche. Observation of cavity-enhanced single-atom spontaneous emission. *Phys. Rev. Lett.*, 50(24):1903–1906 1983.

[18] D Kleppner. Inhibited spontaneous emission. *Phys. Rev. Lett.*, 47(4):233–236, 1981.

[19] AG Vaidyanathan, WP Spencer, and D Kleppner. Inhibited absorption of blackbody radiation. *Phys. Rev. Lett.*, 47(22):1592–1595 1981.

[20] ET Jaynes and FW Cummings. Comparison of quantum and semiclassical radiation theories with application to beam maser. *Proc. IEEE*, 51(1):89 1963.

[21] M Tavis and FW Cummings. Exact solution for an n-molecule—radiation-field hamiltonian. *Phys Rev*, 170(2):379–384, 1968.

[22] M Tavis and FW Cummings. Approximate solutions for an n-molecule-radiation-field hamiltonian. *Phys Rev*, 188(2):692 1969.

[23] M Brune, F SchmidtKaler, A Maali, J Dreyer, E Hagley, JM Raimond, and S Haroche. Quantum rabi oscillation: A direct test of field quantization in a cavity. *Phys. Rev. Lett.*, 76(11):1800–1803 1996.

[24] JJ Sanchez-Mondragon, NB Narozhny, and JH Eberly. Theory of spontaneous-emission line shape in an ideal cavity. *Phys. Rev. Lett.*, 51(7):550–553, 1983.

[25] GS Agarwal. Vacuum-field rabi splittings in microwave absorption by Rydberg atoms in a cavity. *Phys. Rev. Lett.*, 53(18):1732–1734, 1984.

[26] H Carmichael. Photon antibunching and squeezing for a single atom in a resonant cavity. *Phys. Rev. Lett.*, 55(25):2790–2793 1985.

[27] G Rempe and H Walther. Observation of quantum collapse and revival in a one-atom maser. *Phys. Rev. Lett.*, 58(4):353–356 1987.

[28] CF Roos, M Riebe, H Haffner, W Hansel, J Benhelm, GPT Lancaster, C Becher, F Schmidt-Kaler, and R Blatt. Control and measurement of three-qubit entangled states. *Science*, 304(5676):1478–1480 2004.

[29] M Riebe, T Monz, K Kim, A. S Villar, P Schindler, M Chwalla, M Hennrich, and R Blatt. Deterministic entanglement swapping with an ion-trap quantum computer. *Nat Phys*, 4(11):839–842 2008.

[30] D. L Moehring, P Maunz, S Olmschenk, K. C Younge, D. N Matsukevich, L.-M Duan, and C Monroe. Entanglement of single-atom quantum bits at a distance. *Nature*, 449(7158):68–71 2007.

[31] H. G Barros, A Stute, T. E Northup, C Russo, P. O Schmidt, and R Blatt. Deterministic single-photon source from a single ion. *New J. Phys.*, 11:103004 2009.

[32] J Bochmann, M Muecke, C Guhl, S Ritter, G Rempe, and DL Moehring. Lossless state detection of single neutral atoms. *Phys. Rev. Lett.*, 104(20):203601 2010.

[33] KM Fortier, Y Kim, MJ Gibbons, P Ahmadi, and MS Chapman. Deterministic loading of individual atoms to a high-finesse optical cavity. *Phys. Rev. Lett.*, 98(23):233601 2007.

[34] JA Sauer, KM Fortier, MS Chang, CD Hamley, and MS Chapman. Cavity qed with optically transported atoms. *Phys. Rev. A*, 69(5):051804 2004.

[35] M Khudaverdyan, W Alt, T Kampschulte, S Reick, A Thobe, A Widera, and D Meschede. Quantum jumps and spin dynamics of interacting atoms in a strongly coupled atom-cavity system. *Phys. Rev. Lett.*, 103(12):123006 2009.

[36] D Hunger, T Steinmetz, Y Colombe, C Deutsch, T. W Haensch, and J Reichel. A fiber fabry-perot cavity with high finesse. *New J. Phys.*, 12:065038 2010.

[37] M Trupke, J Goldwin, B Darquie, G Dutier, S Eriksson, J Ashmore, and EA Hinds. Atom detection and photon production in a scalable, open, optical microcavity. *Phys. Rev. Lett.*, 99(6):063601 2007.

[38] Y Colombe, T Steinmetz, G Dubois, F Linke, D Hunger, and J Reichel. Strong atom-field coupling for bose-einstein condensates in an optical cavity on a chip. *Nature*, 450(7167):272 2007.

[39] R Gehr, J Volz, G Dubois, T Steinmetz, Y Colombe, BL Lev, R Long, J Esteve, and J Reichel. Cavity-based single atom preparation and high-fidelity hyperfine state readout. *Phys. Rev. Lett.*, 104(20):203602 2010.

[40] Z Kurucz, M. W Sorensen, J. M Taylor, MD Lukin, and M Fleischhauer. Qubit protection in nuclear-spin quantum dot memories. *Phys. Rev. Lett.*, 103(1):010502 2009.

[41] E Togan, Y Chu, A S Trifonov, L Jiang, J Maze, L Childress, MVG Dutt, AS Sørensen, PR Hemmer, AS Zibrov, and MD Lukin. Quantum entanglement between an optical photon and a solid-state spin qubit. *Nature*, 466(7307):730–734 2010.

[42] P Neumann, N Mizuochi, F Rempp, P Hemmer, H Watanabe, S Yamasaki, V Jacques, T Gaebel, F Jelezko, and J Wrachtrup. Multipartite entanglement among single spins in diamond. *Science*, 320(5881):1326–1329 2008.

[43] A Badolato, K Hennessy, M Atatüre, J Dreiser, EL Hu, PM Petroff, and A Imamoğlu. Deterministic coupling of single quantum dots to single nanocavity modes. *Science*, 308(5725):1158–1161 2005.

[44] A Imamoğlu, S Faelt, J Dreiser, G Fernandez, M Atatüre, K Hennessy, A Badolato, and D Gerace. Coupling quantum dot spins to a photonic crystal nanocavity *J. Appl. Phys.* 101(8):081602 2007.

[45] JE Mooij, TP Orlando, L Levitov, L Tian, CH van der Wal, and S Lloyd. Josephson persistent-current qubit. *Science*, 285(5430):1036–1039 1999.

[46] A Wallraff, DI Schuster, A Blais, L Frunzio, RS Huang, J Majer, S Kumar, SM Girvin, and RJ Schoelkopf. Strong coupling of a single photon to a superconducting qubit using circuit quantum electrodynamics. *Nature*, 431(7005):162–167 2004.

[47] M Steffen, M Ansmann, RC Bialczak, N Katz, E Lucero, R McDermott, M Neeley, EM Weig, AN Cleland, and JM Martinis. Measurement of the entanglement of two superconducting qubits via state tomography. *Science*, 313(5792):1423–1425 2006.

[48] J Cho, DG Angelakis, and S Bose. Heralded generation of entanglement with coupled cavities. *Phys. Rev. A*, 78(2):022323 2008.

[49] AS Sorensen and K Mølmer. Probabilistic generation of entanglement in optical cavities. *Phys. Rev. Lett.*, 90(12):127903 2003.

[50] J Metz and A Beige. Macroscopic quantum jumps and entangled-state preparation. *Phys. Rev. A*, 76(2):022331 2007.

[51] J Metz, M Trupke, and A Beige. Robust entanglement through macroscopic quantum jumps. *Phys. Rev. Lett.*, 97(4):040503 2006.

[52] X Wang and SG Schirmer. Arbitrary high steady-state entanglement between non-interacting atoms via collective decay and adiabatic control. *arXiv*, quant-ph 2010.

[53] X Wang and SG Schirmer. Entanglement generation between distant atoms by Lyapunov control. *Phys. Rev. A*, 80(4):042305 2009.

[54] G Vacanti and A Beige. Cooling atoms into entangled states. *New J. Phys.*, 11(8):083008 2009.

[55] L-M Duan, MD Lukin, JI Cirac, and P Zoller. Long-distance quantum communication with atomic ensembles and linear optics. *Nature*, 414(6862):413–418 2001.

[56] B Zhao, M Müller, K Hammerer, and P Zoller. Efficient quantum repeater based on deterministic rydberg gates. *Phys. Rev. A*, 81(5):052329 2010.

[57] T Pellizzari. Quantum networking with optical fibres. *Phys. Rev. Lett.*, 79(26):5242–5245 1997.

[58] SJ van Enk, HJ Kimble, JI Cirac, and Peter Zoller. Quantum communication with dark photons. *Phys. Rev. A*, 59(4):2659–2664 1999.

[59] S Mancini and S Bose. Engineering an interaction and entanglement between distant atoms. *Phys. Rev. A*, 70(2):022307 2004.

[60] P Zoller, M Marte, and DF Walls. Quantum jumps in atomic systems. *Phys. Rev. A*, 35(1):198–207, 1987.

[61] R Blatt and P Zoller. Quantum jumps in atomic systems. *European Journal of Physics*, 9(250):7 1988.

[62] H Dehmelt. *Bull. Am. Phys. Soc.* 20(1):60 1975.

[63] W Nagourney, J Sandberg, and H Dehmelt. Shelved optical electron amplifier - observation of quantum jumps. *Phys. Rev. Lett.*, 56(26):2797–2799 1986.

[64] S Gleyzes, S Kuhr, C Guerlin, J Bernu, S Deléglise, UB Hoff, M Brune, J-M Raimond, and S Haroche. Quantum jumps of light recording the birth and death of a photon in a cavity. *Nature*, 446(7133):297–300 2007.

[65] HJ Carmichael. *An open systems approach to quantum optics* Springer, Berlin 1993.

[66] A Beige, C Schön, and JK Pachos. Interference of spontaneously emitted photons. *Fortschr Phys*, 50(5-7):594–598 2002.

[67] U Eichmann, JC Berquist, JJ Bollinger, JM Gilligan, WM Itano, DJ Wineland, and MG Raizen. Young interference experiment with light scattered from 2 atoms. *Phys. Rev. Lett.*, 70(16):2359–2362 1993.

[68] J Oreg, FT Hioe, and JH Eberly. Adiabatic following in multilevel systems. *Phys. Rev. A*, 29(2):690–697 1984.

[69] K Bergmann, H Theuer, and BW Shore. Coherent population transfer among quantum states of atoms and molecules. *Rev Mod Phys*, 70(3):1003–1025 1998.

[70] R Kosloff, AD Hammerich, and DJ Tannor. Excitation without demolition - radiative excitation of ground-surface vibration by impulsive stimulated raman-scattering with damage control. *Phys. Rev. Lett.*, 69(15):2172–2175 1992.

[71] GM Huang, TJ Tarn, and JW Clark. On the controllability of quantum-mechanical systems. *J. of Math. Phys.*, 24(11):2608–2618 1983.

[72] V Ramakrishna, MV Salapaka, M Dahleh, H Rabitz, and A Peirce. Controllability of molecular-systems. *Phys. Rev. A*, 51(2):960–966 1995.

[73] SG Schirmer, H Fu, and AI Solomon. Complete controllability of quantum systems. *Phys. Rev. A*, 63(6):063410 2001.

Bibliography

[74] L Viola and S Lloyd. Dynamical suppression of decoherence in two-state quantum systems. *Phys. Rev. A*, 58(4):2733–2744 1998.

[75] L Viola, E Knill, and S Lloyd. Dynamical decoupling of open quantum systems. *Phys. Rev. Lett.*, 82(12):2417–2421 1999.

[76] P Zanardi. Symmetrizing evolutions. *Phys Lett A*, 258(2-3):77–82 1999.

[77] B Misra and ECG Sudarshan. Zenos paradox in quantum-theory. *J. of Math. Phys.*, 18(4):756–763 1977.

[78] A Sudbery. The observation of decay. *Ann Phys-New York*, 157(2):512–536 1984.

[79] A Beige and GC Hegerfeldt. Projection postulate and atomic quantum Zeno effect. *Phys. Rev. A*, 53(1):53–65 1996.

[80] GC Hegerfeldt. *The quantum jump approach and quantum trajectories.* Springer LNP: Irreversible Quantum Dynamics 2003.

[81] C Schoen and A Beige. Analysis of a two-atom double-slit experiment based on environment-induced measurements. *Phys. Rev. A*, 64(2):art. no.–023806 2001.

[82] R Loudon. *The quantum theory of light* Oxford University Press 2000.

[83] M A Schlosshauer. *Decoherence and the quantum-to-classical transition.* Springer, Berlin 2007.

[84] GC Hegerfeldt and MB Plenio. Quantum beats revisited - a quantum jump approach. *Quantum Opt*, 6(1):15–25 1994.

[85] GC Hegerfeldt and MB Plenio. Dark periods in the resonance fluorescence of a single lambda-system. *Z Phys B Con Mat*, 96(4):533–539 1995.

[86] GC Hegerfeldt and DG Sondermann. Conditional Hamiltonian and reset operator in the quantum jump approach. *Quantum Semicl Opt*, 8(1):121–132 1996.

[87] J Dalibard, Y Castin, and K Mølmer. Wave-function approach to dissipative processes in quantum optics. *Phys. Rev. Lett.*, 68(5):580–583 1992.

[88] A Beige, GC Hegerfeldt, and DG Sondermann. Laser pulses as measurements: Application to the quantum zeno effect. *Quantum Semicl Opt*, 8(5):999–1015 1996.

[89] H Rabitz, R de Vivie-Riedle, M Motzkus, and K Kompa. Chemistry - whither the future of controlling quantum phenomena? *Science*, 288 (5467): 824-828 2000.

[90] N Khaneja, R Brockett, and SJ Glaser. Time optimal control in spin systems. *Phys. Rev. A*, 63(3):032308 2001.

[91] C Rangan, AM Bloch, C Monroe, and PH Bucksbaum. Control of trapped-ion quantum states with optical pulses. *Phys. Rev. Lett.*, 92(11):113004 2004.

[92] F Schmidt-Kaler, H Haffner, M Riebe, S Gulde, GPT Lancaster, T Deuschle, C Becher, CF Roos, J Eschner, and R Blatt. Realization of the Cirac-Zoller controlled-not quantum gate. *Nature*, 422(6930):408–411 2003.

[93] D Leibfried, B Demarco, V Meyer, D Lucas, M Barrett, J Britton, WM Itano, B Jelenkovic, C Langer, T Rosenband, and DJ Wineland. Experimental demonstration of a robust, high-fidelity geometric two ion-qubit phase gate. *Nature*, 422(6930):412–415 2003.

[94] C Marr, A Beige, and G Rempe. Entangled-state preparation via dissipation-assisted adiabatic passages. *Phys. Rev. A*, 68(3):033817 2003.

[95] JP Palao, R Kosloff, and CP Koch. Protecting coherence in optimal control theory: State-dependent constraint approach. *Phys. Rev. A*, 77(6):063412 2008.

[96] BW Shore. 2-level behavior of coherent excitation of multilevel systems. *Phys. Rev. A*, 24(3):1413–1418 1981.

Bibliography

[97] A Peres. Zeno paradox in quantum-theory. *Am J Phys*, 48(11):931–932 1980.

[98] P Facchi and S Pascazio. Quantum Zeno subspaces. *Phys. Rev. Lett.*, 89(8):080401 2002.

[99] WH Zurek. Reversibility and stability of information-processing systems. *Phys. Rev. Lett.*, 53(4):391–394 1984.

[100] A Beige, D Braun, B Tregenna, and PL Knight. Quantum computing using dissipation to remain in a decoherence-free subspace. *Phys. Rev. Lett.*, 85(8):1762–1765 2000.

[101] JK Pachos and H Walther. Quantum computation with trapped ions in an optical cavity. *Phys. Rev. Lett.*, 89(18):187903 2002.

[102] A Beige. Dissipation-assisted quantum gates with cold trapped ions. *Phys. Rev. A*, 67(2):020301 2003.

[103] A Pechen and H Rabitz. Teaching the environment to control quantum systems. *Phys. Rev. A*, 73(6):062102 2006.

[104] P Facchi, DA Lidar, and S Pascazio. Unification of dynamical decoupling and the quantum Zeno effect. *Phys. Rev. A*, 69(3):032314 2004.

[105] P Facchi, S Tasaki, S Pascazio, H Nakazato, A Tokuse, and DA Lidar. Control of decoherence: Analysis and comparison of three different strategies *Phy. Rev. A* 71 (2):022302 2005.

[106] H Georgi. *Lie algebras in particle physics* Perseus Books 1999.

[107] A Beige and GC Hegerfeldt. Quantum Zeno effect and light-dark periods for a single atom. *J Phys A-Math Gen*, 30(4):1323–1334 1997.

[108] R Cook and H. J Kimble. Possibility of direct observation of quantum jumps. *Phys. Rev. Lett.*, 54(10):1023–1026 1985.

[109] P Facchi and S Pascazio. Quantum Zeno dynamics: mathematical and physical aspects *Phys. Rev. Lett.* 89 (8):080401 2008.

[110] T Pellizzari, SA Gardiner, JI Cirac, and P Zoller. Decoherence, continuous observation, and quantum computing - a cavity QED model. *Phys. Rev. Lett.*, 75(21):3788–3791 1995.

[111] SB Zheng and GC Guo. Efficient scheme for two-atom entanglement and quantum information processing in cavity qed. *Phys. Rev. Lett.*, 85(11):2392–2395 2000.

[112] XX Yi, XH Su, and L You. Conditional quantum phase gate between two 3-state atoms. *Phys. Rev. Lett.*, 90(9):097902 2003.

[113] MB Plenio, S Huelga, A Beige, and PL Knight. Cavity-loss-induced generation of entangled atoms. *Phys. Rev. A*, 59(3):2468–2475 1999.

[114] AS Sorensen and K Mølmer. Measurement induced entanglement and quantum computation with atoms in optical cavities. *Phys. Rev. Lett.*, 91(9):097905 2003.

[115] J Metz, C Schoen, and A Beige. Atomic cluster state build-up with macroscopic heralding. *Phys. Rev. A*, 76(5):052307 2007.

[116] C Cabrillo, JI Cirac, P Garcia-Fernandez, and P Zoller. Creation of entangled states of distant atoms by interference. *Phys. Rev. A*, 59(2):1025–1033 1999.

[117] YL Lim, A Beige, and L Kwek. Repeat-until-success linear optics distributed quantum computing. *Phys. Rev. Lett.*, 95(3):030505 2005.

[118] J Denschlag, D Cassettari, and J Schmiedmayer. Guiding neutral atoms with a wire. *Phys. Rev. Lett.*, 82(10):2014–2017 1999.

[119] EA Hinds and IG Hughes. Magnetic atom optics: mirrors, guides, traps, and chips for atoms *J Phys D Appl Phys* 32(18):R119-R146 1999.

[120] WK Hensinger, S Olmschenk, D Stick, D Hucul, M Yeo, M Acton, L Deslauri-
ers, C Monroe, and J Rabchuk. T-junction ion trap array for two-dimensional
ion shuttling, storage, and manipulation. *Appl Phys Lett*, 88(3):034101 2006.

[121] D Loss and DP DiVincenzo. Quantum computation with quantum dots. *Phys.
Rev. A*, 57(1):120–126 1998.

[122] A Imamoğlu, DD Awschalom, G Burkard, DP DiVincenzo, D Loss, M Sherwin,
and A Small. Quantum information processing using quantum dot spins and
cavity qed. *Phys. Rev. Lett.*, 83(20):4204–4207 1999.

[123] YS Park, AK Cook, and H Wang. Cavity qed with diamond nanocrystals and
silica microspheres. *Nano Lett*, 6(9):2075–2079 2006.

[124] PE Barclay, C Santori, K-M Fu, RG Beausoleil, and O Painter. Coherent
interference effects in a nano-assembled diamond nv center cavity-qed system.
Opt Express, 17(10):8081–8097 2009.

[125] JI Cirac, P Zoller, HJ Kimble, and H Mabuchi. Quantum state transfer and
entanglement distribution among distant nodes in a quantum network. *Phys.
Rev. Lett.*, 78(16):3221–3224 1997.

[126] A Serafini, S Mancini, and S Bose. Distributed quantum computation via
optical fibers. *Phys. Rev. Lett.*, 96(1):010503 2006.

[127] S Clark, A Peng, M Gu, and AS Parkins. Unconditional preparation of
entanglement between atoms in cascaded optical cavities. *Phys. Rev. Lett.*,
91(17):177901 2003.

[128] W Vogel and D-G Welsch. *Lectures on quantum optics* Wiley-VCH 1994.

[129] JD Franson, BC Jacobs, and TB Pittman. Quantum computing using single
photons and the zeno effect. *Phys. Rev. A*, 70(6):062302 2004.

[130] A Stiebeiner, O Rehband, R Garcia-Fernandez, and A Rauschenbeutel. Ultra-sensitive fluorescence spectroscopy of isolated surface-adsorbed molecules using an optical nanofiber. *Opt Express*, 17(24):21704–21711 2009.

[131] JD Jackson. *Classical electrodynamics* Wiley 1999.

[132] M Poellinger, D O'Shea, F Warken, and A Rauschenbeutel. Ultrahigh-q tunable whispering-gallery-mode microresonator. *Phys. Rev. Lett.*, 103(5):053901 2009.

[133] B Hecht, B Sick, U Wild, and V Deckert. Scanning near-field optical microscopy with aperture probes. *J. Chem. Phys.* 2000.

[134] TI Kuznetsova, VS Lebedev, and AM Tsvelik. Optical fields inside a conical waveguide with a subwavelength-sized exit hole. *Journal of Optics A Pure and Applied Optics*, 6(4):338–348, 2004.

[135] L Novotny, DW Pohl, and P Regli. Light-propagation through nanometer-sized structures - the 2-dimensional-aperture scanning near-field optical microscope. *J Opt Soc Am A*, 11(6):1768–1779 1994.

[136] L Novotny, DW Pohl, and B Hecht. Light confinement in scanning near-field optical microscopy *Ultramicroscopy* 61:1–9 1995.

[137] TJAT Szoplik. Description of near–and far–field light emitted from a metal–coated tapered fiber tip. *Opt. Express*, 15:7845–7852, 2007.

[138] L Novotny and C Hafner. Light propagation in a cylindrical waveguide with a complex, metallic, dielectric function. *Phys. Rev. E* 1994.

[139] L Novotny, DW Pohl, and B Hecht. Scanning near-field optical probe with ultrasmall spot size. *Opt Lett*, 20(9):970–972 1995.

[140] CWJ Beenakker, DP DiVincenzo, C Emary, and M Kindermann. Charge detection enables free-electron quantum computation. *Phys. Rev. Lett.*, 93(2):020501 2004.

Bibliography

[141] TP Spiller, K Nemoto, SL Braunstein, WJ Munro, P Van Loock, and G Milburn. Quantum computation by communication. *New J. Phys.*, 8(2):30–30 2006.

[142] V Cerletti, WA Coish, O Gywat, and D Loss. Recipes for spin-based quantum computing *Nanotechnology* 16(4):R27-R49 2005.

[143] G Burkard and A Imamoğlu. Ultra-long-distance interaction between spin qubits. *Phys. Rev. B*, 74(4):4 2006.

[144] JP Reithmaier, G Sęk, A Löffler, C Hofmann, S Kuhn, S Reitzenstein, LV Keldysh, VD Kulakovskii, TL Reinecke, and A Forchel. Strong coupling in a single quantum dot–semiconductor microcavity system. *Nature*, 432(7014):197–200 2004.

[145] T Yoshie, A Scherer, J Hendrickson, G Khitrova, HM Gibbs, G Rupper, C Ell, OB Shchekin, and DG Deppe. Vacuum rabi splitting with a single quantum dot in a photonic crystal nanocavity. *Nature*, 432(7014):200–3 2004.

[146] K Srinivasan and O Painter. Linear and nonlinear optical spectroscopy of a strongly coupled microdisk-quantum dot system. *Nature*, 450(7171):862–U15 2007.

[147] D Englund, A Faraon, B Zhang, Y Yamamoto, and J Vuckovic. Generation and transfer of single photons on a photonic crystal chip. *Opt Express*, 15(9):5550–5558 2007.

[148] D Englund, A Faraon, I Fushman, NG Stoltz, PM Petroff, and J Vuckovic. Controlling cavity reflectivity with a single quantum dot. *Nature*, 450(7171):857–861 2007.

[149] M Atatüre, J Dreiser, A Badolato, A Hogele, K Karrai, and A Imamoğlu. Quantum-dot spin-state preparation with near-unity fidelity. *Science*, 312(5773):551–553 2006.

[150] WA Coish and D Loss. Hyperfine interaction in a quantum dot: Non-markovian electron spin dynamics. *Phys. Rev. B*, 70(19):21 2004.

[151] J Taylor, C Marcus, and M Lukin. Long-lived memory for mesoscopic quantum bits. *Phys. Rev. Lett.*, 90(20):206803 2003.